Sensitivity Analysis of the Static Aeroelastic Response of a Wing

by

Lloyd B. Eldred

Dissertation submitted to the Faculty of the

Virginia Polytechnic Institute and State University

in partial fulfillment of the requirements for the degree of

Doctor of Philosophy

in

Aerospace Engineering

APPROVED:

Rakesh K. Kapania (Chairman)

Raphael T. Haftka

Eric R. Johnson

Liviu Librescu

William Mason

February, 1993

Blacksburg, Virginia

Abstract

A technique to obtain the sensitivity of the static aeroelastic response of a three dimensional wing model is designed and implemented. The formulation is quite general and accepts any aerodynamic and structural analysis capability. A program to combine the discipline level, or local, sensitivities into global sensitivity derivatives is developed. A variety of representations of the wing pressure field are developed and tested to determine the most accurate and efficient scheme for representing the field outside of the aerodynamic code. Chebyshev polynomials are used to globally fit the pressure field. This approach had some difficulties in representing local variations in the field, so a variety of local interpolation polynomial pressure representations are also implemented. These panel based representations use a constant pressure value, a bilinearly interpolated value, or a biquadratically interpolated value. The interpolation polynomial approaches do an excellent job of reducing the numerical problems of the global approach for comparable computational effort. Regardless of the pressure representation used, sensitivity and response results with excellent accuracy have been produced for large integrated quantities such as wing tip deflection and trim angle of attack. The sensitivities of such things as individual generalized displacements have been found with fair accuracy. In general, accuracy is found to be proportional to the relative size of the derivatives to the quantity itself.

Acknowledgements

This thesis is dedicated to my family and friends for their support throughout the years of work leading to this document. I would also like to acknowledge the support, advice, and assistance of Dr. Rakesh Kapania, without whom this would not have been possible. Further, I would like to ackowledge the financial support of NASA, Langley Research Center, and the aid of Dr. Jean-Francois M. Barthelemy and Mr. E. Carson Yates. Thanks are also due to Drs. Raphael Haftka, Eric Johnson, Liviu Librescu and William Mason for serving on my committee. I would also like to thank Dr. Ron Kriz and the Scientific Visualization Lab for the tools to help analyze where problems existed early on in the work.

Table of Contents

List of Figures

List of Tables

1.0 Introduction

During the design phase of an engineering system, numerous analyses are conducted to predict changes in the characteristics of the system due to changes in design variables. Usually, this process entails perturbing each variable in turn, recalculating the characteristics, and evaluating the sensitivities by a finite-difference calculation. These repeated analyses can drive the cost of design very high. An approach that has found increased interest recently in engineering design is analytical calculation of the sensitivity derivatives[1]. Typically, the analytical approach requires less computational resources than a finite-difference approach and is less subject to numerical errors (round-off or truncation). The analytical approach is best developed in parallel with the baseline analysis capability since it uses a significant portion of the numerical information generated during that baseline analysis. In the design of modern aircraft, airframe flexibility is a concern from strength, control, and performance standpoints. To properly account for the aerodynamic and structural implications of flexibility, reliable aeroelastic sensitivity analysis is needed. Therefore, both structural and aerodynamic sensitivity analysis capabilities are necessary.

1.1 Sensitivity Analysis

Structural sensitivity analysis methodology has been available for over two decades for both sizing (thickness, cross-section properties) and shape (configuration) variables[2]. However, aerodynamic sensitivity analysis has been nonexistent until relatively recently. Some limited aerodynamic sensitivity analysis capability was developed for aircraft in

subcritical compressible flow by Hawk and Bristow[3], but it only handled perturbations in the direction of the thickness of the wing (thickness, camber, or twist distribution). Yates[4] proposed a new approach that considers general geometry variations including planform for subsonic, sonic, and supersonic unsteady, nonplanar lifting-surface theory. This work is still under progress.

Aeroelastic sensitivity analysis methodology has also been available for more than two decades for structural sizing variables (Haftka and Yates[5]). This is because changes in sizing variables exclusively affect the structural stiffness and mass distribution of the airframe and not its basic geometry. Therefore, structural sensitivity analysis capability is sufficient. However, the lack of development in aerodynamic shape sensitivity analysis explains why there are very few results in aeroelastic shape sensitivity analysis. In a notable exception, Haftka et al[6] designed a sailplane wing under aeroelastic constraints and analyzed the design model with vortex lattice and finite element methods. A finite-difference (for GSE derivatives) aeroelastic sensitivity analysis capability is made possible by (1) devising a reduced order model to describe the wing static aeroelastic response and (2) using exact perturbation analysis to approximate changes in the vorticity vector with changes in the geometry. Follow up work used semi-analytical derivatives.

Barthelemy and Bergen[7] demonstrated the feasibility of calculating analytically the sensitivity of wing static aeroelastic characteristics to changes in wing shape. Of interest also was the fact that the curvature of the aeroelastic characteristics was small enough that analytical sensitivity derivatives could be used to approximate them without costly reanalyses for large perturbations of the design variables.

The dynamic aeroelastic phenomena is also of interest to designers and it would be advantageous to the aircraft designers to have a tool that can be used to predict the changes in flutter speed with the changes in basic shape parameters.

As is the case for static aeroelastic response, sensitivity calculations have only been available for structural sizing parameters. For example, Rudisill and Bhatia[8] developed expressions for the analytical derivatives of the eigenvalues, reduced frequency and flutter

speed with respect to structural parameters for use in minimizing the total mass. However, this method is limited because the structural parameters are sizing variables such as cross-sectional areas, plate thickness and diameters of spars.

Pedersen and Seyranian[9] examined the change in flutter load as a function of change in stiffness, mass, boundary conditions or load distribution. They showed how sensitivity analysis can be performed without any new eigenvalue analysis. The solution to the main and adjoint problem provide all the necessary information for evaluating sensitivities. Their paper mainly focuses on column and beam critical load distributions.

In a recent study, Kapania, Bergen and Barthelemy[10] obtained the sensitivity of a wing flutter response to changes in its geometry. Specifically, the objective was to determine the derivatives of flutter speed and frequency with respect to wing area, aspect ratio, taper ratio, and sweep angle. The study used Giles'[11,12] equivalent plate model to represent the wing structure. The aerodynamic loads were obtained using Yates[13] modified strip analysis to analyze flutter characteristics for finite span swept and unswept wings. It is noted that Yates modified strip theory was used quite recently by Landsberger and Dugundji[14], with a modification for camber effects given by Spielberg[15], to study the flutter and divergence of a composite plate.

Unger, Hutchison, Rais-Rohani, Haftka, and Grossman[16] recently demonstrated a variable-complexity approach to the multidisciplinary design of a transport wing. Their approach optimizes based on a relatively simple and inexpensive model. Then, this approximate optimal wing is reoptimized using a more complex model.

An excellent examination of various issues involved in aeroelastic analysis was recently published by Borland[17]. The study compares and contrasts "integrated" aeroelastic systems versus "interfaced" systems. Borland refers to packages designed to produce aeroelastic results from a single program as "integrated". Packages that have separate modules for each discipline that each write as their output the input for another package are termed "interfaced". As is discussed in section 2.1 of this dissertation, the current work's scheme is a variation on the "interfaced" approach.

1.2 Current Work

The current work develops techniques to determine the sensitivity of the various static aeroelastic responses to the variations in various shape parameters, namely: (i) wing area, (ii) sweep, (iii) aspect ratio and (iv) the taper ratio. The aeroelastic responses were the generalized aeroelastic displacements and the trim angle of attack. The sensitivities were obtained by differentiating the constitutive equations. It was shown that the resulting sensitivity equations can be reformulated into a variation of the Sobieski's Global Sensitivity Equations[19] (G.S.E.) approach. Both schemes gave the various global sensitivities (i.e. the sensitivity including all interdisciplinary interactions) in terms of local sensitivities (i.e. the sensitivities obtained at the discipline level). A key feature that distinguished this study from the study by Barthelemy and Bergen[7] is the use of a more realistic aerodynamic model, FAST[20], that uses a lifting surface theory as opposed to a lifting line theory employed in the earlier study. The formulation was designed to be quite general so that it was applicable with any aerodynamic code which, for a given geometry and structural deformations, provides aerodynamic pressures on the wing surface. To facilitate the calculation of the shape sensitivities of various quantities (required in aeroelastic analyses), the pressure distribution was represented as a double series of global Chebyshev polynomials. The displacements of the wing were obtained using an iterative scheme. To validate this more general formulation, sensitivity of the static aeroelastic response of an example wing was obtained. The results were compared with those obtained by using a purely finite difference approach. A good agreement was obtained.

During the course of the work [Ref. 18], it was found that the generalized pressure coefficients, due to the global nature of the interpolation polynomials, may be sensitive to small changes in independent variables. As a result, the determination of the local derivatives of some of the generalized aerodynamic coefficients was found to be difficult when forward or central differences were used. A higher order finite difference scheme using

a large step size was emplyed so that the effect of local wiggles can be reduced. Obviously, this was an expensive option. Other more robust techniques are therefore needed to express the aerodynamic pressure. A representation of the aerodynamic loads that is piece-wise polynomial should be used. Some of the advantages of piece-wise representation over global representation are discussed by Burden and Faires[21] and by de Boor[22].

In addition, the piece-wise polynomial pressure approach will have a major application in representing the aerodynic pressure of the High Speed Civil Transport Wing. This wing's flow regime will be transonic, thereby having pressure discontinuities from shock waves. A piece-wise function is often better represented by piece-wise polynomials as opposed to globally defined polynomials.

2.0 Aeroelastic Response

A scheme was developed to interface arbitrary aerodynamic and structural codes in order to calculate the aeroelastic response of a wing. Anticipating the availability of nonlinear aerodynamic models in the future, the formulation does not assume a linear dependence between the lift generated and the generalized coordinates and the initial angle of attack. This formulation needs an iterative process to calculate the angle of attack to which the aircraft is trimmed to produce the required lift.

This analysis is performed for the wing shown in figure 1. This forward swept wing has its coordinate origin at the root quarter chord. The y-axis is perpendicular to the root chord, in the span-wise direction. The x-axis is in the chord-wise direction, with positive values being aft of the quarter-chord.

2.1 Overview

The combination of realistic aerodynamics and structural models in a modular manner with shape sensitivity code requires a systematic approach. A scheme of calling the aerodynamic and structural codes to produce a converged static wing loading and shape was developed. In addition a set of "neutral format" data files were defined. Here, a "neutral format" data file is a file that is defined to contain certain data at certain spots, regardless of the package that originally generated the data. This scheme makes the replacement of analysis packages practical and relatively simple. These files include the base geometry and initial deflection values, the intermediate pressure loading and structural deflections, and the final converged wing loading and deflection.

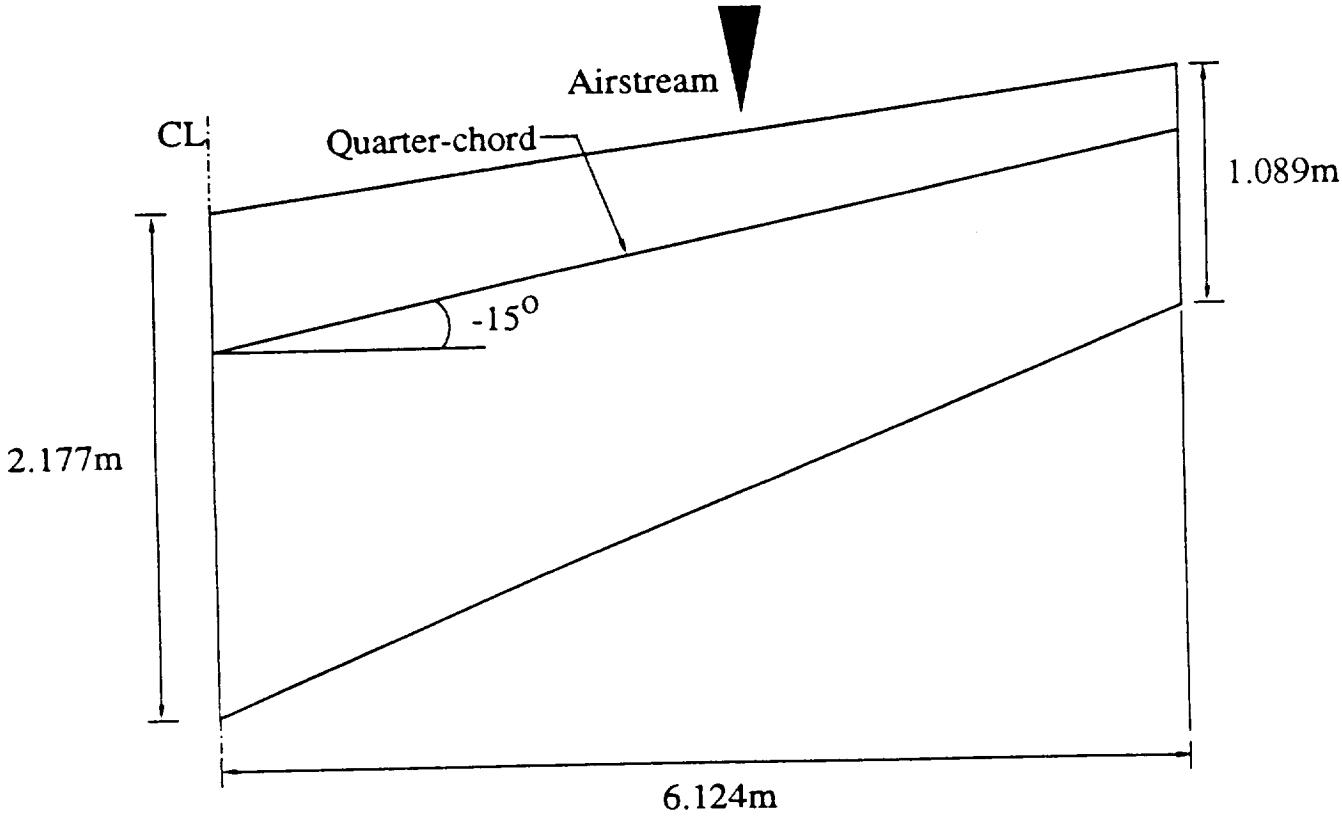

Figure 1. Baseline Wing

The aeroelastic problem is broken into subproblems (or blocks) by discipline. The aerodynamic and structural blocks are called iteratively to produce a converged static wing loading and shape. Shape sensitivity values for this converged wing are then obtained (discussed in chapter 3). Figure 1 is a flow chart illustrating this scheme.

Each block operates completely independently of the other. It reads from several "neutral format" input files, performs its calculations and generates one or more neutral format output files. Thus, any aerodynamic and structural analysis capability may be used. Only new input and output "adapter" programs need be written to add a new analysis package to the system. These two adapter programs must convert the neutral format data files to and from the new package's native format.

2.11 Aerodynamics:

The aerodynamic block is responsible for generating the loads on the wing. It reads as input the wing geometry parameters and the current wing deflections. It is able to output the pressure on the wing at arbitrary points. Figure 2 illustrates the aerodynamic section. Currently, the aerodynamic analysis is being performed by program FAST. This lifting surface code was developed at NASA, Langley. It is based on a kernal-function based theory developed by Yates, and was implemented by Desmarais and Bennett[20]. Originally developed for a CDC Cyber computer, this program, with considerable effort, has been ported to the VAX/VMS and IBM-CMS operating systems. Adapter programs to convert to and from native FAST data files to the defined neutral format were also developed.

2.12 Structures:

The structural block is responsible for calculating the deflection of the wing. It is given the wing geometry and wing loading. It calculates the deflected shape of the wing. Figure 3 illustrates the structural section. Currently, Giles' ELAPS[12] code is being used to perform the structural analysis. This Ritz method program was developed at NASA, Langley. It has been adapted for use on both the VAX and IBM systems. Adapter programs have been developed to convert wing pressures to ELAPS generalized forces and

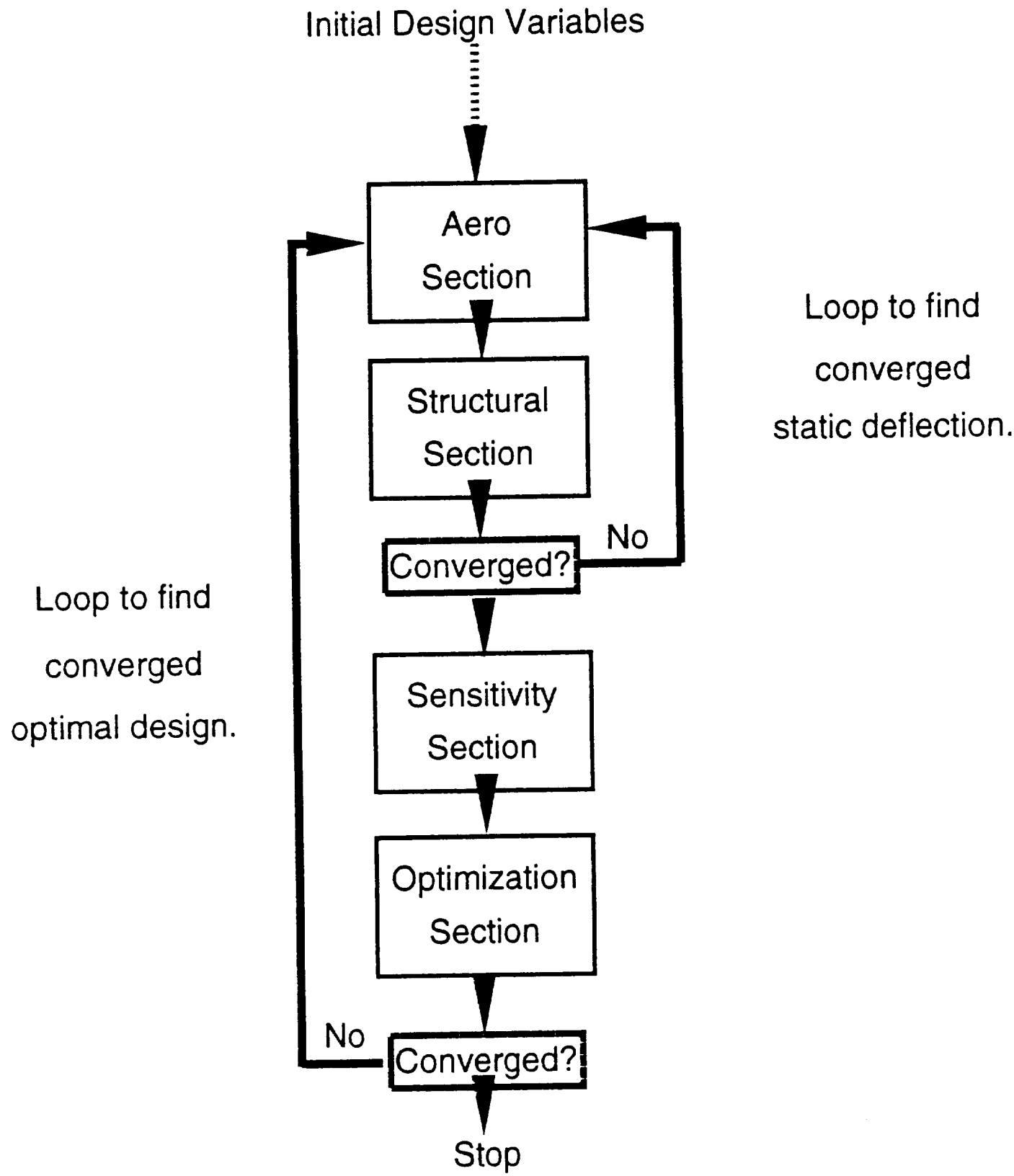

Figure 2. Overall Flow Chart

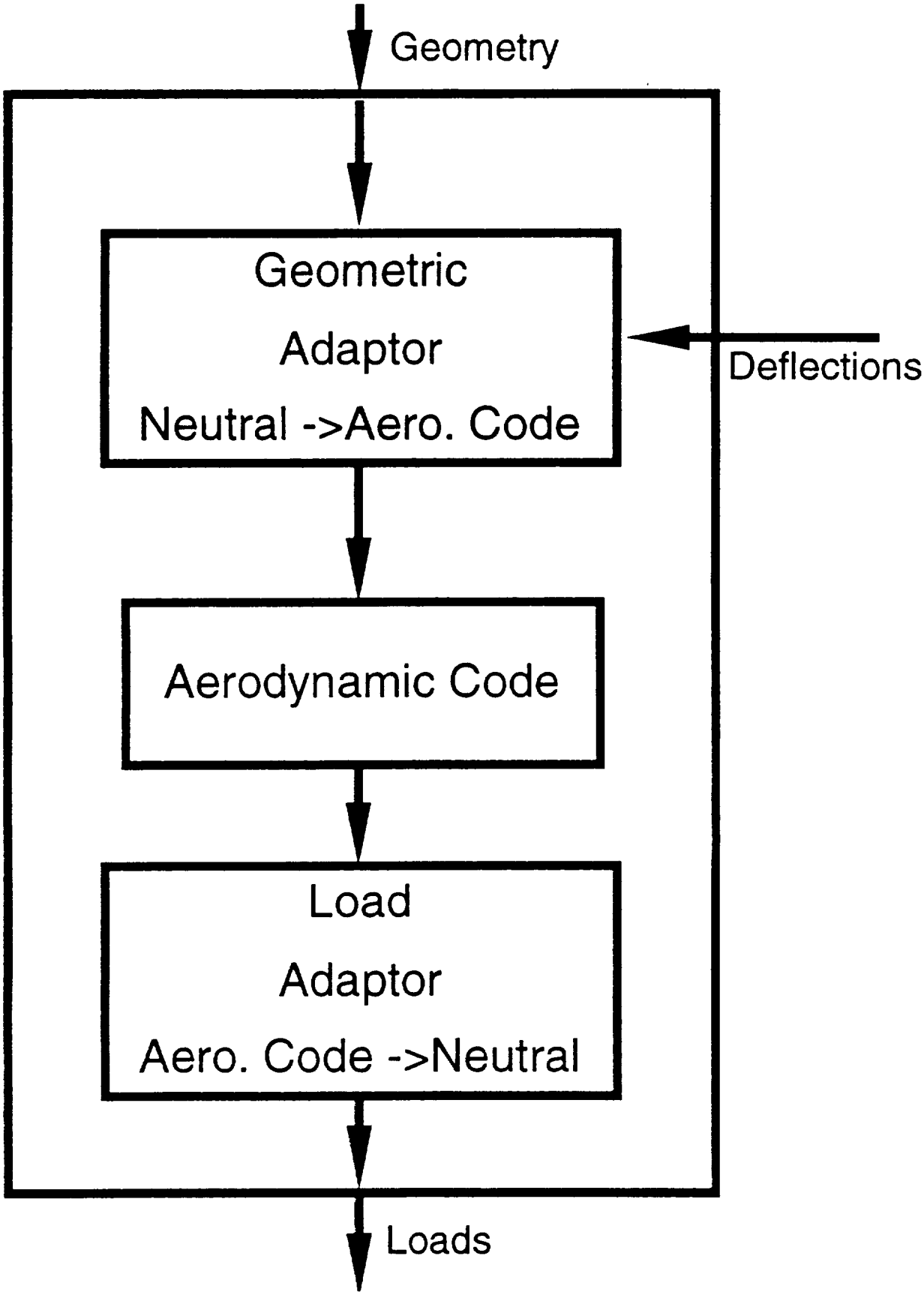

Figure 3. Aerodynamic Section

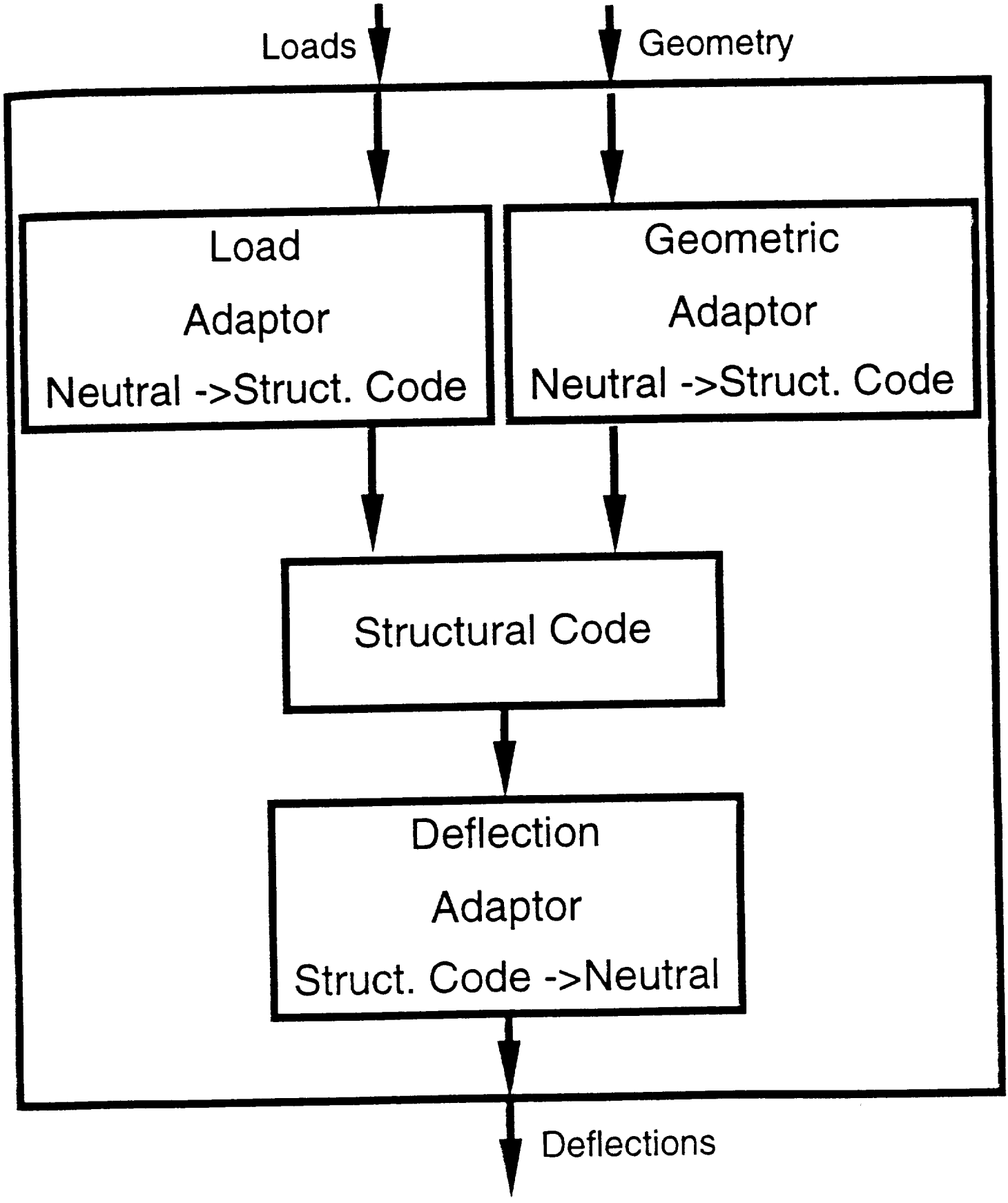

Figure 4. Structural Section

to convert its deflection outputs to neutral form.

2.2 Governing Equations

The governing equations of motion for the aeroelastic analysis and the lift can be written as

$$[K]\{C\} = \{Q\} \tag{2.1}$$

and

$$\frac{nW}{2} = \int\int_{\Omega} p(x,y)d\Omega \tag{2.2}$$

where

$[K]$ is the stiffness matrix,

$\{C\}$ is the vector of unknown generalized displacements,

$\{Q\}$ is the vector of generalized forces,

n is the load factor,

W is the aircraft weight,

$p(x,y)$ is the wing pressure field, and

Ω is the wing surface area.

The vector of generalized forces can be obtained as:

$$Q_i = \int\int_{\Omega} p(x,y)\gamma_i(x,y)dxdy \tag{2.3}$$

where $\gamma_i(x,y)$ is the ith nondimensional displacement function used in the displacement

model:

$$w(x,y) = \sum_{i=1}^{np} \gamma_i(x,y) C_i \tag{2.4}$$

with

$$\gamma_i(x,y) = (\frac{x}{x_{max}})^m (\frac{y}{y_{max}})^n \tag{2.5}$$

where m varies from 0 to mw and n varies from 2 to $nw + 2$ with n varying more rapidly than m. The terms mw and nw are configurable options. For this work, $mw = 5$ and $nw = 6$.

These γ's satisfy the geometric boundary conditions for a cantilever plate. The C's in (2.4) are the generalized displacements.

To facilitate both the integration and subsequent sensitivity calculations, a coordinate transformation was used to simplify the integration limits. This was accomplished using the following transformation:

$$x(\eta,\xi) = \sum_{j=1}^{4} N_j(\eta,\xi) x_j \tag{2.6}$$

$$y(\eta,\xi) = \sum_{j=1}^{4} N_j(\eta,\xi) y_j \tag{2.7}$$

where

$N_j(\eta,\xi)$ are the shape functions, and the

x_j and y_j are the coordinates of the four corner points of the wing.

The shape functions are given as

$$N_i(\eta,\xi) = (1 + \xi\xi_i)(1 + \eta\eta_i)/4 \tag{2.8}$$

where η_i and ξ_i are the coordinates of the node i in the $\eta - \xi$ system. Note that this transformation will change the domain of the wing to a square ($-1 \leq \eta \leq 1; -1 \leq \xi \leq 1$). The transformed wing is shown in figure 5.

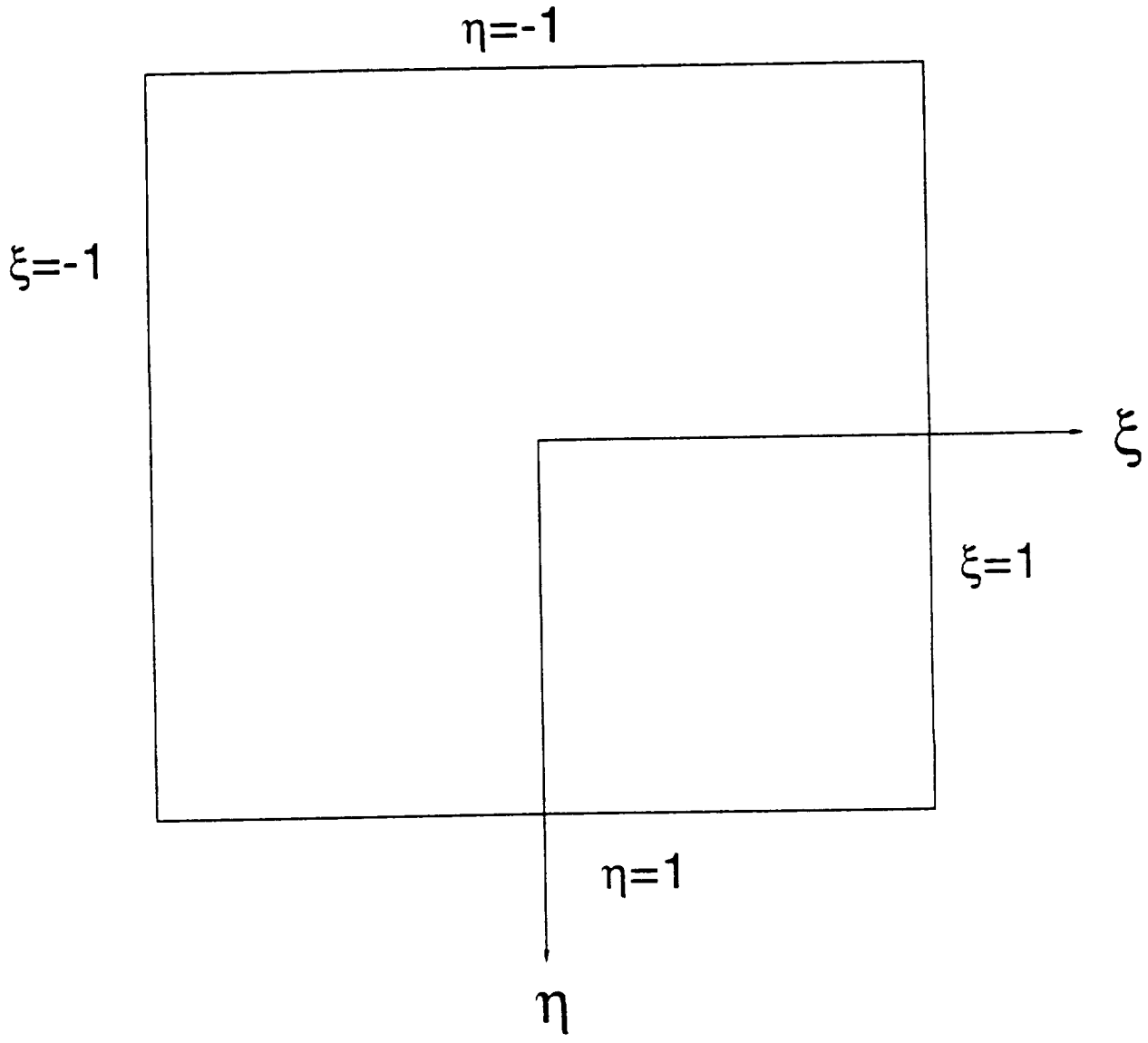

Figure 5. Transformed Wing

As a first step to obtain the generalized forces, the pressure distribution on the wing was represented as a series of either global interpolation functions or interpolation polynomials that have local support over a wing panel. This can be represented in a generic form as:

$$p(\eta,\xi) = \sum_{j=1}^{M} \beta^j(\eta,\xi) a^j \tag{2.9}$$

where a^j can be considered as the generalized pressure coefficients and $\beta^j(\eta,\xi)$ are some known interpolation functions of η and ξ.

A large number of interpolating polynomials are available in the literature[21,22]. First, a global tensor product of Chebyshev polynomials was used. Then, a variety of local polynomials were studied. Details of these approaches and their results are in chapters 4-7.

Generically, the integral for a generalized force Q_i, is

$$Q_i = \int_{-1}^{1}\int_{-1}^{1} p(\eta,\xi)\ \gamma_i(\eta,\xi)\ |J_1(\eta,\xi)|\ d\eta d\xi \tag{2.10}$$

where $|J_1(\eta,\xi)|$ is the Jacobian of the coordinate transformation specified by Eqs. 2.6 and 2.7. The generalized force Q_i can be written as

$$Q_i = \sum_{j=1}^{M} A_{ij} a^j \tag{2.11}$$

In matrix form

$$\{Q\} = [A]\{a\} \tag{2.12}$$

Similarly, the lift equation can be written as:

$$\frac{nW}{2} = \sum_{j=1}^{M} a^j L^j = \{L\}^T\{a\} \tag{2.13}$$

2.3 Aeroelastic Response

The aeroelastic response was obtained in an iterative fashion. In that, the pressure distribution on the wing is first obtained by assuming the wing to be rigid and having an angle of attack of 1° (throughout the span). The pressure distribution thus obtained is used to obtain the vector of generalized forces (Eq. 2.9) which in turn is used to obtain the vector of generalized displacements (Eq. 2.1). The elastic displacements are superimposed on the rigid wing and a new pressure distribution on the wing is obtained. This pressure distribution is then used to obtain the generalized displacements. The total lift on the wing is calculated, and a new trim angle of attack is obtained by dividing the total required lift by the current calculated lift and multiplying by the current trim angle of attack. This process is repeated until a converged value of the trim angle of attack is achieved for the wing. No relaxation is necessary to achieve convergence for the cases studied.

An alternative technique has also been developed to compute the trim angle of attack and wing generalized deflections. This technique involves significantly more setup effort, but gives the converged displacement and angle of attack in one step. It should be noted that only the linearity of the two current analysis programs makes this one step solution possible.

For the case of linear aerodynamics, one is not required to use an iterative scheme to obtain the aeroelastic solution. For such a case the vector of aerodynamic pressures, p_i, at some discrete points can be written as

$$\{p\} = [\bar{A}]\{C\} + \alpha \left\{\frac{\partial p}{\partial \alpha}\right\} \tag{2.14}$$

where $\bar{A}_{ij} = \dfrac{\partial p_i}{\partial C_j}$.

The generalized aerodynamic coefficients can be written as

$$\{a\} = [R]\{p\} \tag{2.15}$$

where R is an interpolation matrix that converts discrete p's to our generalized a's. For our case, $\{p\}$ is taken at Chebychev points. Eqn. 2.13 is substituted into eqn. 2.14. Then, the equilibrium equations for the structure are updated from eqns. 2.1 and 2.8.

$$[K]\ \{C\} \ = \ [A]\ [R]\ [\bar{A}]\ \{C\} \ + \ \alpha[A]\ [R] \left\{ \frac{\partial p}{\partial \alpha} \right\} \tag{2.16}$$

The trim equation is adapted from eqn. 2.12.

$$n\frac{W}{2} \ = \ \{L\}^T\ [R]\ [\bar{A}]\ \{C\} \ + \ \alpha\ \{L\}^T [R] \left\{ \frac{\partial p}{\partial \alpha} \right\} \tag{2.17}$$

Note that for our case: $[R]\ [\bar{A}] \ = \ \dfrac{\partial \{a\}}{\partial \{C\}}$

The governing equations, for the case of linear aerodynamics, are:

$$\begin{bmatrix} [K] - [A]\ \frac{\partial \{a\}}{\partial \{C\}} & [A]\ \frac{\partial \{a\}}{\partial \alpha} \\ \{L\}^T \left[\frac{\partial \{a\}}{\partial \{C\}} \right] & \{L\}^T\ \frac{\partial \{a\}}{\partial \alpha} \end{bmatrix} \begin{Bmatrix} C \\ \alpha \end{Bmatrix} = \begin{Bmatrix} 0 \\ \frac{nW}{2} \end{Bmatrix} \tag{2.18}$$

The left hand side matrix is identical to the sensivity matrix to be derived in the next chapter. If linear aerodynamics are to be used and a sensitivity analysis is desired, this result can result in a slight savings of computational effort over the iterative approach.

In order to get a feel for the performance of the aeroelastic system, the spanload was plotted at a couple of constant chord positions for both rigid and flexible wings. Figure 6 shows the spanload along the nodes closest to the leading edge of the wing. Figure 7 shows the spanload along a spanwise line approximately along the wing quarter chord. The differences between the flexible and rigid wings are small, indicating a rather stiff wing.

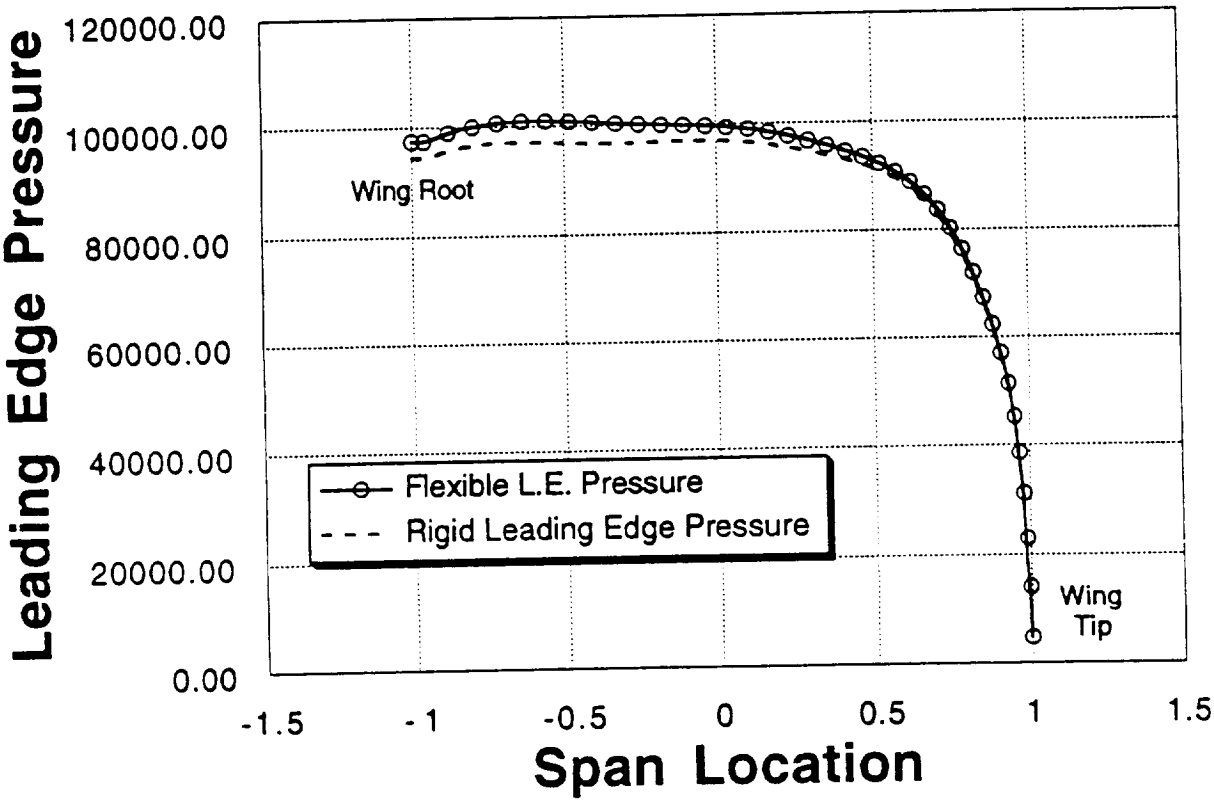

Figure 6. Pressure near Wing Leading Edge

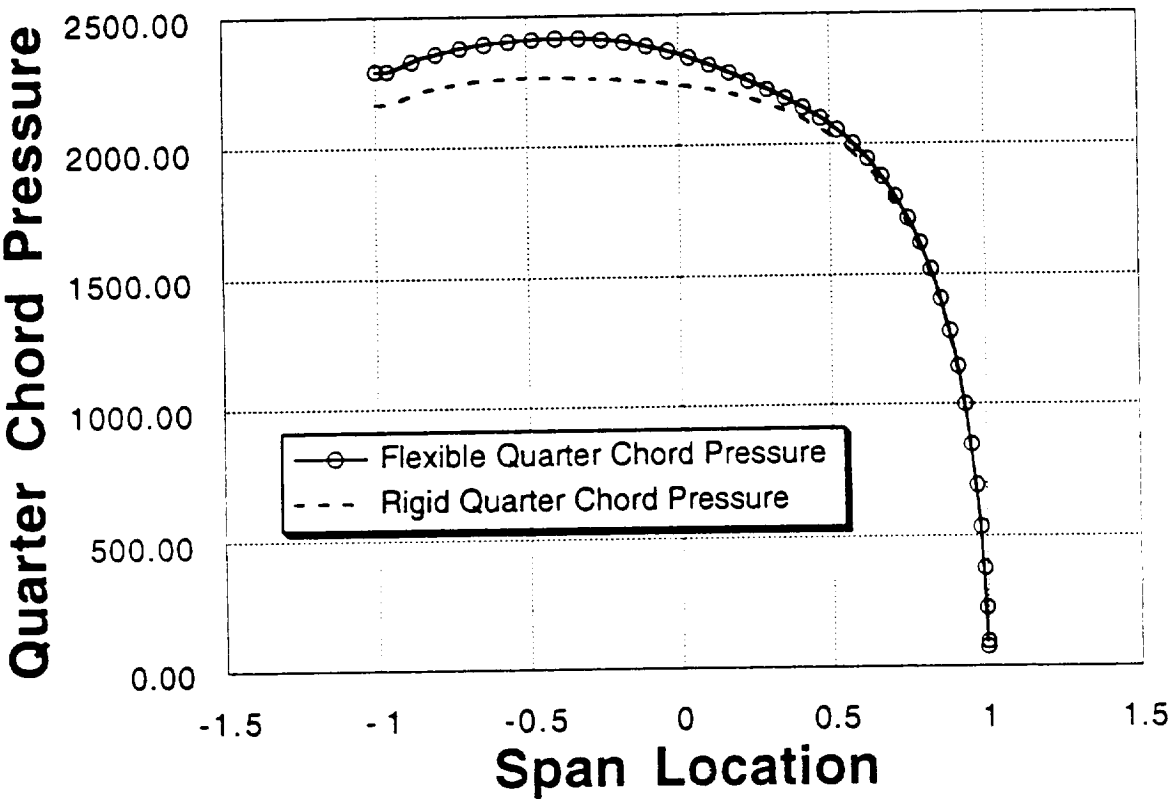

Figure 7. Pressure along Wing Quarter Chord

3.0 Senstitivity Equations

A scheme for determining the global sensitivities of the aeroelastic system to changes in shape parameters is developed. This scheme can be shown to be a variation of Sobieski's Global Sensitivity Equations. A variety of local sensitivity data is combined to produce global sensitivity results. Here, the term local sensitivity refers to the sensitivity of an item within a particular discipline, such as the sensitivity of the wing stiffness matrix to a change in wing sweep. Global sensitivities are dependent on the interaction of the disciplines. A global sensitivity example is the variation of wing deflected shape with respect to a change in wing taper ratio.

The goal of this analysis is to produce values for the global sensitivities dC/dr_l and $d\alpha/dr_l$. Here, r_l represents any of the wing shape parameters: area, aspect ratio, sweep, or taper ratio. Equations 2.1, 2.9, and 2.12 can be used to perform the shape sensitivity analysis of static aeroelastic response. In the following development $\partial()/\partial()$ indicates a local, single discipline, term and $d()/d()$ indicates a global or total derivative. Taking derivatives of the equilibrium and the trim equation, with respect to the shape variable r_l (namely sweep, aspect ratio, wing area, taper ratio), we obtain

$$[K]\{\frac{dC}{dr_l}\} + [\frac{dK}{dr_l}]\{C\} = \{\frac{dQ}{dr_l}\} \tag{3.1}$$

$$\frac{d(nW/2)}{dr_l} = \{\frac{\partial L}{\partial r_l}\}^T\{a\} + \{L\}^T\{\frac{da}{dr_l}\} = 0 \tag{3.2}$$

Note that the derivative of lift is zero, because we require the total lift acting on the wing to remain constant. Additionally, L is purely a function of geometry, so its partial derivative is the same as its total derivative.

The vector $\{dQ/dr_l\}$ can be obtained as

$$\frac{dQ_i}{dr_l} = \sum_{j=1}^{M}([\frac{\partial A_{ij}}{\partial r_l}]a^j + A_{ij}\frac{da^j}{dr_l}) \tag{3.3}$$

where

$$\frac{da^j}{dr_l} = \frac{\partial a^j}{\partial r_l} + \sum_{n=1}^{np}(\frac{\partial a^j}{\partial C_n}\frac{dC_n}{dr_l}) + \frac{\partial a^j}{\partial \alpha}\frac{d\alpha}{dr_l} \tag{3.4}$$

and where

$\partial a^j/\partial r_l$ is the local sensitivity of the aerodynamic generalized pressure coefficients and can be obtained while performing the aerodynamic analysis;

$\partial a^j/\partial C_n$ is the derivative of the generalized pressure coefficient with respect to a generalized displacement C_n, and

$d\alpha/dr_l$ is the derivative of the trim angle of attack with respect to r_l.

Note that the matrix [A] is also purely a function of geometry: thus its partial and total derivative are the same.

In matrix form, the global sensitivity of generalized forces becomes

$$\{\frac{dQ}{dr_l}\} = [\frac{\partial A}{\partial r_l}]\{a\} + [A]\{\frac{\partial a}{\partial r_l}\} + [A][\frac{\partial\{a\}}{\partial\{C\}}]\{\frac{dC}{dr_l}\} + \frac{d\alpha}{dr_l}[A]\{\frac{\partial a}{\partial \alpha}\} \tag{3.5}$$

It is noted that the major computational expense is the determination of $\partial\{a\}/\partial\{C\}$.

The sensitivity of generalized displacements, therefore, becomes (combining Eqs. 3.1 and 3.5)

$$\left[[K] - [A][\frac{\partial\{a\}}{\partial\{C\}}]\right]\{\frac{dC}{dr_l}\} = [\frac{\partial A}{\partial r_l}]\{a\} + [A]\{\frac{\partial a}{\partial r_l}\} + \frac{d\alpha}{dr_l}[A]\{\frac{\partial a}{\partial \alpha}\} - [\frac{dK}{dr_l}]\{C\} \tag{3.6}$$

In this equation, all the terms on the right hand side are known except for $d\alpha/dr_l$. This can be obtained by considering the sensitivity of the lift equation, Eq. 3.2. This equation can be written as:

$$\{\frac{\partial L}{\partial r_l}\}^T\{a\} + \{L\}^T\{\frac{\partial a}{\partial r_l}\} + \{L\}^T[\frac{\partial\{a\}}{\partial\{C\}}]\{\frac{dC}{dr_l}\} + \frac{d\alpha}{dr_l}\{L\}^T\{\frac{da}{d\alpha}\} = 0 \tag{3.7}$$

The required sensitivity derivatives can be then obtained by simultaneously solving the sets of eqns 3.6 and 3.7. With a little rearranging they become:

$$\begin{bmatrix} [K]-[A][\frac{\partial\{a\}}{\partial\{C\}}] & -[A]\{\frac{\partial\{a\}}{\partial\alpha}\} \\ \{L\}^T[\frac{\partial\{a\}}{\partial\{C\}}] & \{L\}^T\{\frac{\partial\{a\}}{\partial\alpha}\} \end{bmatrix} \begin{Bmatrix} \frac{d\{C\}}{dr_l} \\ \frac{d\alpha}{dr_l} \end{Bmatrix} = \begin{Bmatrix} [\frac{\partial A}{\partial r_l}]\{a\}+[A]\{\frac{\partial a}{\partial r_l}\}-[\frac{\partial K}{\partial r_l}]\{C\} \\ -\{\frac{\partial L}{\partial r_l}\}^T\{a\}-\{L\}^T\{\frac{\partial a}{\partial r_l}\} \end{Bmatrix} \quad (3.8)$$

Generating this left hand "sensitivity" matrix by finite differences is extremely computationally expensive. The term $\partial\{a\}/\partial\{C\}$ is particularly expensive. It requires calling the aerodynamic code one time for each element in the $\{C\}$ vector. The sensitivity matrix is valid for a particular base geometry, regardless of which r_l is of interest. It is only generated once and saved for future uses. The left hand sensitivity matrix may be used with a different right hand side to determine the converged wing aeroelastic response. This equation is given by Eqn 2.18.

$$\begin{bmatrix} [K]-[A][\frac{\partial\{a\}}{\partial\{C\}}] & -[A]\{\frac{\partial\{a\}}{\partial\alpha}\} \\ \{L\}^T[\frac{\partial\{a\}}{\partial\{C\}}] & \{L\}^T\{\frac{\partial\{a\}}{\partial\alpha}\} \end{bmatrix} \begin{Bmatrix} \{C\} \\ \alpha \end{Bmatrix} = \begin{Bmatrix} \{0\} \\ nW/2 \end{Bmatrix} \quad (2.18)$$

If a sensitivity calculation is to be performed as well, then this approach to determining the aeroelastic response is more efficient. If only the converged wing configuration is needed, the iterative approach is slightly better. The iterative approach is also more general; it can be directly applied to non-linear aerodynamic codes, whereas Eqn. 2.18 is only applicable for linear aerodynamics.

3.1 Comparison Between the Present Formulation and Sobieski's Global Sensitivities Equations (GSE)

In Ref. 18, Sobieski presented two different formulations (GSE1 and GSE2) to obtain the global sensitivities of a multi-disciplinary system in terms of the sensitivities of the

subsystems, called local sensitivities. It is of interest to compare the present formulation (Eq. 3.8) with Sobieski's Global Sensitivity Equations.

In terms of the Sobieski's first formulation, called GSE1, the governing equations for the wing can be written as:

Trim:

$$f_a = L^T(\{r_\ell\}, \alpha)\ \{a\} - \frac{nW}{2} = 0 \tag{3.10}$$

Aerodynamics:

$$\{f_a\ (\alpha,\ \{a\},\ \{C\})\} = \{0\} \tag{3.11}$$

Structures:

$$\{f_C\} = [K(r_\ell)]\{C\} - [A(r_\ell)]\{a\} = \{0\} \tag{3.12}$$

Then the GSE's are:

$$\begin{bmatrix} \frac{\partial f_a}{\partial \alpha} & \frac{\partial f_a}{\partial \{a\}} & \frac{\partial f_a}{\partial \{C\}} \\ \frac{\partial \{f_a\}}{\partial \alpha} & \frac{\partial \{f_a\}}{\partial \{a\}} & \frac{\partial \{f_a\}}{\partial \{C\}} \\ \frac{\partial \{f_C\}}{\partial \alpha} & \frac{\partial \{f_C\}}{\partial \{a\}} & \frac{\partial \{f_C\}}{\partial \{C\}} \end{bmatrix} \begin{Bmatrix} \frac{d\alpha}{dr_\ell} \\ \frac{d\{a\}}{dr_\ell} \\ \frac{d\{C\}}{dr_\ell} \end{Bmatrix} = - \begin{Bmatrix} \frac{\partial f_a}{\partial r_\ell} \\ \frac{\partial \{f_a\}}{\partial r_\ell} \\ \frac{\partial \{f_C\}}{\partial r_\ell} \end{Bmatrix} \tag{3.13}$$

or

$$\begin{bmatrix} 0 & \{L\}^T & 0 \\ \frac{\partial \{f_a\}}{\partial \alpha} & \frac{\partial \{f_a\}}{\partial \{a\}} & \frac{\partial \{f_a\}}{\partial \{C\}} \\ 0 & -[A] & [K] \end{bmatrix} \begin{Bmatrix} \frac{d\alpha}{dr_\ell} \\ \frac{d\{a\}}{dr_\ell} \\ \frac{d\{C\}}{dr_\ell} \end{Bmatrix} = - \begin{Bmatrix} \frac{\partial}{\partial r_\ell}\{L\}^T\{a\} \\ \frac{\partial \{f_a\}}{\partial r_\ell} \\ \frac{\partial}{\partial r_\ell}[K]\{C\} - \frac{\partial}{\partial r_\ell}[A]\{a\} \end{Bmatrix} \tag{3.14}$$

Note that, since $\{f_a\}$ is not directly accessable, the above form of the Sobieski's Global Sensitivity Equations could not be used.

In terms of Sobieski's GSE2 formulation, the governing equations, for the system at hand are:

Trim:

$$\alpha = \alpha\left(\{a\},\ r_\ell\right) \tag{3.15}$$

Aerodynamics:

$$\{a\} = \{a(\alpha,\ \{C\},\ r_\ell)\} \tag{3.16}$$

Structures:

$$\{C\} = [K(r_\ell)]^{-1}\ [A(r_\ell)]\ \{a\} \tag{3.17}$$

The global sensitivity equations are:

$$\begin{bmatrix} I & -\frac{\partial\alpha}{\partial\{a\}} & -\frac{\partial\alpha}{\partial\{C\}} \\ -\frac{\partial\{a\}}{\partial\alpha} & I & -\frac{\partial\{a\}}{\partial\{C\}} \\ -\frac{\partial\{C\}}{\partial\alpha} & -\frac{\partial\{C\}}{\partial\{a\}} & I \end{bmatrix} \begin{Bmatrix} \frac{d\alpha}{dr_\ell} \\ \frac{d\{a\}}{dr_\ell} \\ \frac{d\{C\}}{dr_\ell} \end{Bmatrix} = \begin{Bmatrix} \frac{\partial\alpha}{\partial r_\ell} \\ \frac{\partial\{a\}}{\partial r_\ell} \\ \frac{\partial\{C\}}{\partial r_\ell} \end{Bmatrix} \tag{3.18}$$

Using Eqs. 3.15 - 3.17, the above set of equations becomes

$$\begin{bmatrix} I & -\frac{\partial\alpha}{\partial\{a\}} & 0 \\ -\frac{\partial\{a\}}{\partial\alpha} & I & -\frac{\partial\{a\}}{\partial\{C\}} \\ 0 & -[K]^{-1}[A] & I \end{bmatrix} \begin{Bmatrix} \frac{d\alpha}{dr_\ell} \\ \frac{d\{a\}}{dr_\ell} \\ \frac{d\{C\}}{dr_\ell} \end{Bmatrix} = \begin{Bmatrix} 0 \\ \frac{\partial\{a\}}{\partial r_\ell} \\ \frac{\partial}{\partial r_\ell}\left[[K]^{-1}[A]\right]\{a\} \end{Bmatrix} \tag{3.19}$$

Since $\partial\alpha/\partial\{a\}$ cannot be found easily, this formulation could not be used. The first equation from 3.14 and the last two equations from 3.19 can be combinted to form a system as follows:

$$\begin{Bmatrix} \frac{\partial\{a\}}{\partial r_l} \\ \frac{\partial\{C\}}{\partial r_l} \\ \{\frac{\partial L}{\partial r_l}\}^T\{a\} \end{Bmatrix} = \begin{bmatrix} [I] & -[\frac{\partial\{a\}}{\partial\{C\}}] & -\frac{d\{a\}}{d\alpha} \\ -[K]^{-1}[A] & [I] & [0] \\ -\{L\}^T & 0 & 0 \end{bmatrix} \begin{Bmatrix} \frac{d\{a\}}{dr_l} \\ \frac{d\{C\}}{dr_l} \\ \frac{d\alpha}{dr_l} \end{Bmatrix} \tag{3.20}$$

For the current study, the global derivatives of $\{a\}$ aren't necessary, so eliminating the first line of 3.20 and rearranging it will give us equation 3.9. Thus, our formulation is a mix of GSE1 and GSE2.

3.2 Solving the System

The terms $[K]$,$[A]$,$\{a\}$,$\{C\}$, and $\{L\}$ are all quantities known from the converged baseline configuration. A finite difference technique is used to calculate the terms , $\partial\{a\}/\partial\alpha$, $\partial[K]/\partial r_l$, and $\partial\{a\}/\partial r_l$. The terms $\partial[A]/\partial r_l$ and $\partial\{L\}/\partial r_l$ are computed analytically. The terms $d\{C\}/dr_l$ and $d\alpha/dr_l$ are the unknowns found by solving this system of equations.

3.3 Derivatives of $[A]$ and $\{L\}$

These derivatives are calculated by using the chain rule and the derivatives of each of their elements. Each element's derivative will be reduced to derivatives of one of our coordinates (u, η, etc.). Thus, derivatives of these coordinates will be found first, then the derivatives of the elements will be found.

Coordinate Derivatives

u, v - **Local panel coordinates.** The panel based pressure interpolations discussed in chapters 5-7 use the coordinates u and v for on-panel coordinates. They are based on the gauss points on a particular panel. Thus, they don't change with our shape parameters.

$$\frac{du}{dr_l} = \frac{dv}{dr_l} = 0 \tag{3.21}$$

η, ξ - **Transformed wing coordinates** The square η, ξ $(-1, 1)$ planform doesn't change with wing geometry changes.

$$\frac{d\eta}{dr_l} = \frac{d\xi}{dr_l} = 0 \tag{3.22}$$

x, y - **True Planform Coordinates** These do change with wing geometry.

$$y = \frac{b}{2}(1+\eta) = \frac{1}{2}\sqrt{SAR}(1+\eta) \tag{3.23}$$

where b is the single-wing span, S is the single-wing area, and AR is the aspect ratio of the single-wing/

$$\frac{dy}{dS} = \frac{(1+\eta)}{4}\sqrt{\frac{AR}{S}} \tag{3.24}$$

$$\frac{dy}{dAR} = \frac{(1+\eta)}{4}\sqrt{\frac{S}{AR}} \tag{3.25}$$

$$\frac{dy}{d\Lambda} = \frac{dy}{d\lambda} = 0 \tag{3.26}$$

where λ is the wing taper ratio.

x is a function of the local chord length, so $\frac{dC_r}{dr_l}$ and $\frac{dC(y)}{dr_l}$ are derived first.

$$C_r = \frac{2S}{b(1+\lambda)} = \frac{2\sqrt{\frac{S}{AR}}}{1+\lambda} \tag{3.27}$$

$$\frac{dC_r}{dS} = \frac{1}{b(1+\lambda)} \tag{3.28}$$

$$\frac{dC_r}{dAR} = \frac{-1}{(1+\lambda)}\frac{1}{AR}\sqrt{\frac{S}{AR}} \tag{3.29}$$

$$\frac{dC_r}{d\Lambda} = 0 \tag{3.30}$$

$$\frac{dC_r}{d\lambda} = \frac{-2}{(1+\lambda)^2}\sqrt{\frac{S}{AR}} \tag{3.31}$$

$$C(y) = C_r\left[1 - \frac{1}{2}(1-\lambda)(1+\eta)\right] \tag{3.32}$$

where $C(y)$ is the local chord length as a function of the span-wise coordinate, y.

$$\frac{dC(y)}{dS} = \frac{dC_r}{dS}\frac{C(y)}{C_r} \tag{3.33}$$

$$\frac{dC(y)}{dAR} = \frac{dC_r}{dAR}\frac{C(y)}{C_r} \tag{3.34}$$

$$\frac{dC(y)}{d\Lambda} = \frac{dC_r}{d\Lambda}\frac{C(y)}{C_r} = 0 \tag{3.35}$$

$$\frac{dC(y)}{d\lambda} = \frac{dC_r}{d\lambda}\frac{C(y)}{C_r} + \frac{C_r}{2}(1+\eta) \tag{3.36}$$

Now, back to x:

$$x = \left(\frac{1+\xi}{2} - \frac{1}{4}\right)C(y) + y\tan\Lambda \tag{3.37}$$

$$\frac{dx}{dS} = \left(\frac{1+\xi}{2} - \frac{1}{4}\right)\frac{dC(y)}{dS} + \frac{dy}{dS}\tan\Lambda \tag{3.38}$$

$$\frac{dx}{dAR} = \left(\frac{1+\xi}{2} - \frac{1}{4}\right)\frac{dC(y)}{dAR} + \frac{dy}{dAR}\tan\Lambda \tag{3.39}$$

$$\frac{dx}{d\Lambda} = \frac{y}{\cos^2 \Lambda} \tag{3.40}$$

$$\frac{dx}{d\lambda} = \left(\frac{1+\xi}{2} - \frac{1}{4}\right) \frac{dC(y)}{d\lambda} + \frac{dy}{d\lambda} \tan \Lambda \tag{3.41}$$

w_x, w_y - **Gauss weights.** These don't change with respect to geometry.

$\gamma_i(x,y)$ - **Generalized mode shapes.** As given in equation 2.5.

$$\gamma_i(x,y) = \left(\frac{x}{x_{max}}\right)^m \left(\frac{y}{y_{max}}\right)^n \tag{3.42}$$

where $m = 0$ to mw and $n = 2$ to $nw + 2$. N is looped over first. Thus,

$$\gamma_1(x,y) = \left(\frac{x}{x_{max}}\right)^0 \left(\frac{y}{y_{max}}\right)^2 \tag{3.43}$$

$$\gamma_2(x,y) = \left(\frac{x}{x_{max}}\right)^0 \left(\frac{y}{y_{max}}\right)^3 \tag{3.44}$$

If $m = 0$,

$$\frac{d\gamma}{dr_l} = \frac{n y^{n-1}}{y_{max}^n} \frac{dy}{dr_l} \tag{3.45}$$

otherwise ($m \neq 0$),

$$\frac{d\gamma}{dr_l} = \frac{x^{m-1} y^{n-1}}{x_{max}^m y_{max}^n} \left[my \frac{dx}{dr_l} + nx \frac{dy}{dr_l} \right] \tag{3.46}$$

J_1 - **First Jacobian.** The Jacobian of the x, y to η, ξ coordinate transformation is

$$J_1 = \frac{S}{4}\left(1 - \eta\frac{(1-\lambda)}{(1+\lambda)}\right) \tag{3.47}$$

Then,

$$\frac{dJ_1}{dS} = \frac{1}{4}\left(1 - \eta\frac{(1-\lambda)}{(1+\lambda)}\right) - \frac{S}{4}\frac{(1-\lambda)}{(1+\lambda)}\frac{d\eta}{dS} \tag{3.48}$$

recalling that $\frac{d\eta}{dr_i} = 0$ we get

$$\frac{dJ_1}{dS} = \frac{J_1}{S} \tag{3.49}$$

$$\frac{dJ_1}{dAR} = 0 \tag{3.50}$$

$$\frac{dJ_1}{d\Lambda} = 0 \tag{3.51}$$

$$\frac{dJ_1}{d\lambda} = \frac{S\eta}{2(1+\lambda)^2} \tag{3.52}$$

J_2 - **Second Jacobian.** The panel based interpolation schemes discussed in chapters 5-7 use rectangular sub-sections of the square η, ξ wing defined such that the local corrdinates $(u, v) = (-1, 1)$ The Jacobian of the η, ξ to u, v coordinate transformation is

$$J_2 = \frac{S_{\eta,\xi}}{S_{u,v}} \tag{3.53}$$

where $S_{\eta,\xi}$ is the panel area measured in the (η, ξ) system and $S_{u,v}$ is the panel area measured in the (u, v) system which always equals 4.

The derivatives of J_2 are

$$\frac{dJ_2}{dr_l} = 0. \tag{3.54}$$

3.4 Deflection Sensitivities

These results can be used to calculate a variety of other useful results. For instance, equation (2.4) can be differentiated and combined with the equations in section 3.4 to produce the sensitivity of the deflection of any point of the wing to changes in the shape parameters. Recalling

$$W(x,y) = \sum_{i=1}^{np} \gamma_i(x,y) C_i \tag{3.55}$$

with

$$\gamma_i(x,y) = (\frac{x}{x_{max}})^m (\frac{y}{y_{max}})^n \tag{3.56}$$

where m varies from 0 to mw and n varies from 2 to $nw+2$ with n varying more rapidly than m. Then

$$\frac{dW(x,y)}{dr_l} = \sum_{m=0}^{mw} \sum_{n=2}^{nw+2} \left\{ \frac{dc_i}{dr_l} \left[\frac{x}{x_{max}}\right]^m \left[\frac{y}{y_{max}}\right]^n \right.$$

$$\left. + \frac{mc_i}{x_{max}} \left[\frac{x}{x_{max}}\right]^{m-1} \left[\frac{y}{y_{max}}\right]^n \frac{dx}{dr_l} + \frac{nc_i}{y_{max}} \left[\frac{x}{x_{max}}\right]^m \left[\frac{y}{y_{max}}\right]^{n-1} \frac{dy}{dr_l} \right\} \tag{3.57}$$

4.0 Chebyshev Pressure Representation

The wing pressure field is represented first by a tensor product of Chebyshev polynomials. They were chosen for their ability to accurately fit a curve with a small number of terms, due to their orthogonality properties. The pressure distribution can thus be written

$$p(\eta,\xi) = \sum_{q=0}^{Q}\sum_{p=0}^{P} a_{pq} T_p(\eta) T_q(\xi) \tag{4.1}$$

Here T_p is the Chebyshev polynomial of order p.

$$T_p(x) = cos(ncos^{-1}(x)) \tag{4.2}$$

Thus,

$$T_0(x) = 1, \tag{4.3}$$

$$T_1(x) = x, \tag{4.4}$$

$$T_2(x) = 2x^2 - 1, \tag{4.5}$$

and in general

$$T_{n+1} = 2xT_n(x) - T_{n-1}(x). \tag{4.6}$$

A quick comparison of Eqns. 4.1 and 2.9 shows that the generic β^j is

$$\beta^j(\eta,\xi) = T_p(\eta) T_q(\xi) \tag{4.7}$$

4.1 Chebyshev Results

The aeroelastic code does an excellent job of calculating the converged wing loading and deflections for a particular flight condition. The sensitivity derivative calculations do

an excellent job of predicting shape sensitivities. Slight difficulty has been encountered in the exact calculation of derivatives with very small values. It was modeled structurally using a box beam model detailed in Ref. 10. The material properties were $E_{11} = E_{22} = 6.89 \times 10^{10}$, $G_{12} = 2.65 \times 10^{10}$, and $\nu_{12} = 0.3$.

The behavior of the chebyshev aerodynamic coeffients, a, are of interest because several perturbed runs of the program are needed to produce finite difference derivatives for later use by the sensitivity program. As Figures 8-9 show, the overall trend of these aerodynamic coefficients is smooth, but with significant sharp "wiggle" in these curves. This wiggle makes accurate finite differencing problematical on the affected a's. These curves are the worst cases; many of the other curves are much smoother.

To overcome this problem, a higher-order finite difference scheme using a large step size was used. This scheme

$$f'(x) \approx \frac{1}{12h}[f(x-2\Delta x) - 8f(x-\Delta x) + 0f(x) + 8f(x+\Delta x) - f(x+2\Delta x)] \qquad (4.8)$$

has an accuracy of $O(\Delta x^4)$.

Note, these figures are for single elements of the sixty element $\{a\}$ vector. These graphs can be used to estimate the best step size for a single element, but not for the entire vector. In an attempt to discover an optimal step size to maximize the accuracy of the vector as a whole, the L-2 norm of the difference between two finite differences was minimized. In this case, for each of a wide variety of step sizes, a forward and central first derivative finite difference was calculated with the central difference used as a reference. The logarithm of the average of the square of the difference of these two values was plotted. The step size that produced the minimum difference was chosen as our optimal step size for use in eqn. 4.7. Note, this is not in any way a percentage error, but instead the average absolute squared error. Figure 10 shows the variation of this pseudo-error with step size in α and aspect ratio. Similar curves were generated for the other three r_l's.

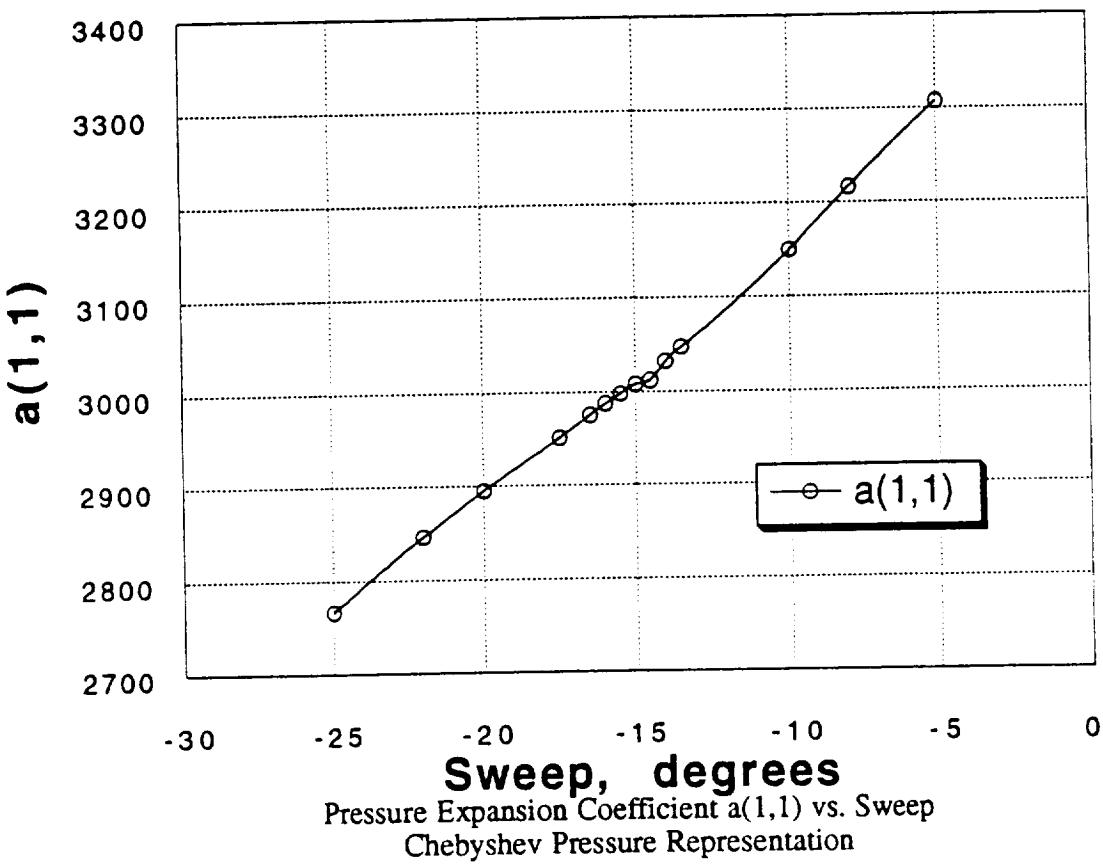

Figure 8. Pressure Expansion Coefficient a(1,1) vs. Sweep

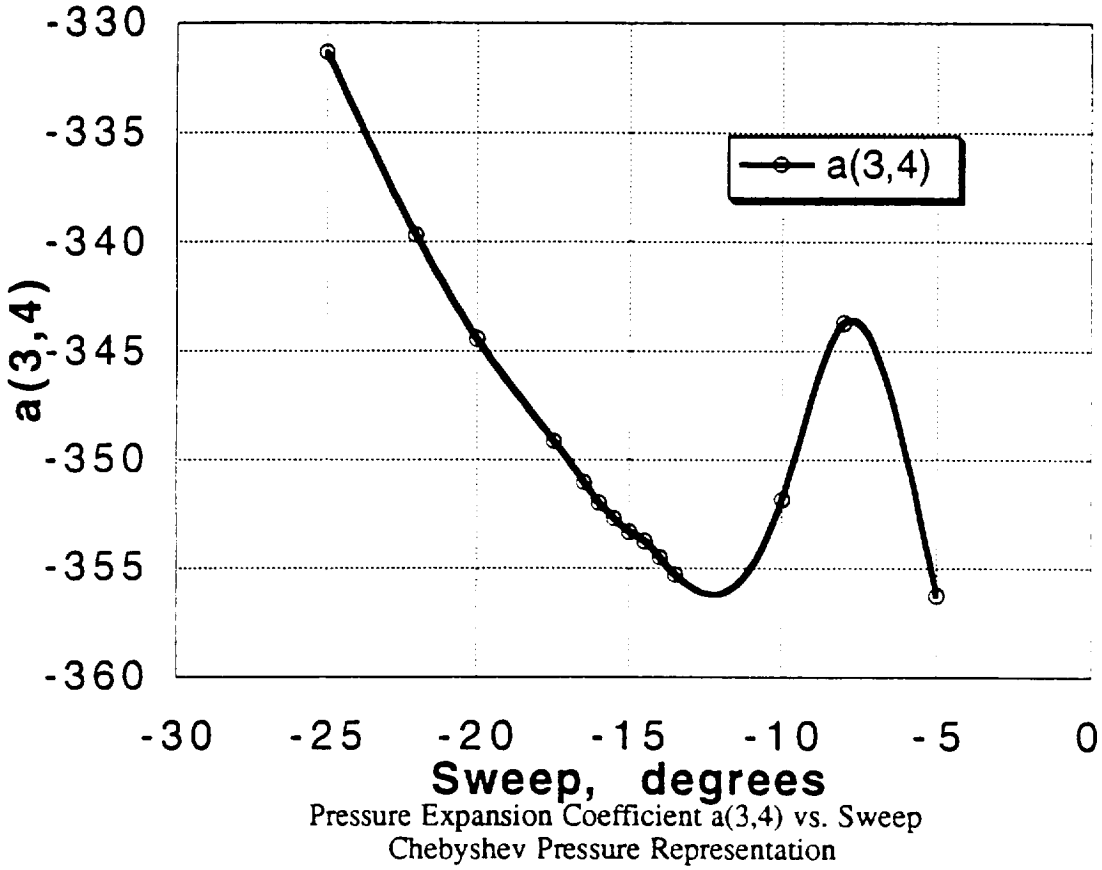

Figure 9. Pressure Expansion Coefficient a(3,4) vs. Sweep

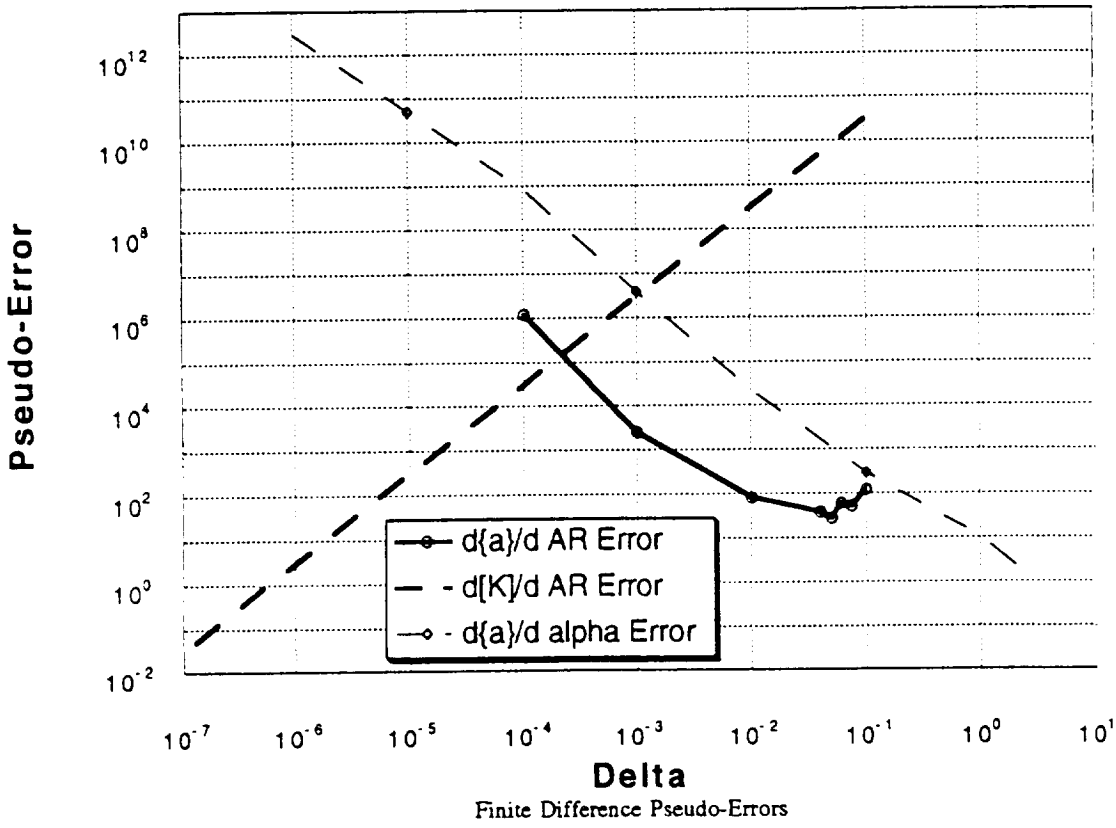

Finite Difference Pseudo-Errors

Figure 10. Finite Difference Pseudo-Errors

The individual deflection coefficients, C, show some wiggle, similar to the aerodynamic terms, but the effect is much smaller. Since these derivatives are only used to confirm the sensitivity results, a step size study was less important. Nevertheless, one was performed to insure that these derivatives would be as accurate as possible.

Derivatives of the stiffness matrix are also calculated by finite difference for use in the sensitivity code. A step size study identical to the aerodynamic code study was undertaken. While the term "L-2 Norm" is not strictly accurate for a matrix operation, the process was the same. The difference between each term of a central and a forward differenced derivative was squared and summed. The behavior of this pseudo-error measurement is also plotted in Figure 10. The optimal step size was used by a central difference in the actual sensitivity calculation.

The variation of the trim angle of attack with respect to the wing area is shown in Figure 11. The solid line shows the converged results from the iterative aerodynamic and structures combination. The various dashed lines show the variation predicted by the sensitivity derivatives at the different base configurations. The prediction goes through the converged value at the base geometry and is linear with a slope equal to the sensitivity derivative. The desired result is for this line to be tangent to the converged data curve.

Similarly, the sensitivity of the trim angle of attack to changes in the wing aspect ratio is shown in Figure 12. The solid line shows the converged iterative results and the dashed lines show the predicted variation by having a slope equal to the calculated sensitivity derivative.

Figures 13 and 14 show the converged and predicted values for the angle of attack variation with respect to taper ratio and sweep. It is obvious from Fig. 7 that the obtained value of the sensitivity of the angle of attack with respect to the taper ratio is not very accurate corresponding to the taper ratio values of 0.5 and 0.8. However, note that the value of the converged angle of attack is almost insensitive to the variation in taper ratio at those values of taper ratio. The inaccuracy in the present results can be attributed to the numerical problems associated with determining derivatives that are almost zero.

Also of interest are deflection sensitivities. Figures 15-18 show the predicted and

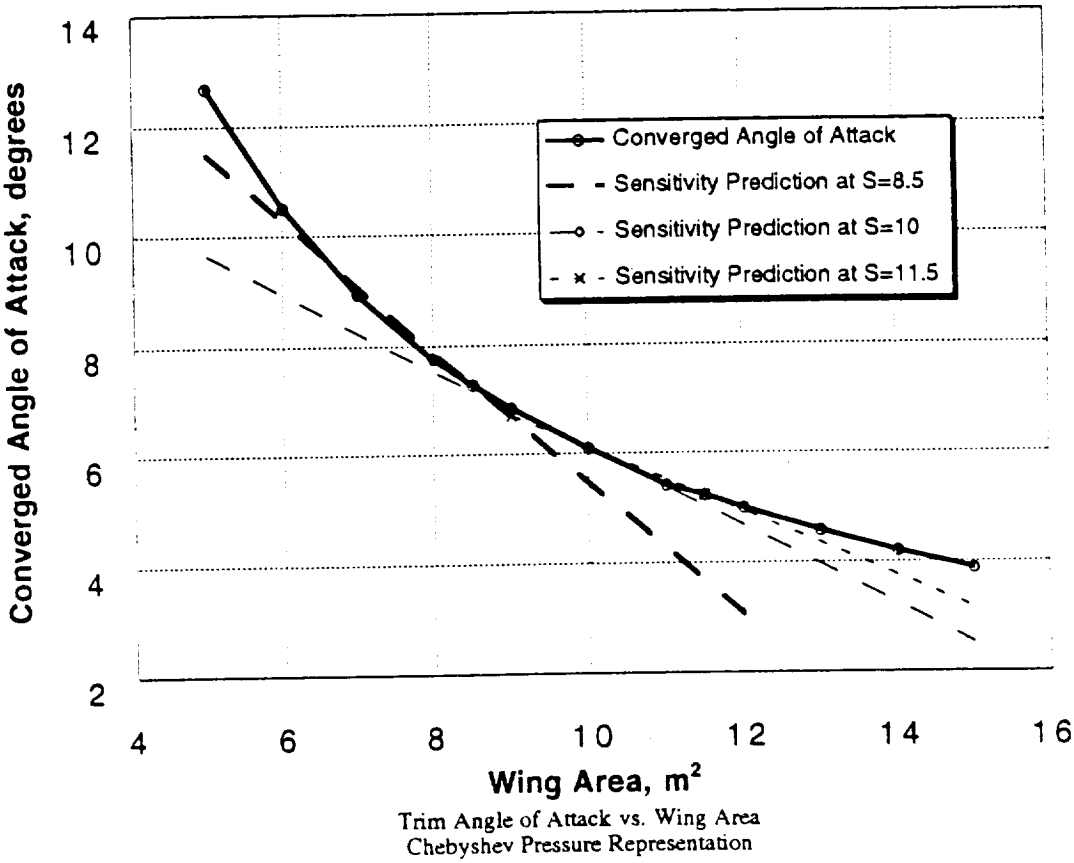

Trim Angle of Attack vs. Wing Area
Chebyshev Pressure Representation

Figure 11. Trim Angle of Attack vs. Wing Area, Chebyshev Pressure Representation

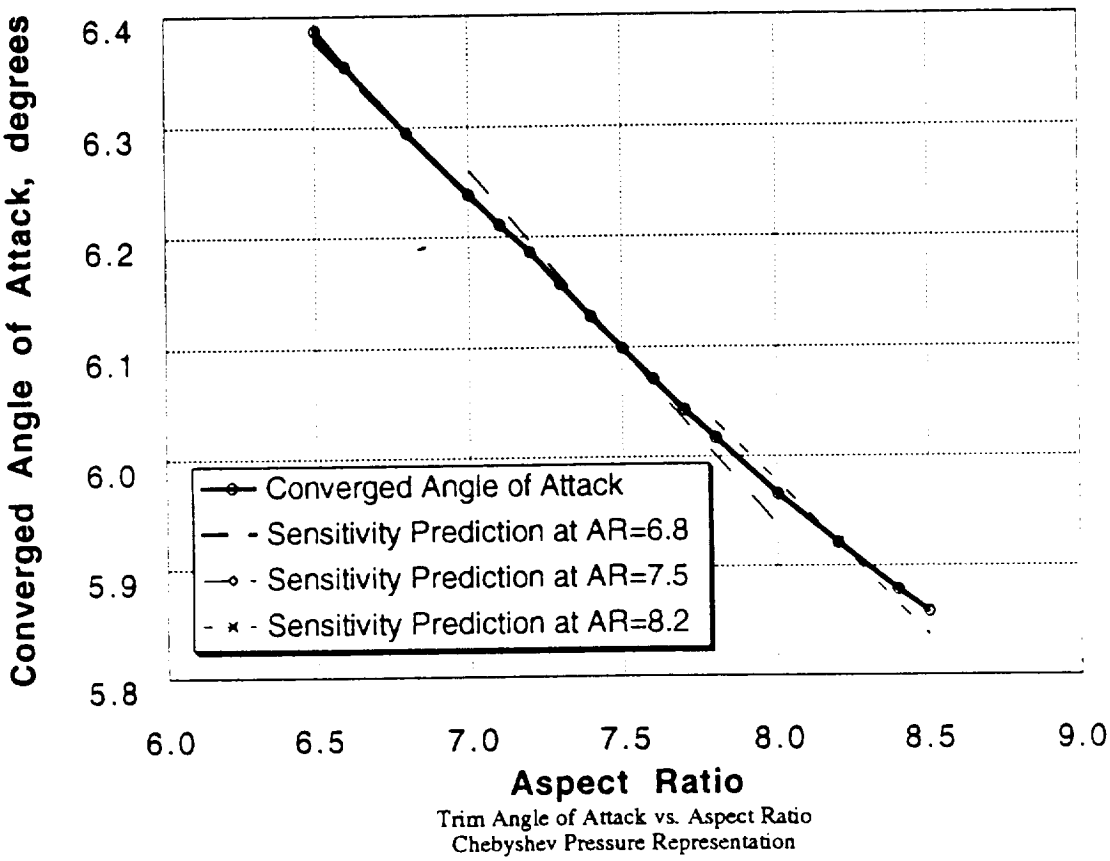

Figure 12. Trim Angle of Attack vs. Wing Aspect Ratio, Chebyshev Pressure Representation

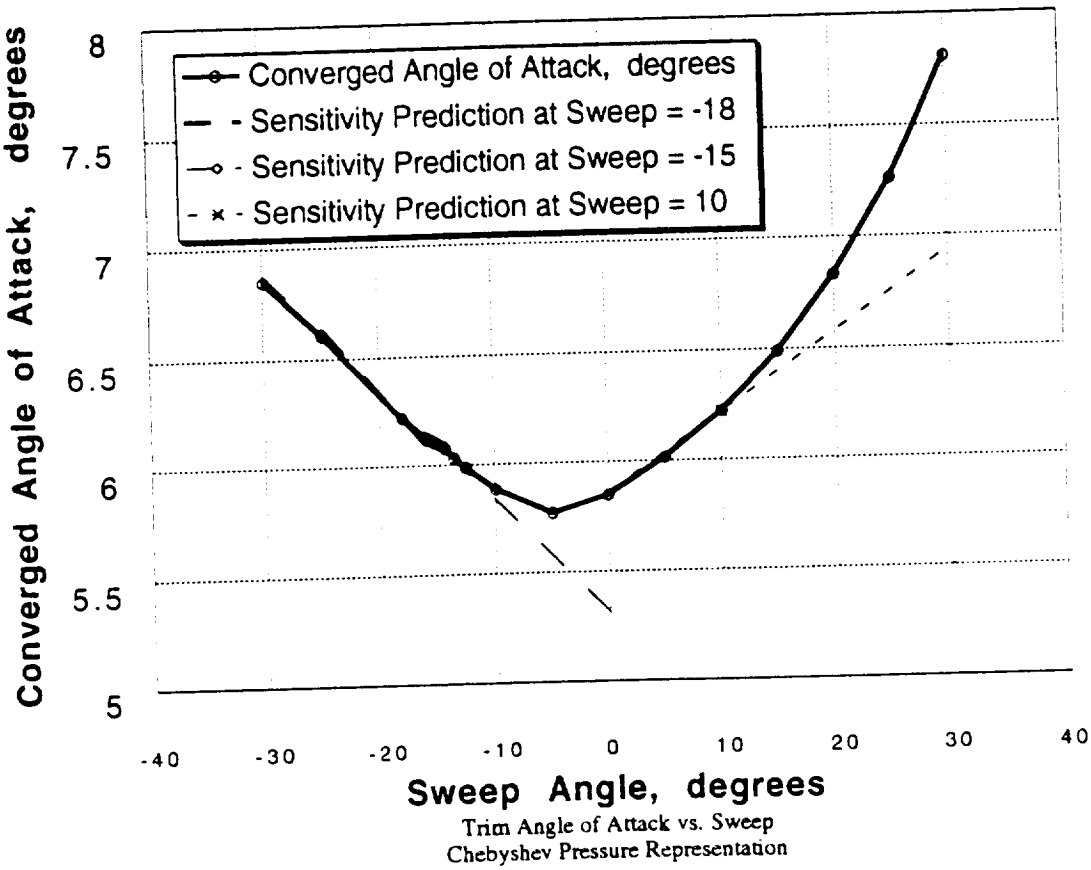

Figure 13. Trim Angle of Attack vs. Wing Sweep, Chebyshev Pressure Representation

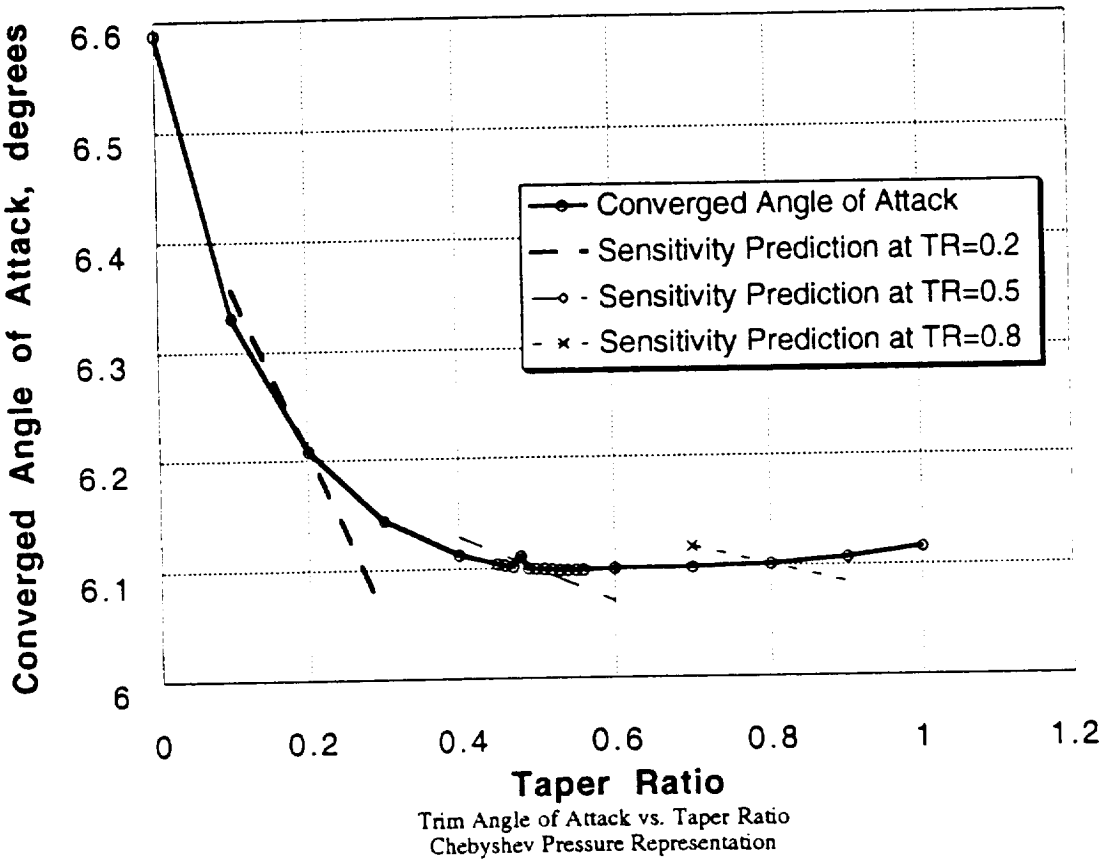

Trim Angle of Attack vs. Taper Ratio
Chebyshev Pressure Representation

Figure 14. Trim Angle of Attack vs. Wing Taper Ratio, Chebyshev Pressure Representation

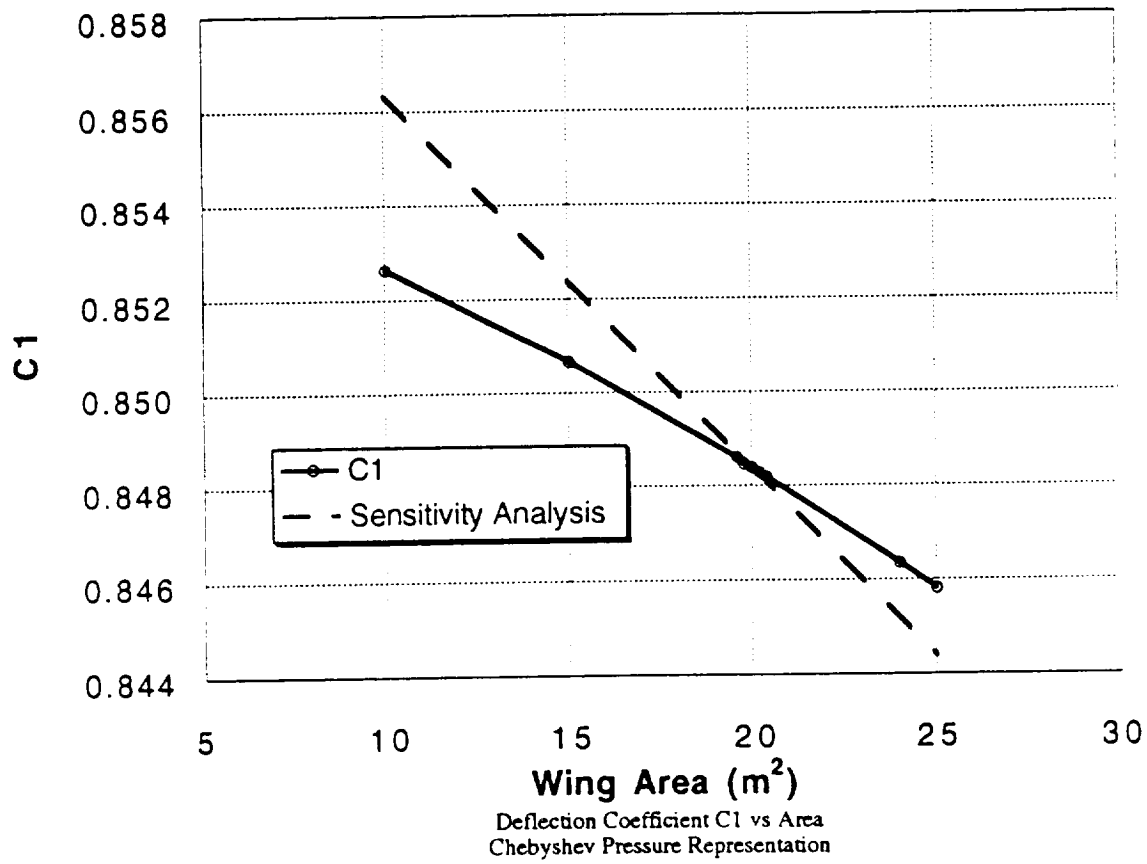

Figure 15. Deflection Coefficient C1 vs. Wing Area, Chebyshev Pressure Representation

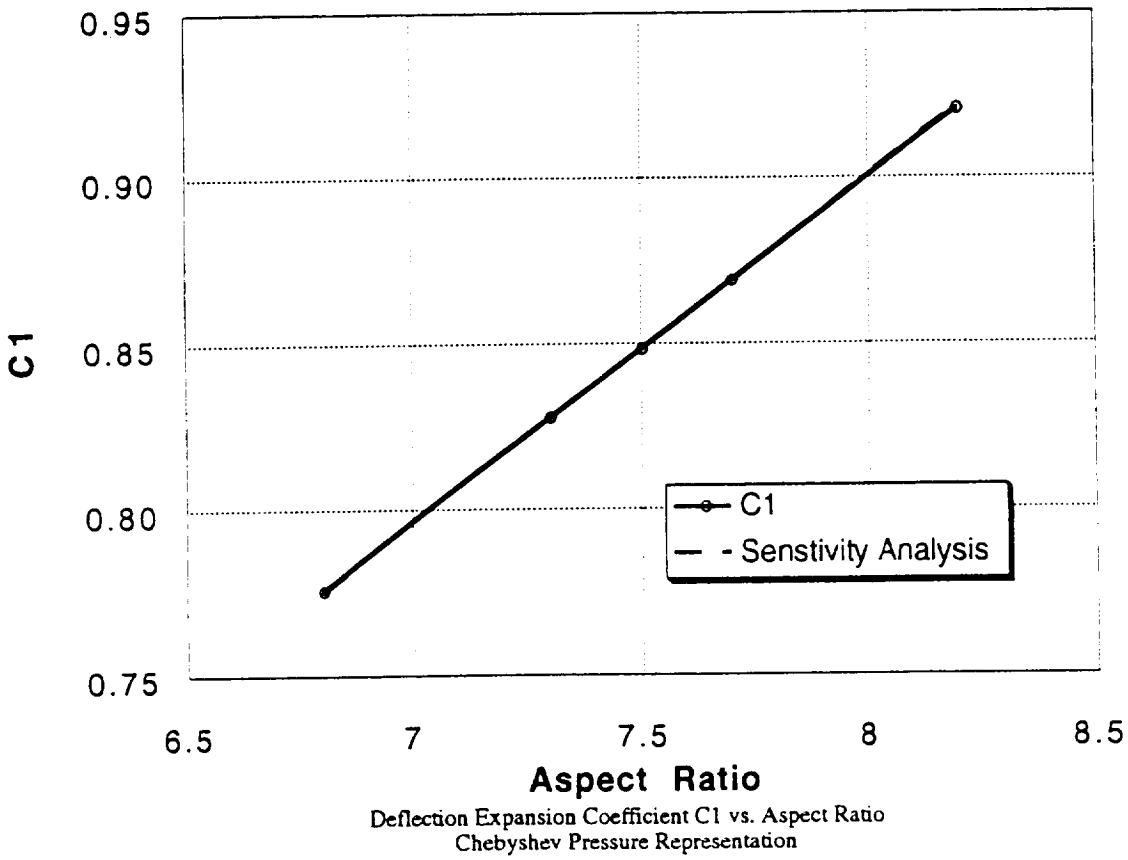

Figure 16. Deflection Coefficient C1 vs. Wing Aspect Ratio, Chebyshev Pressure Representation

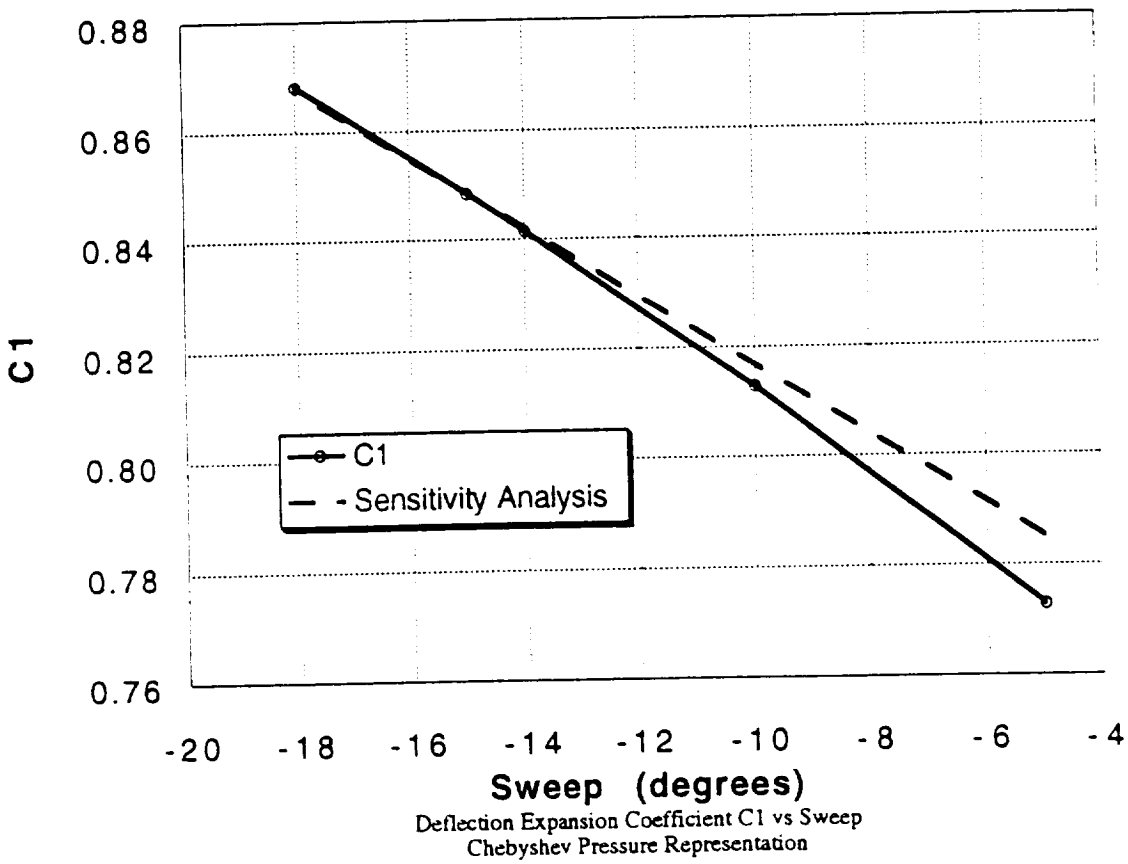

Figure 17. Deflection Coefficient C1 vs. Wing Sweep, Chebyshev Pressure Representation

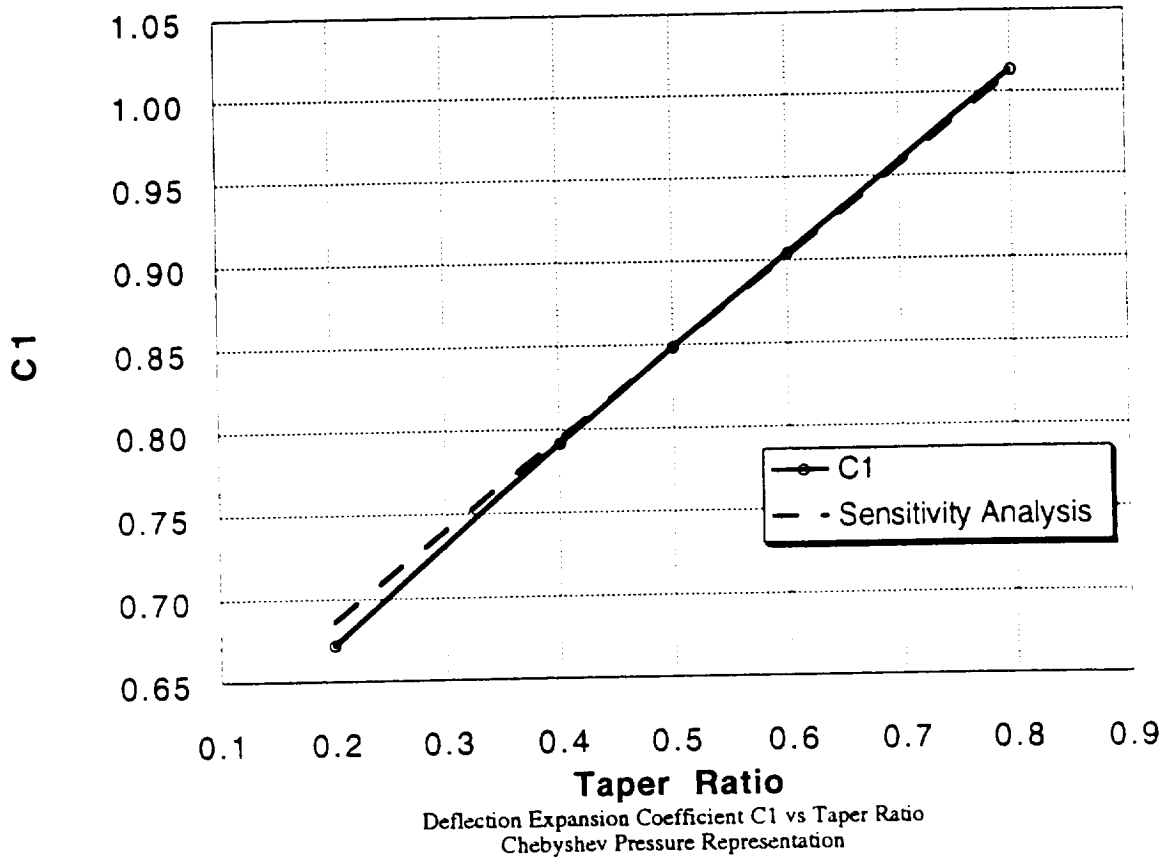

Figure 18. Deflection Coefficient C1 vs. Wing Taper Ratio, Chebyshev Pressure Representation

actual variation of a few of the deflection expansion coefficients. Figure 15 is the worst of all of the plots in this report. Note the relative scaling of the axes in this plot. The sensitivity is very near zero. Perhaps more important is the sensitivity of the deflections themselves. Figures 19-22 show the sensitivity of the leading edge tip deflection (measured in meters). The sensitivity of the coefficient C_1 with respect to wing area is not very accurate (see Fig. 15) as C_1 is almost insensitive to the variation in the wing area. The inaccuracies obtained in calculating this sensitivity do not however affect the sensitivity of the tip deflection with respect to wing area. This can be observed in Fig. 17. From Figs. 17-20 it is clear that the present formulation yields very accurate shape sensitivities for the aeroelastic tip deflections and can be used in optimization studies. The coefficient errors largely disappear in the integrated quantities.

Table 1: Comparison of Finite Difference and Analytic Logarithmic Derivatives

Term	*Finite Difference*	*Analytic*	*% Error*
$\frac{d\alpha}{dS}$	-1.188194	-1.129775	4.917
$\frac{d\alpha}{dAR}$	-0.366320	-0.463287	29.906
$\frac{d\alpha}{d\lambda}$	$-1.85613\text{x}10^{-2}$	$-2.40882\text{x}10^{-2}$	29.777
$\frac{d\alpha}{d\Lambda}$	0.098611	0.126455	28.236
$\frac{dc_1}{dS}$	$-5.83136\text{x}10^{-4}$	$-9.77324\text{x}10^{-3}$	40.333
$\frac{dc_1}{dAR}$	0.122537	0.123591	0.8581
$\frac{dc_1}{d\lambda}$	0.332564	0.329906	-3.957
$\frac{dc_1}{d\Lambda}$	0.122932	0.112007	-8.887
$\frac{dTipDef}{dS}$	0.984423	0.978191	0.2812
$\frac{dTipDef}{dAR}$	1.888806	1.916328	1.457
$\frac{dTipDef}{d\lambda}$	0.273598	0.265756	2.866
$\frac{dTipDef}{d\Lambda}$	0.262560	0.258709	1.467

These errors are largely numerical in origin. Variables with very small logarithmic derivatives will be difficult to differentiate numerically regardless of the scheme used[21]. Table 1 shows a variety of variables, their logarithmic derivatives, and the error in calculating them. As can be seen from the table, some of the intermediate results with very low logarithmic derivatives show as much as a 40% error. However, sensitivities of the final

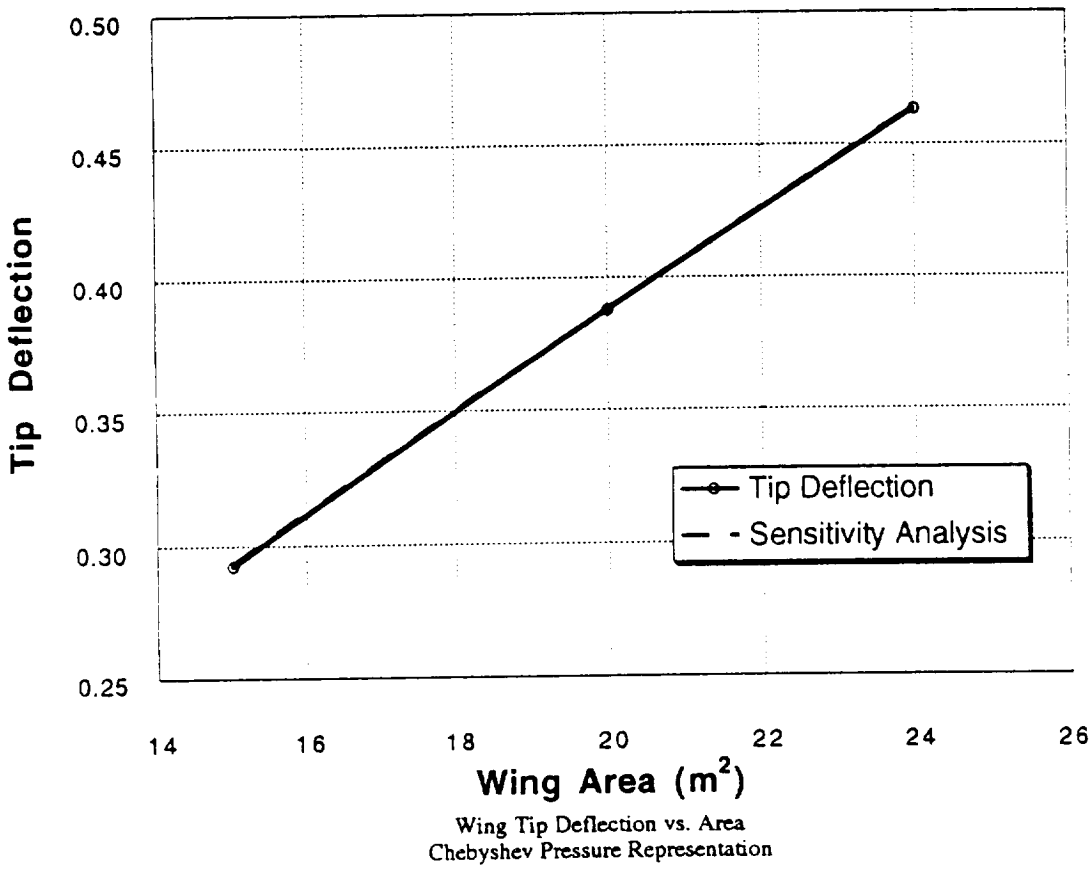

Wing Tip Deflection vs. Area
Chebyshev Pressure Representation

Figure 19. Tip Deflection vs. Wing Area, Chebyshev Pressure Representation

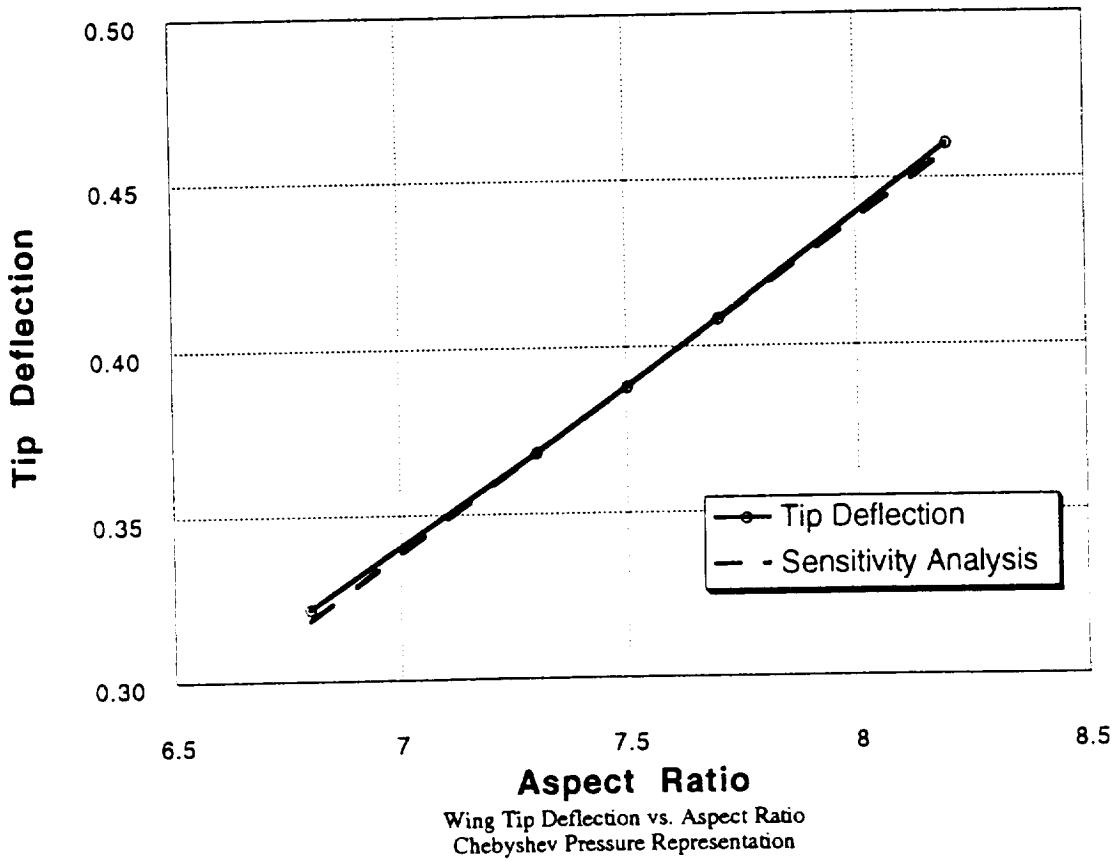

Figure 20. Tip Deflection vs. Wing Aspect Ratio, Chebyshev Pressure Representation

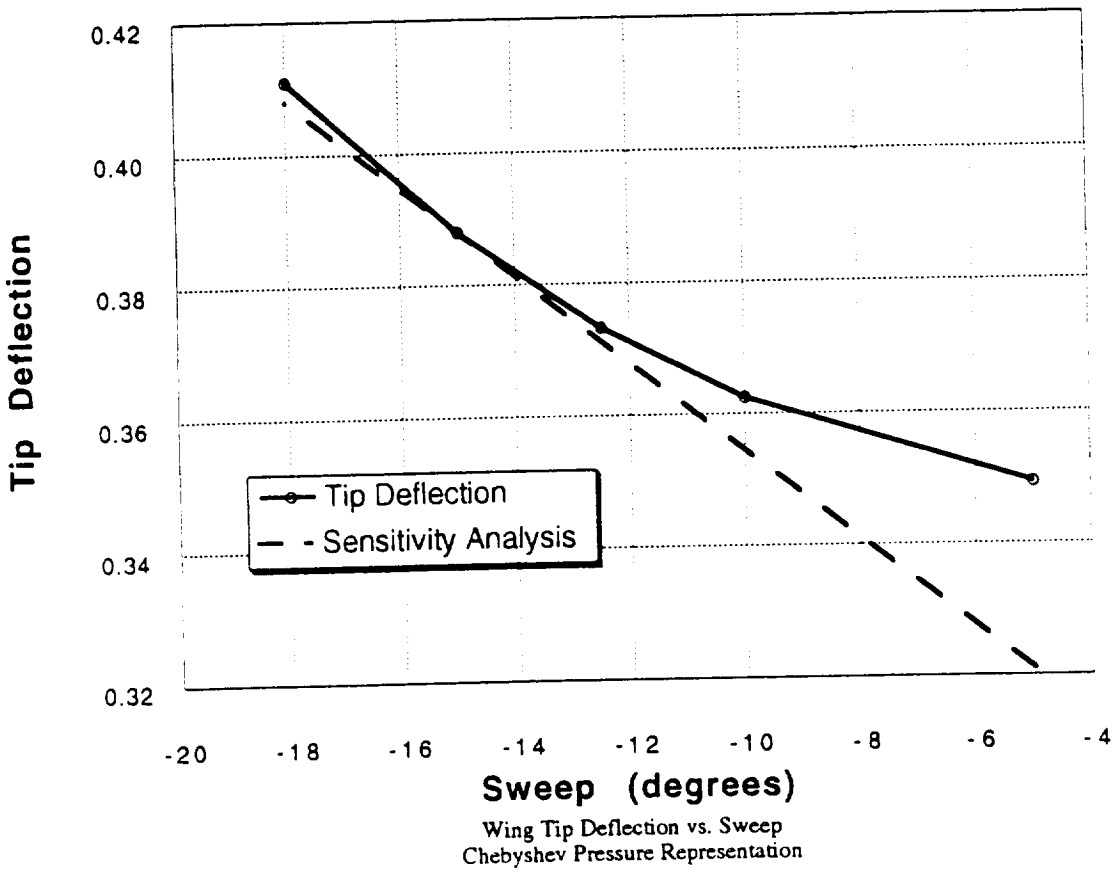

Figure 21. Tip Deflection vs. Wing Sweep, Chebyshev Pressure Representation

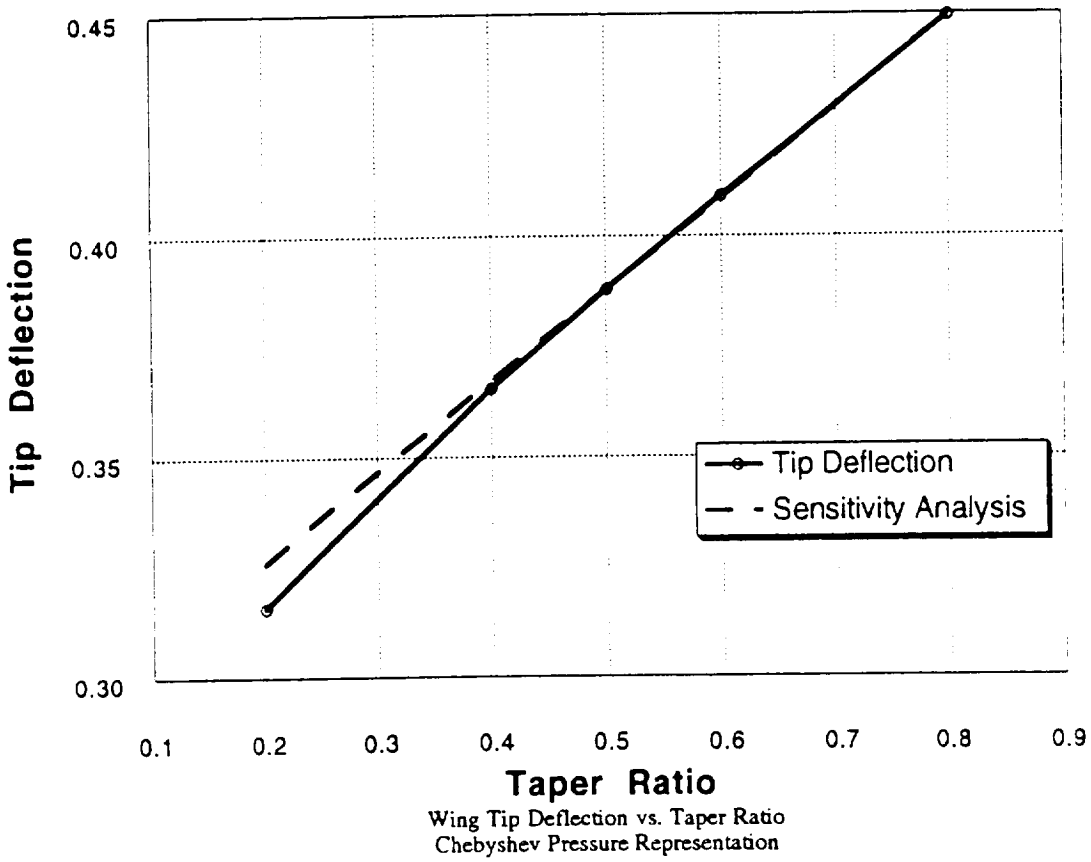

Figure 22. Tip Deflection vs. Wing Taper Ratio, Chebyshev Pressure Representation

integrated tip deflection results show a maximum of a 3% error.

The results show good accuracy for integrated quantities such as tip displacements but less accuracy for individual displacement coefficients or trim angle of attack. In general, the accuracy decreases noticably when the size of the derivative decreases.

The global sensitivities of the aerodynamic coeffients were also studied. Equation 3.4 was used to calculate these sensitivities. As with the deflection coefficient sensitivities, it was difficult to accurately model the sensitivities of individual coefficients. A wide variety of coefficients were examined for each of the four shape parameters. Figures 23-30 are representative of the overall results. Figures 23-24 show the mediocre modeling of da/dS. The similarly bad modeling of da/dAR is shown in figures 25-26. Despite more eratic behavior in the variation of the a's with respect to sweep and taper, the modelings of $da/d\Lambda$ and $da/d\lambda$ are much better. These are shown in figures 27-28 and 29-30 respectively.

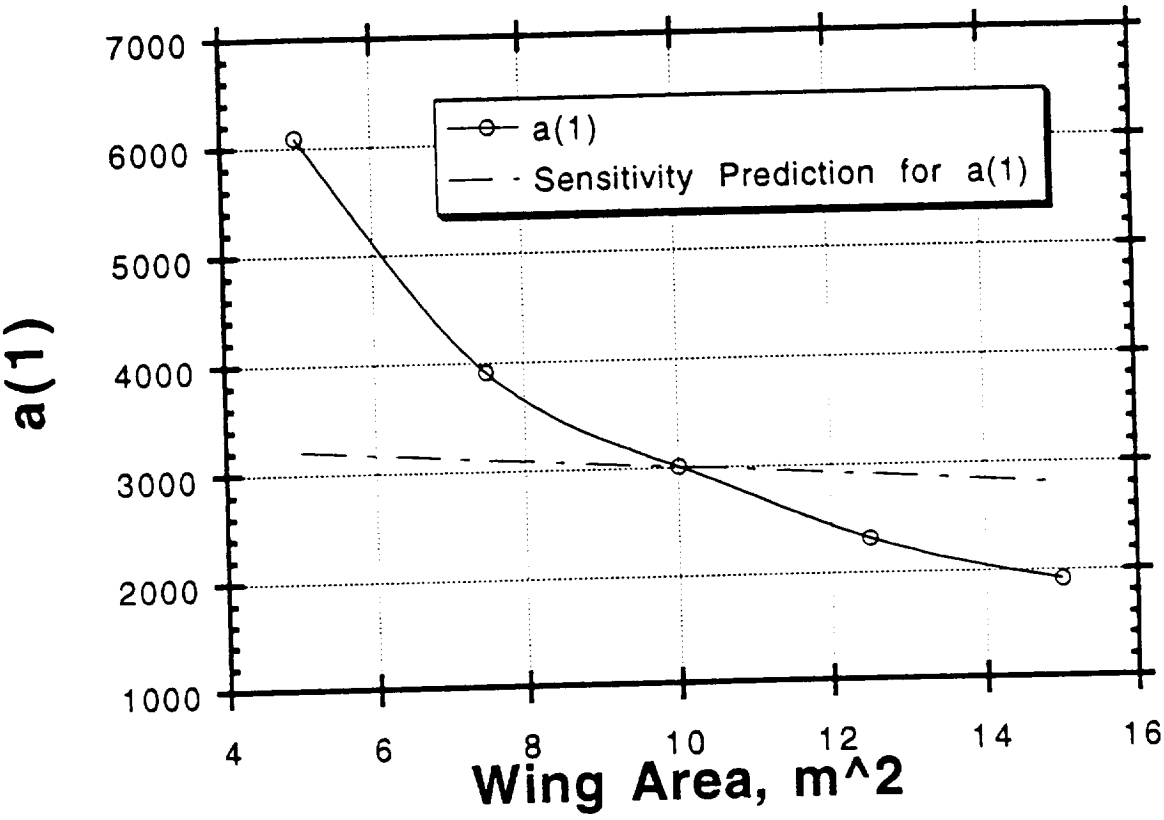

Figure 23. a(1) vs. Wing Area, Chebyshev Pressure Representation

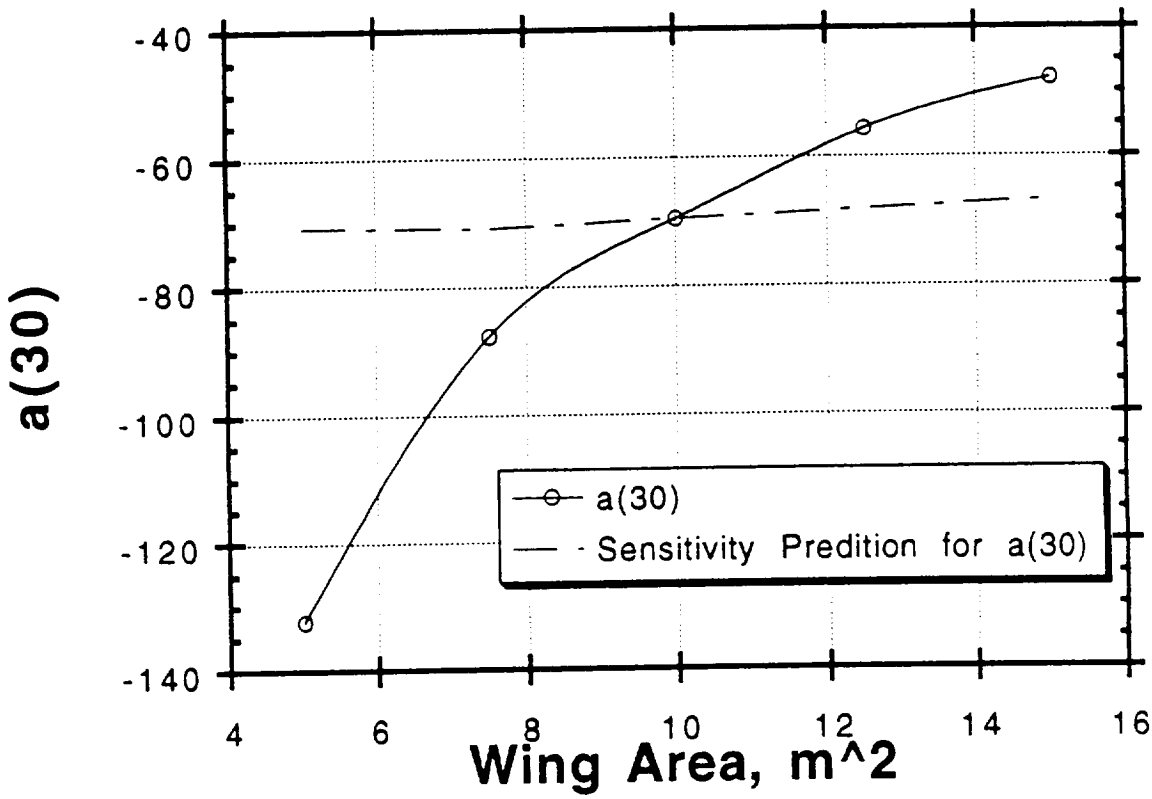

Figure 24. a(30) vs. Wing Area, Chebyshev Pressure Representation

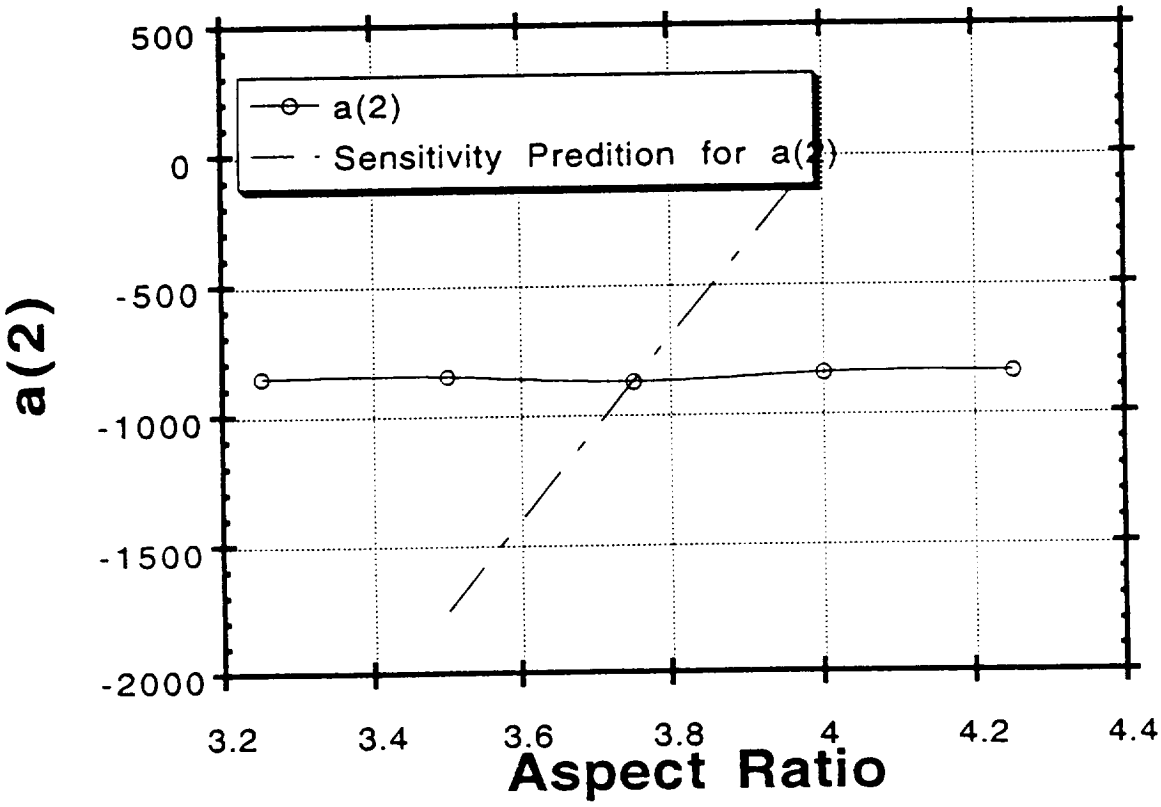

Figure 25. a(2) vs. Aspect Ratio, Chebyshev Pressure Representation

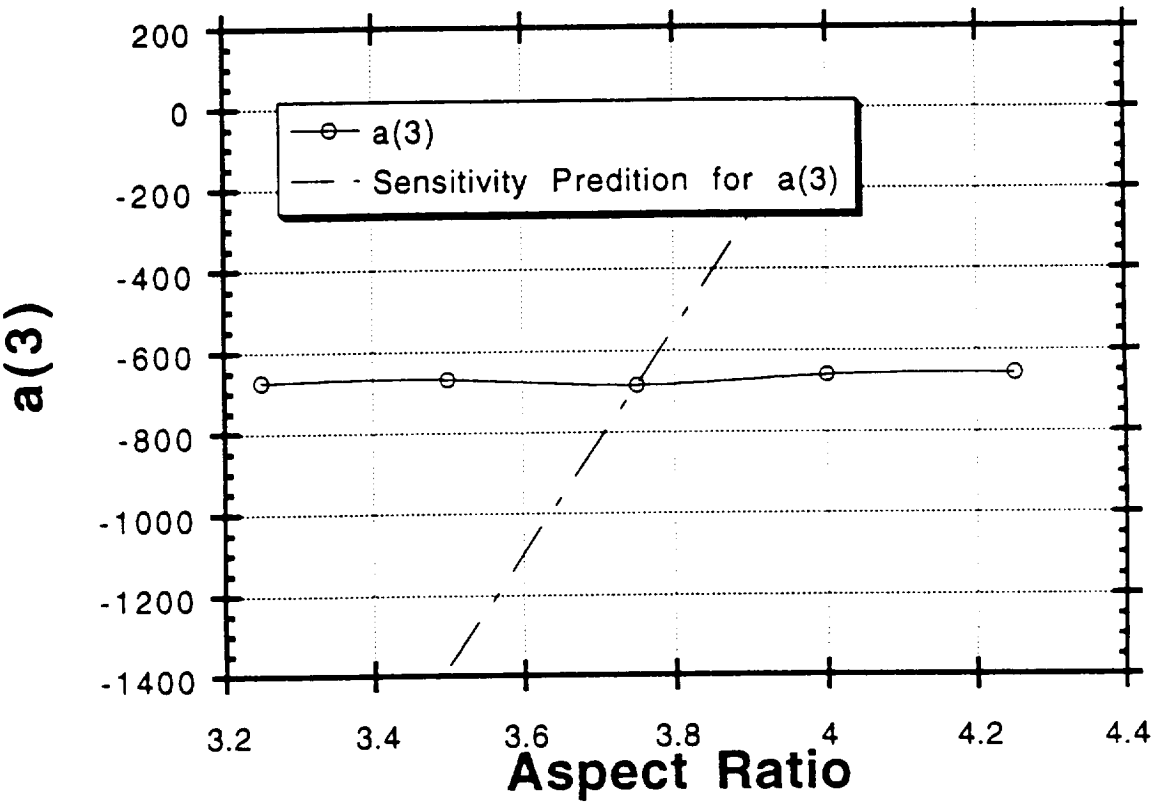

Figure 26. a(3) vs. Aspect Ratio, Chebyshev Pressure Representation

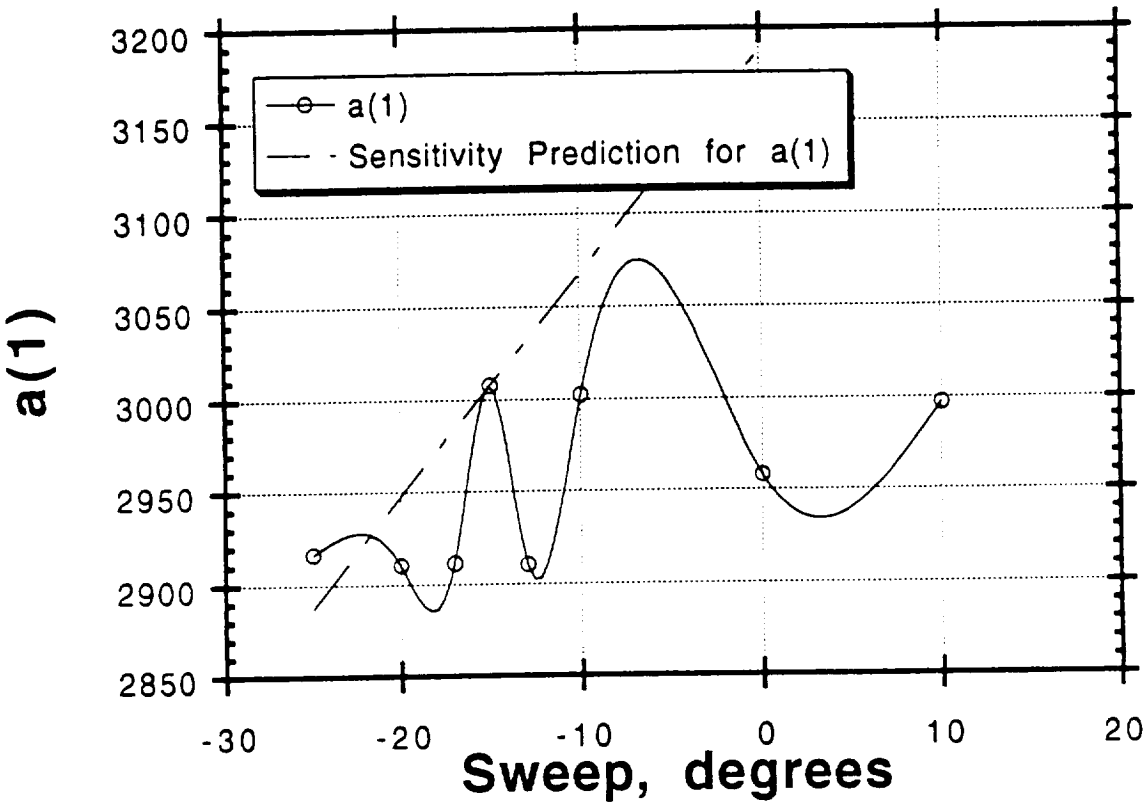

Figure 27. a(1) vs. Sweep, Chebyshev Pressure Representation

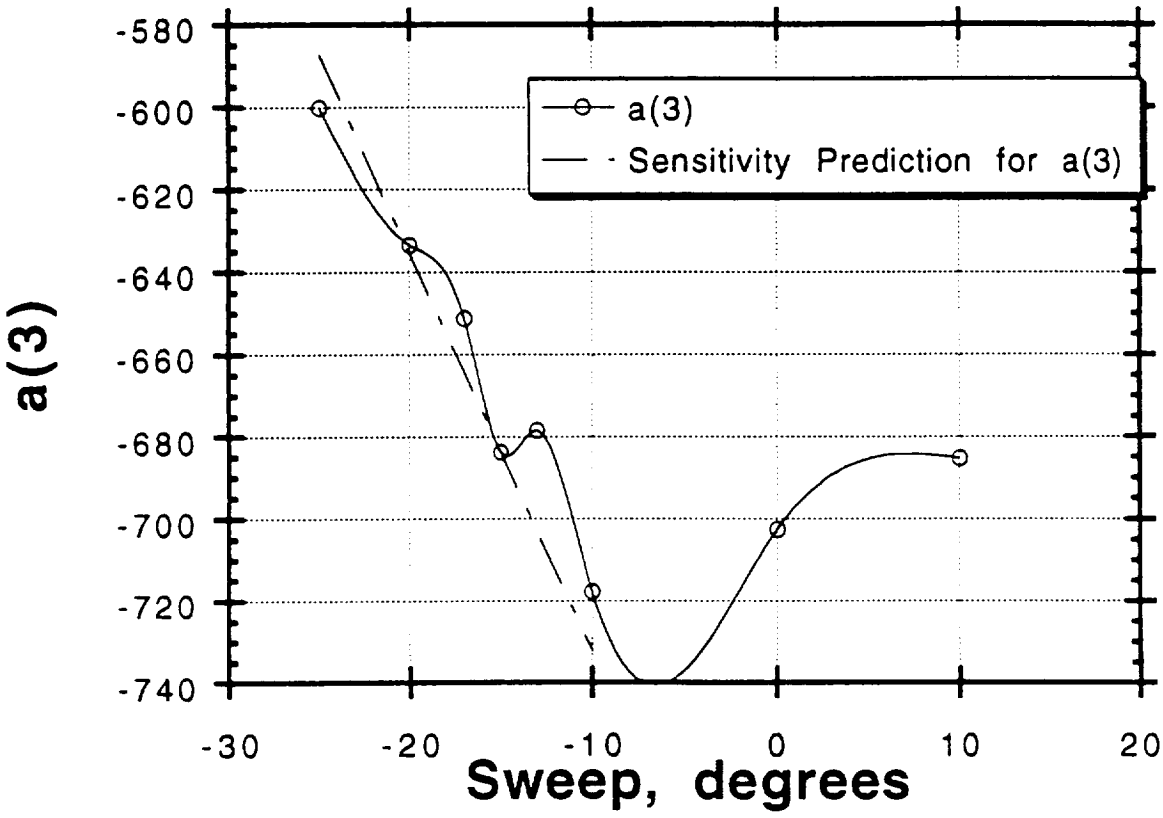

Figure 28. a(3) vs. Sweep, Chebyshev Pressure Representation

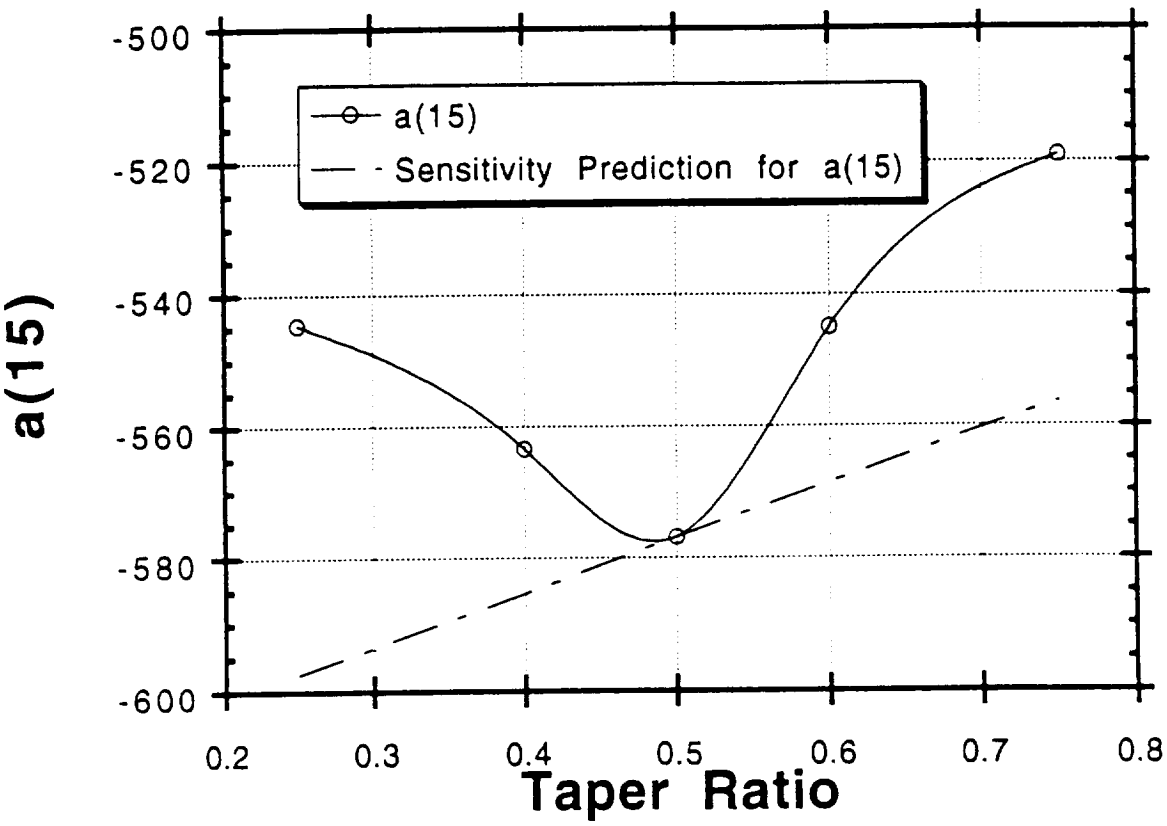

Figure 29. a(15) vs. Taper Ratio, Chebyshev Pressure Representation

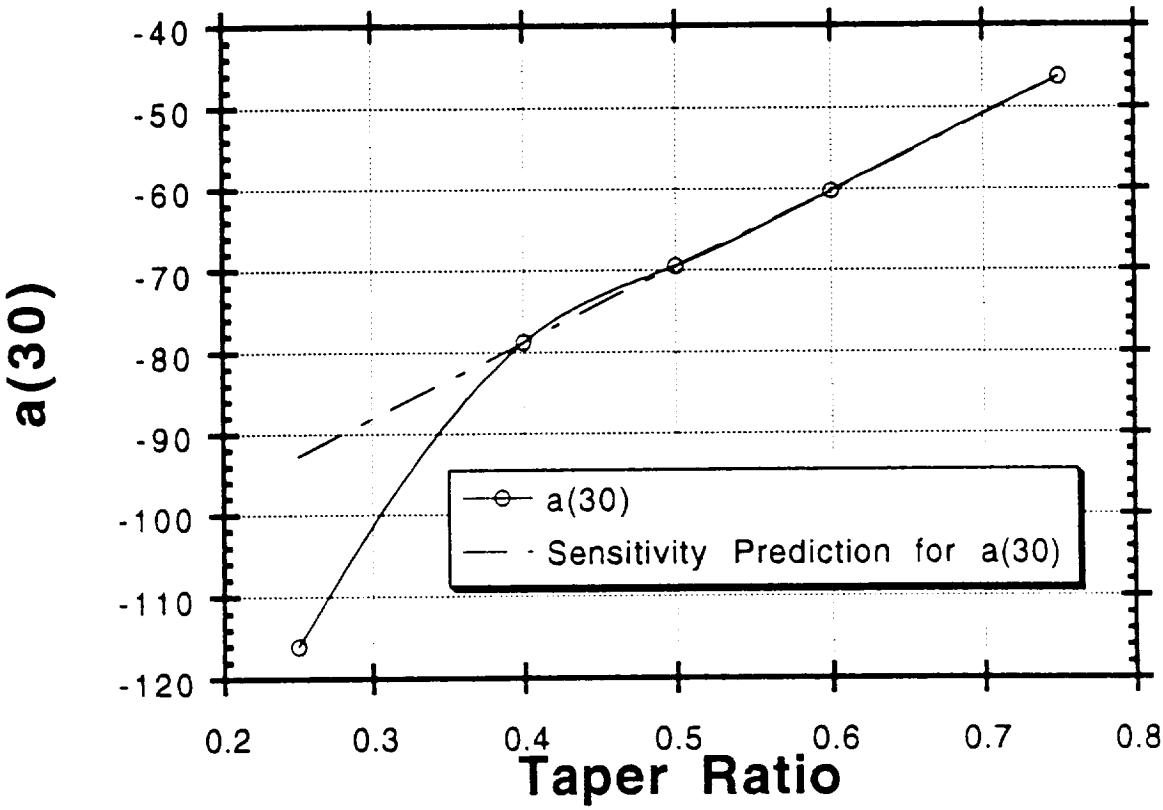

Figure 30. a(30) vs. Taper Ratio, Chebyshev Pressure Representation

5.0 Constant Local Pressure Representation

The global Chebyshev pressure representation will not adequately capture small, local, details in the pressure field unless a very large number of terms are used. Thus, an alternative scheme was employed. The pressure is represented by using interpolation polynomials that have local support over the wing panel. It is expected that a larger aerodynamic coefficient vector, $\{a\}$, will be necessary for similarly accurate results. This relationship is examined.

Any number of polynomials are available for this purpose. To begin with a scheme that represented panels each having constant pressure was used. Given a square panel defined as $(u, v) = (-1, 1)$, and the values at the four corners of the panel as b_{00}, b_{01}, b_{10}, b_{11}. Then the interpolated value p at any point (u, v) on that panel is given by:

$$p(u, v) = \frac{1}{4}[1 \quad 1] \begin{bmatrix} b_{00} & b_{01} \\ b_{10} & b_{11} \end{bmatrix} \begin{Bmatrix} 1 \\ 1 \end{Bmatrix} \tag{5.1}$$

This can be rearranged by multiplication to become:

$$p(u, v) = \frac{1}{4}[1 \quad 1 \quad 1 \quad 1] \begin{Bmatrix} b_{00} \\ b_{01} \\ b_{10} \\ b_{11} \end{Bmatrix} \tag{5.2}$$

In other words, the pressure on a panel is represented by the average of the pressures at the four corners of that panel. The symbol $R_i(u, v)$ is used in the following chapters to represent the interpolation polynomials used by the bilinear and biquadratic interpolation. For completeness sake, the constant pressure panel representation's interpolation polynomials are

$$R_i(u,v) = \frac{1}{4} \tag{5.3}$$

where i varies from 1 to 4.

This form is suitable for the integration of the forces. If we call the right hand side our aerodynamic coefficients (actually true pressures), $\{a\}$, we get

$$p(u,v) = \{R\}^T\{a\} \tag{5.4}$$

This pressure representation can be used in eqns. 2.10 and 2.12. These equations allow us to produce the $[A]$, aerodynamic kernal matrix, for the constant pressure panel case. A typical term in $[A_C]$, our constant panel aerodynamic matrix, is:

$$[A_C] = \sum_{panels} \int_{-1}^{1}\int_{-1}^{1} R(u,v)\gamma_i(x,y)|J_1(\eta,\xi)||J_2(u,v)|dudv \tag{5.5}$$

where $J_2(u,v)$ is the Jacobian of the transformation from the (η,ξ) to (u,v) coordinate system, and the subscript C indicates the constant pressure representation of the aerodynamic pressure over the wing panels.

$[A_C]$ has the following properties:

1) Each row corresponds to a particular Q_i (corresponding to γ_i).

2) Each column corresponds to the contribution of a particular point pressure.

3) Each wing panel will add to 4 columns in $[A]$. For instance, panel "j" will add to each element "i" in the column corresponding to the upper left node:

$$\int_{-1}^{1}\int_{-1}^{1} \frac{1}{4}\ \gamma_i(\eta,\xi)\ |J_1(\eta,\xi)||J_2(u,v)|\ du\ dv \tag{5.6}$$

The constant-panel version of $\{L\}$ is very similar. Each panel contributes to the four elements of the vector corresponding to its four corner nodes.

$$L_C = \sum_{panels} \int_{-1}^{1} \int_{-1}^{1} R(u,v)\ |J_1(\eta,\xi)||J_2(u,v)|\ du\ dv \tag{5.7}$$

A Gauss integration scheme was used to perform the double integrals in the $[A_C]$ and $\{L_C\}$ equations.

The first step was to verify $[A_C]$ and $\{L_C\}$. Recalling that $Q_i = [A_C]\{a\}$ and $Lift = \{L_C\}^T\{a\}$ gives us an easy way to test the terms. Comparing Q_i and the lift to results earlier obtained from using global Chebyshev polynomials eventually gave very good results.

An evenly distributed rectangular grid was first used. A computer graphics visualization of the error field confirmed that significant error was concentrated in the region very near the leading edge.

A revised gridding scheme was devised. This had two refinements. The inability of FAST to produce pressure data at the wing edges was initially a problem. Under the original local bilinear scheme, panels were assembled away from the edge, resulting in a 100% error band around the boundary of the wing. The current scheme puts the panels nearer to the wing edges and also specifies a zero pressure along the edges, allowing panels to be placed along the wing edges.

Second, a variable spacing technique was used to put improved resolution where it was needed. This used a modified half-Gauss-Lobatto grid. The phase and frequency of the cosine term in the Gauss-Lobatto equation was changed to give high resolution at the wing leading edge and tip, and low resolution along the trailing edge and wing root.

$$\xi(i) = -2cos(\frac{\pi}{2}\frac{i-1}{N_\xi}) + 1 \tag{5.8}$$

$$\eta(j) = -2cos(\frac{\pi}{2}\frac{j-1}{N_\xi} + \frac{\pi}{2}) - 1 \tag{5.9}$$

This scheme captures the leading edge peak of the pressure field much better than the earlier scheme employing a uniformly distributed grid and also better than the global chebyshev scheme employed in Chapter 4.

Then, the derivatives of $[A]$ and $\{L\}$, taking into account all the zero coordinate derivatives, are:

$$\frac{dA_C}{dr_l} = \sum_{kgx} \sum_{kgy} Rw_x w_y J_2 \left(\frac{d\gamma_i}{dr_l} J_1 + \gamma_i \frac{dJ_1}{dr_l} \right) \tag{5.10}$$

and

$$\frac{dL}{dr_l} = \sum_{kgx} \sum_{kgy} Rw_x w_y J_2 \frac{dJ_1}{dr_l}. \tag{5.11}$$

where kgx and kgy are the number of gauss points in the x and y directions. (Typically, $kgx = kgy = 2$). Note that $dJ_2/dr_l = 0$.

Tables 4 - 13 (in Chapter 8) show the results from the constant pressure panel versions of the analysis. Comparisons with the other approaches show very close results.

6.0 Bilinear Local Pressure Representation

Next, a bilinear scheme was used to represent the wing pressure. Given the same square panel defined as $(u, v) = (-1, 1)$, and the values at the four corners of the panel as b_{00}, b_{01}, b_{10}, b_{11}. Then the interpolated value p at any point (u, v) is given by:

$$p(u,v) = \frac{1}{4}[1-u \quad 1+u] \begin{bmatrix} b_{00} & b_{01} \\ b_{10} & b_{11} \end{bmatrix} \begin{Bmatrix} 1-v \\ 1+v \end{Bmatrix} \tag{6.1}$$

This can be rearranged by multiplication to become:

$$p(u,v) = \frac{1}{4}\left[(1-u)(1-v) \quad (1-u)(1+v) \quad (1+u)(1-v) \quad (1+u)(1+v)\right] \begin{Bmatrix} b_{00} \\ b_{01} \\ b_{10} \\ b_{11} \end{Bmatrix} \tag{6.2}$$

If we call the left hand vector R, our interpolation vector, and the right hand side is our aerodynamic coefficients (actually true pressures), $\{a\}$, we get

$$p(u,v) = \{R\}^T\{a\} \tag{6.3}$$

where a typical term in $[A_{BL}]$,our bilinear aerodynamic matrix, is:

$$[A_{BL}] = \sum_{panels} \int_{-1}^{1}\int_{-1}^{1} R(u,v)\gamma_i(x,y)|J_1(\eta,\xi)||J_2(u,v)|dudv \tag{6.4}$$

where $J_2(u, v)$ is the Jacobian of the transformation from the (η, ξ) to (u, v) coordinate system, and the subscript BL indicates the bilinear representation of the aerodynamic pressure over the wing panels.

$[A_{BL}]$ has the same properties discussed for $[A_C]$. For instance, panel "j" will add to each element "i" in the column corresponding to the upper left node:

$$\int_{-1}^{1}\int_{-1}^{1} \frac{1}{4}(1-u)(1-v)\ \gamma_i(\eta,\xi)\ |J_1(\eta,\xi)||J_2(u,v)|\ du\ dv \tag{6.5}$$

The bilinear version of $\{L\}$ is very similar. Each panel contributes to the four elements of the vector corresponding to its four corner nodes.

$$L_{BL} = \sum_{panels} \int_{-1}^{1}\int_{-1}^{1} R(u,v)\ |J_1(\eta,\xi)||J_2(u,v)|\ du\ dv \tag{6.6}$$

A Gauss integration scheme was used to perform the double integrals in the A_{BL} and L_{BL} equations.

The next thing to test was the derivatives of $[A_{BL}]$ and $\{L\}$. This was accomplished by comparing the analytic derivatives to finite difference derivatives calculated by recalling the subroutines with slight changes to the shape parameters.

The new bilinear-interpolation versions of the terms $\{d\{a\}/d\alpha\}$, $[d\{a\}/d\{C\}]$, and $\{d\{a\}/dr_\ell\}$ remained. Each was calculated by appropriate finite differences. Then, the sensitivity code had to be modified to allow easy switching between the two (and other future) schemes.

$R(u,v)$ - **Bilinear interpolator**. R has 4 different values, one at a time, depending on which term of $[A]$ is under consideration.

$$R_1 = 0.25(1-u)(1-v) = 0.25(1-u-v+uv) \tag{6.7}$$

$$R_2 = 0.25(1+u)(1-v) = 0.25(1+u-v-uv) \tag{68}$$

$$R_3 = 0.25(1-u)(1+v) = 0.25(1-u+v-uv) \tag{6.9}$$

$$R_4 = 0.25(1+u)(1+v) \tag{6.10}$$

Since the derivatives du/dr_ℓ and dv/dr_ℓ are zero, the derivatives of R_4 is also zero.

6.1 Bilinear Pressure Interpolation

The motivating factor for attempted local or panel based schemes was to try to improve the accuracy of the local derivatives of the aerodynamic loads. A major factor in the inaccuracy of the Chebyshev approach's aerodynamic derivatives were the "wiggles" in the data being differentiated.

A study was undertaken to determine if the new aerodynamic coefficients, actually point pressures, were any smoother in their behaviors. Each of the four shape parameters was varied and pressures at three points on the wing were stored. These points were the nodes nearest to the wing leading-edge-root, the wing center, and the wing trailing-edge-tip. Nearly all of the data was if not linear, at least very smoothly varying. Figures 31 - 34 show the four worst cases. Only the trailing-edge-root pressure vs. Sweep plot indicates a potential problem. The other sweep plots were perfectly smooth. The pressures shown are measured in Pascals.

6.2 Bilinear Results

The variation of the trim angle of attack with respect to the wing area is shown in Figure 35. The solid line shows the converged results from the iterative aerodynamic and structures combination. The various dashed lines show the variation predicted by the sensitivity derivatives at the different base configurations. The prediction goes through the converged value at the base geometry and is linear with a slope equal to the sensitivity derivative. The desired result is for this line to be tangent to the converged data curve.

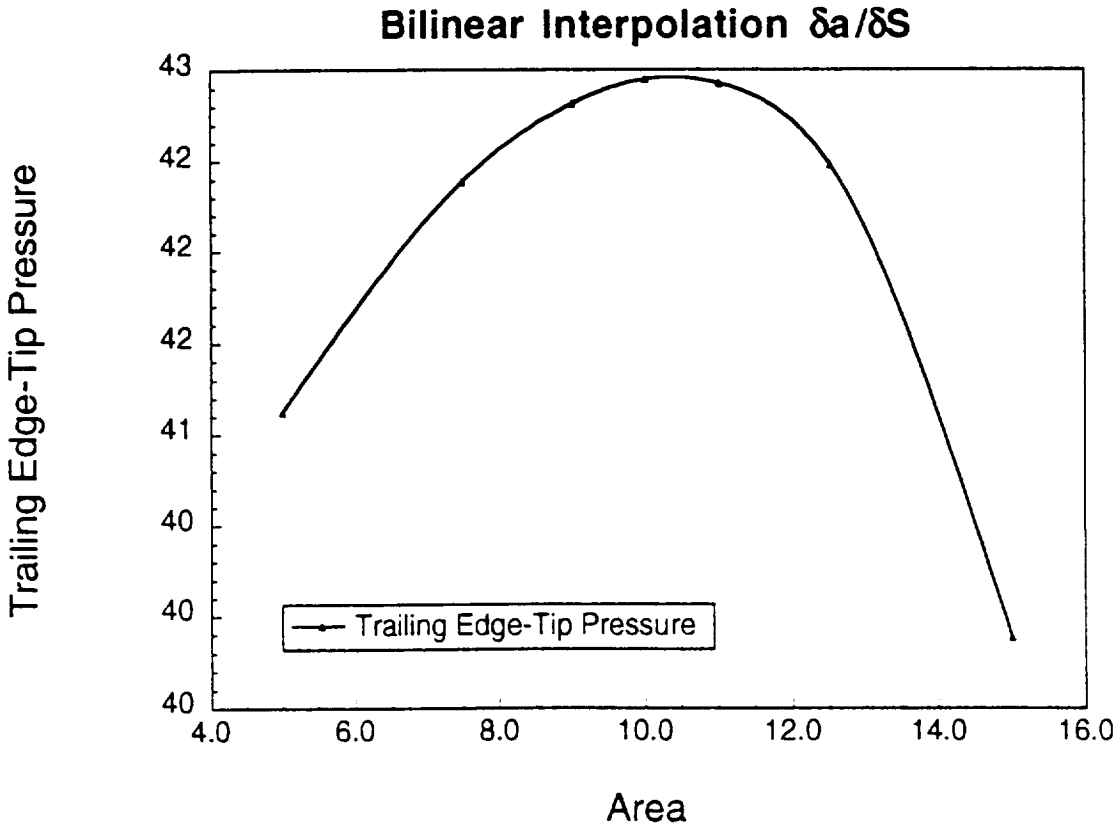

Figure 31. Trailing Edge-Tip Pressure vs. Wing Area

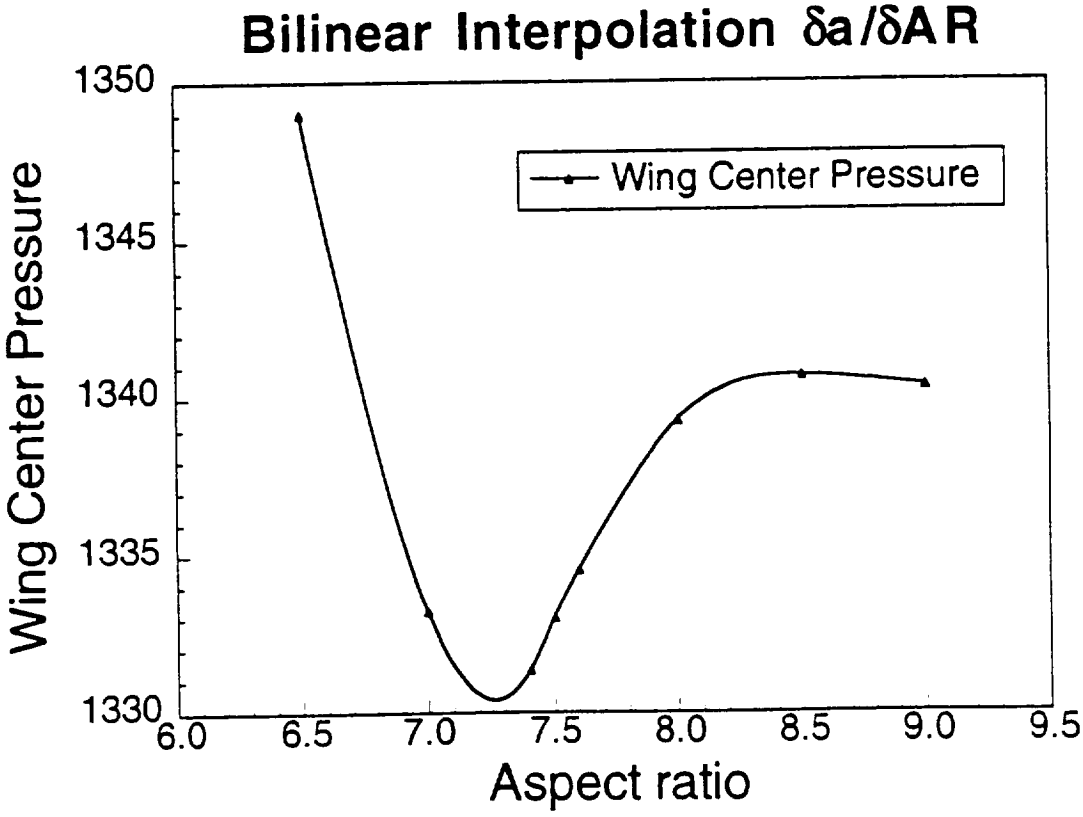

Figure 32. Wing Center Pressure vs. Aspect Ratio

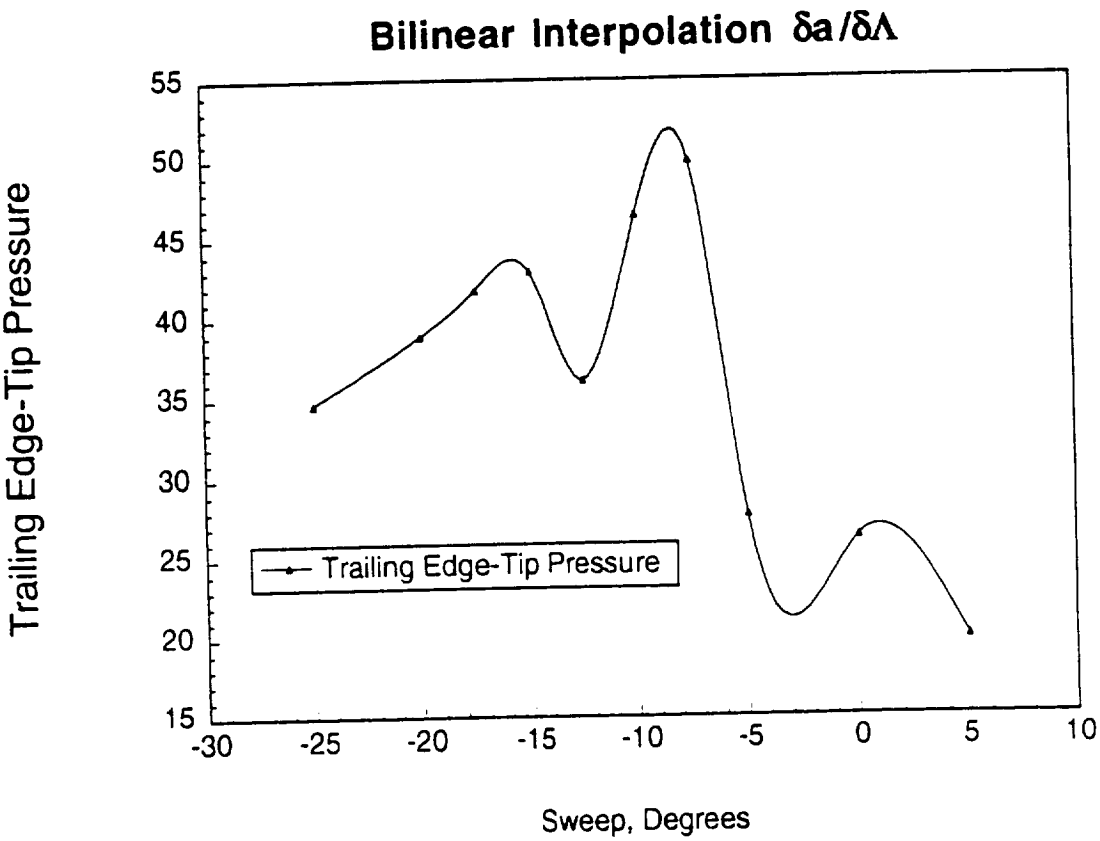

Figure 33. Trailing Edge-Tip Pressure vs. Sweep

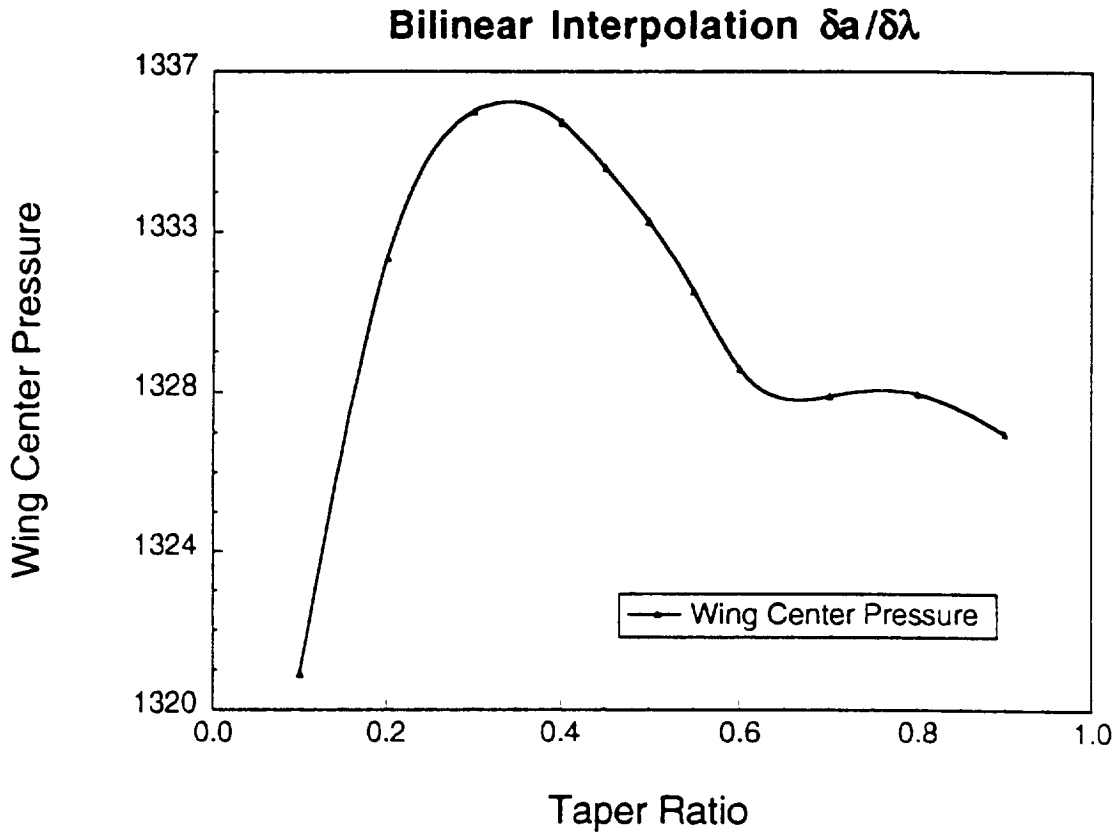

Figure 34. Wing Center Pressure vs. Taper Ratio

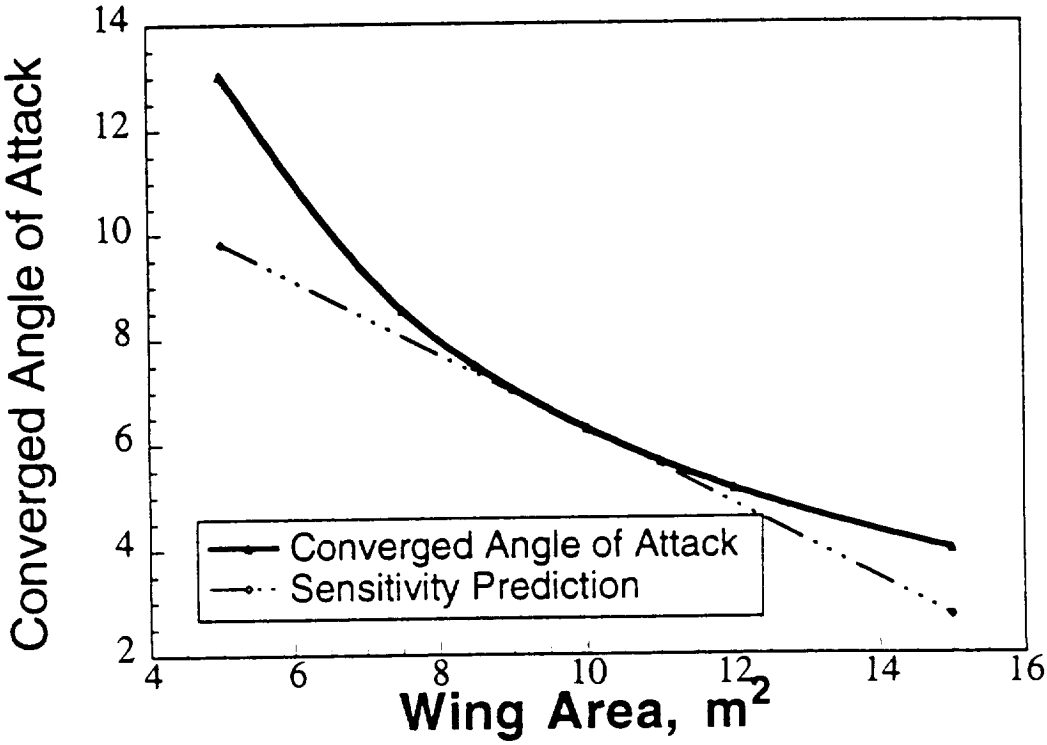

Trim Angle of Attack vs. Wing Area
Bilinear Pressure Representation

Figure 35. Trim Angle of Attack vs. Wing Area, Bilinear Pressure Representation

Similarly, the sensitivity of the trim angle of attack to changes in the wing aspect ratio is shown in Figure 36. The solid line shows the converged iterative results and the dashed lines show the predicted variation by having a slope equal to the calculated sensitivity derivative.

Figures 37 and 38 show the converged and predicted values for the angle of attack variation with respect to taper ratio and sweep. It is obvious from Fig. 38 that the obtained value of the sensitivity of the angle of attack with respect to the taper ratio is not as accurate as one would like. However, note that the value of the converged angle of attack is almost insensitive to the variation in taper ratio at those values of taper ratio. The inaccuracy in the present results can be attributed to the numerical problems associated with determining derivatives that are almost zero.

Also of interest are deflection sensitivities. Figures 39-42 show the sensitivity of the leading edge tip deflection. From these figures it is clear that the present formulation yields very accurate shape sensitivities for the aeroelastic tip deflections and can be used in optimization studies. The coefficient errors largely disappear in the integrated quantities.

These few errors are largely numerical in origin. Variables with very small logarithmic derivatives will be difficult to differentiate numerically regardless of the scheme used (Haftka[23]). The final comparisions between the current versions of both schemes is also of interest. The following chart, Table 2, compares the various results. The finite difference derivatives are all forward derivatives where the step size was decreased until the derivative converged:

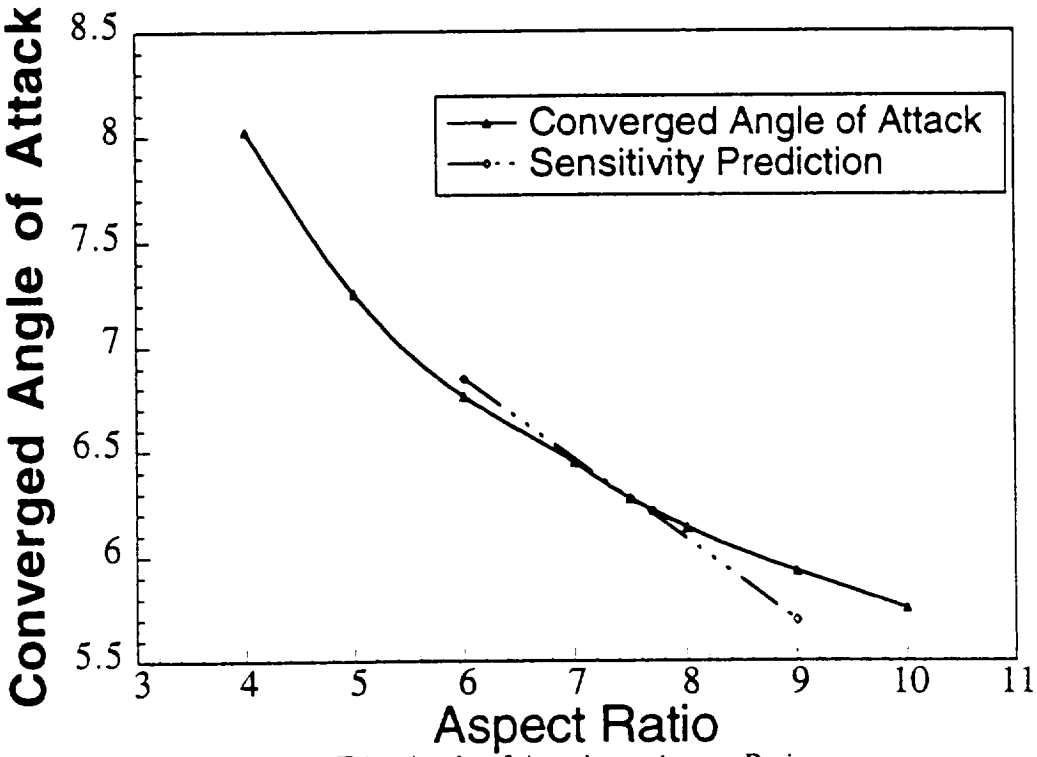

Trim Angle of Attack vs. Aspect Ratio
Bilinear Pressure Representation

Figure 36. Trim Angle of Attack vs. Wing Aspect Ratio, Bilinear Pressure Representation

Table 2: Comparison of Bilinear and Chebyshev approach Derivatives

Term	Bilinear Analytic	Chebyshev Analytic	Bilinear Fin. Dif.	Chebyshev Fin. Dif.
α_{trim}	6.2686	6.0987		
TD^*	0.4086	0.3879		
TDw/α	0.6179	0.5915		
$d\alpha/dS$	-0.710	-0.689	-0.686	-0.725
dTD/dS	0.040	0.038	0.040	0.038
$d\alpha/dAR$	-0.766	-0.775	-0.579	-0.596
dTD/dAR	0.209	0.274	0.209	0.195
$d\alpha/d\Lambda$	-0.056	-0.051	-0.032	-0.040
$dTD/d\Lambda$	$-7.2\text{x}10^{-3}$	$-6.7\text{x}10^{-3}$	$-7.2\text{x}10^{-3}$	$-6.8\text{x}10^{-3}$
$d\alpha/d\lambda$	-0.359	-0.294	-0.188	-0.226
$dTD/d\lambda$	0.213	0.266	0.227	0.212

* Tip Deflection

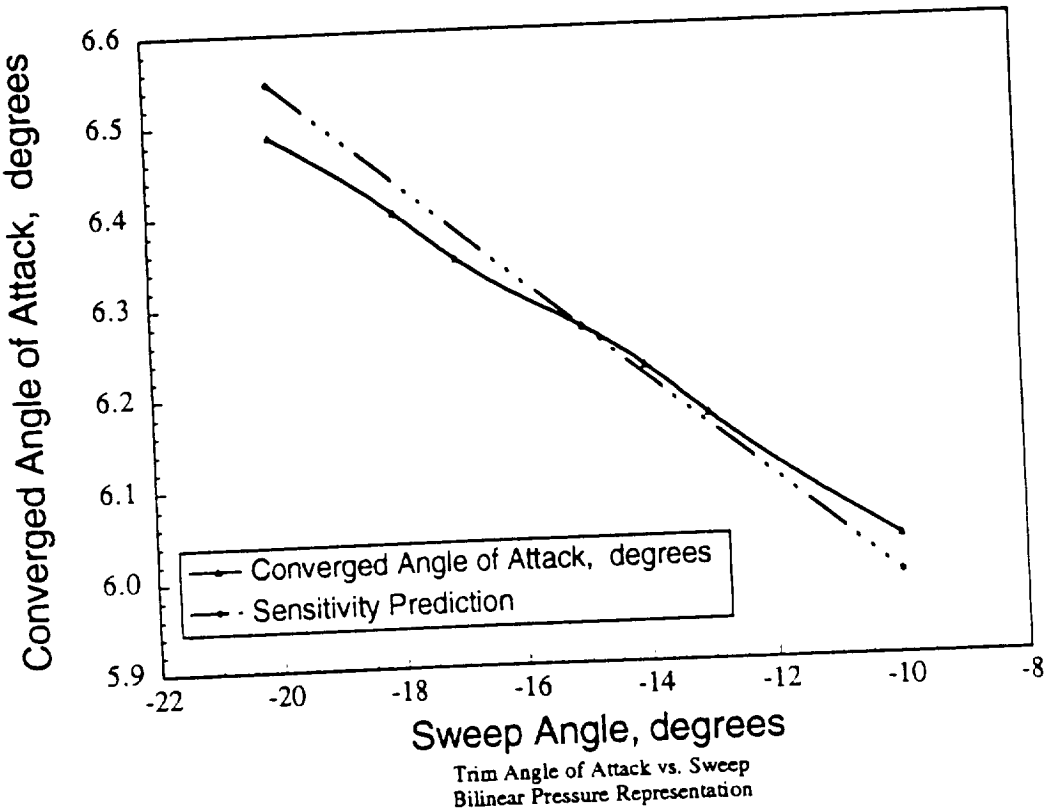

Figure 37. Trim Angle of Attack vs. Wing Sweep, Bilinear Pressure Representation

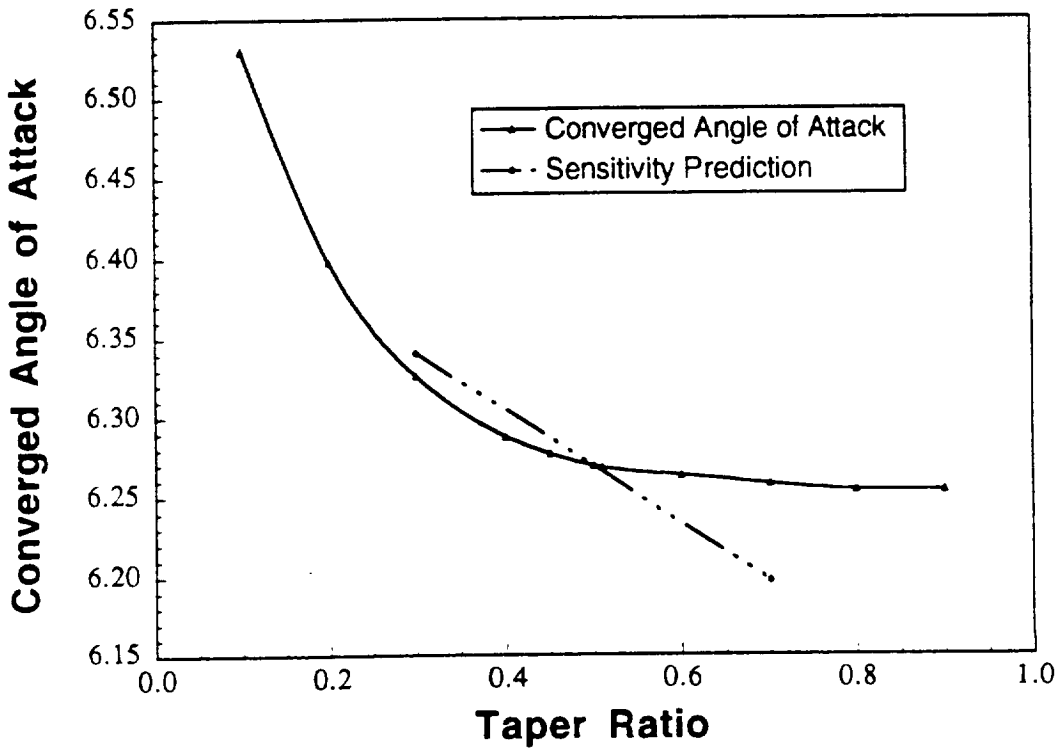

Trim Angle of Attack vs. Taper Ratio
Bilinear Pressure Representation

Figure 38. Trim Angle of Attack vs. Wing Taper Ratio, Bilinear Pressure Representation

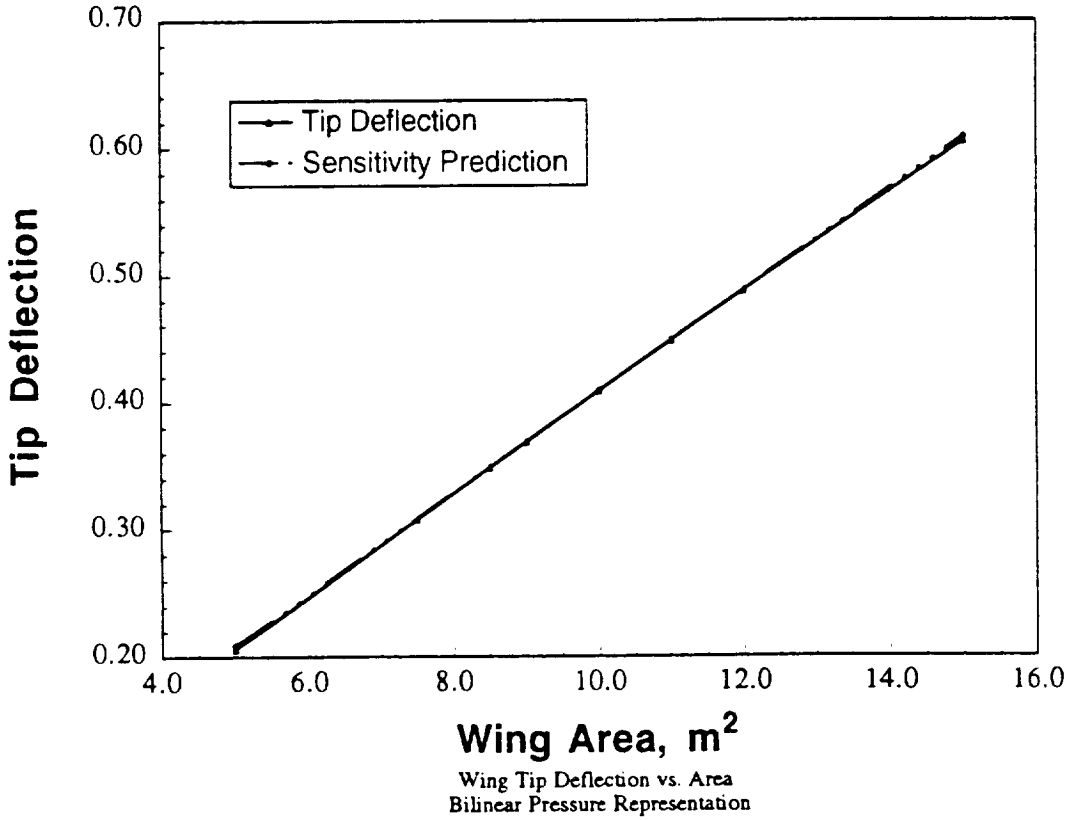

Figure 39. Tip Deflection vs. Wing Area, Bilinear Pressure Representation

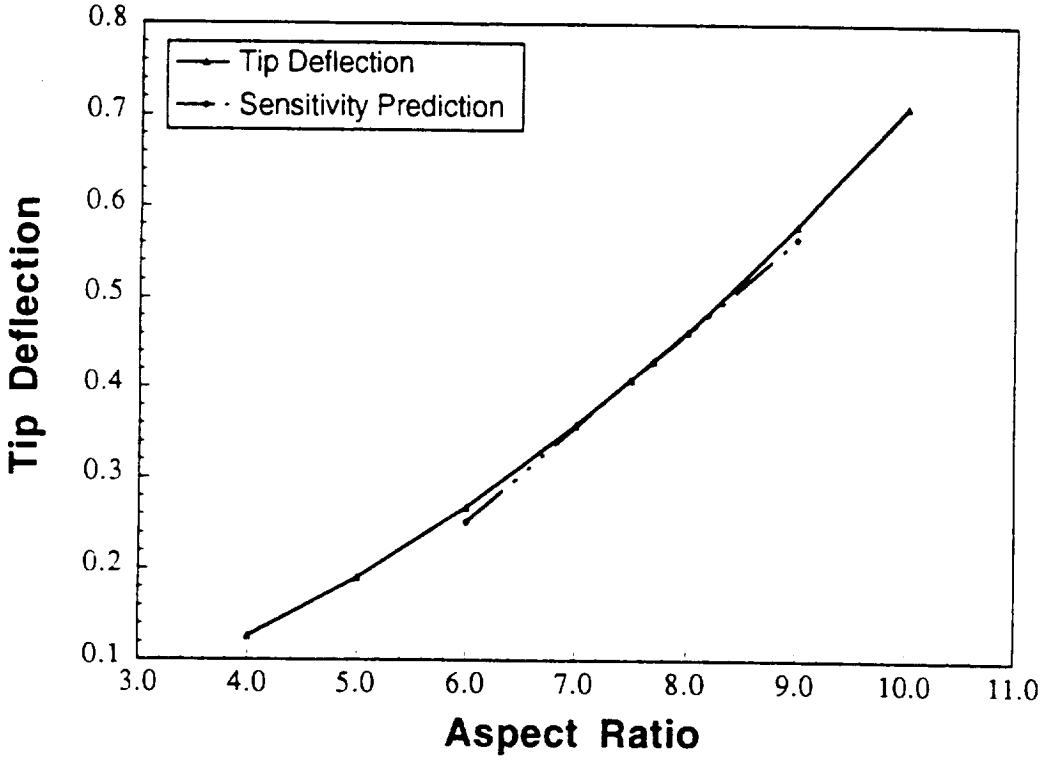

Tip Deflection vs. Aspect Ratio
Bilinear Pressure Representation

Figure 40. Tip Deflection vs. Wing Aspect Ratio, Bilinear Pressure Representation

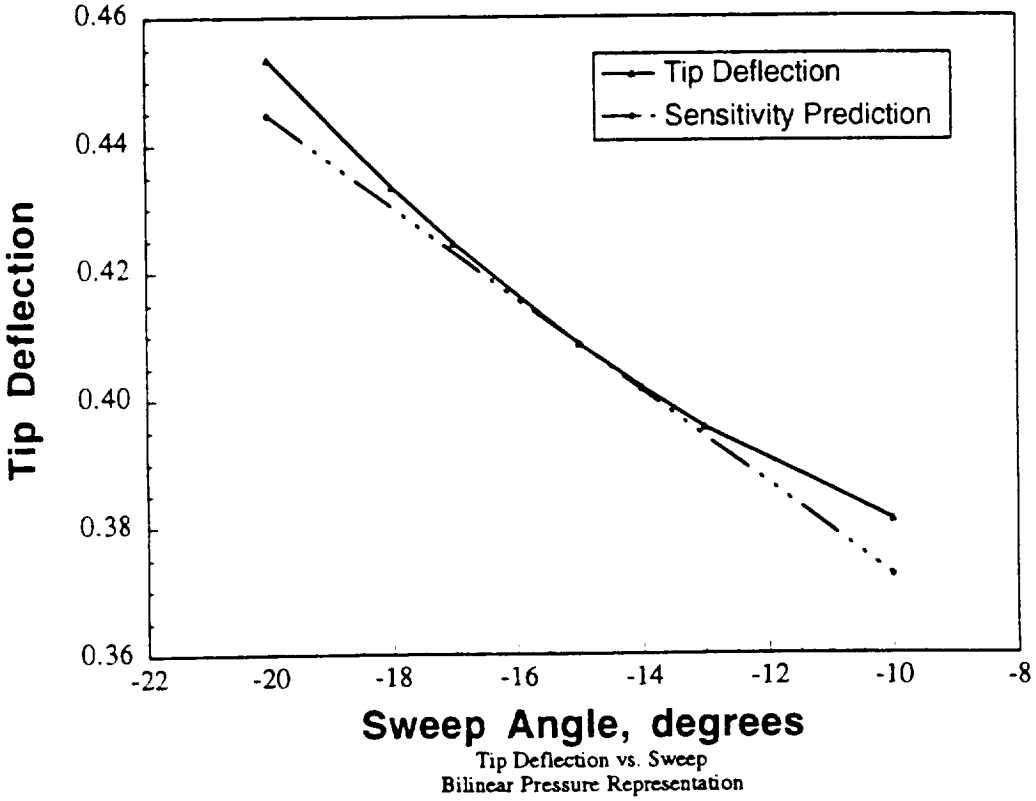

Figure 41. Tip Deflection vs. Wing Sweep, Bilinear Pressure Representation

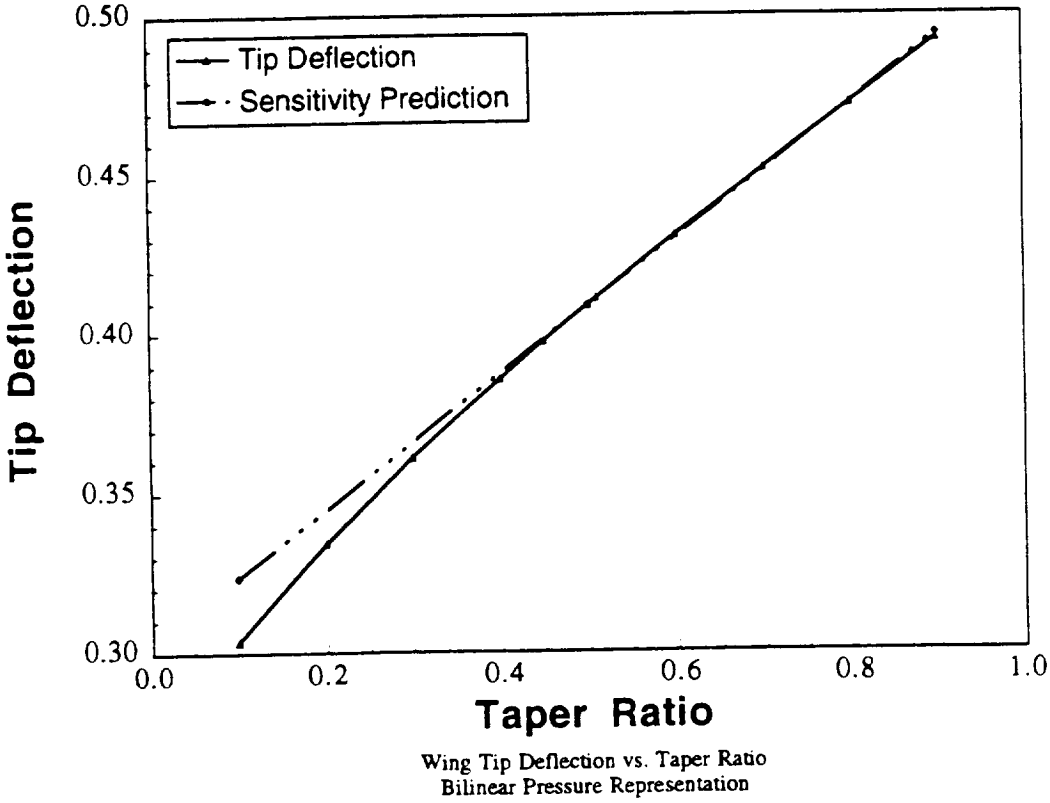

Figure 42. Tip Deflection vs. Wing Taper Ratio, Bilinear Pressure Representation

7.0 Biquadratic Local Pressure Representation

A biquadratic pressure panel representation was developed next. Again, a panel was designated as having $(u, v) = (-1, 1)$. For this scheme, the panel has nine input pressure nodes.

The interpolation polynomials R_i were derived from Langrangian polynomials. The two dimensional R's are products of the one dimensional quadratic Lagrangian polynomials. These Lagrangian polynomials with an arbitrarily positioned middle node are:

$$L_1(u) = \frac{1}{2}\frac{(u - u_2)(u - 1)}{(1 + u_2)} \tag{7.1}$$

$$L_2(u) = \frac{(u + 1)(u - 1)}{(u_2 + 1)(u_2 - 1)} \tag{7.2}$$

$$L_3(u) = \frac{1}{2}\frac{(u - u_2)(u + 1)}{(1 - u_2)} \tag{7.3}$$

where

u is the location to be interpolated to and

u_2 is the coordinate of the middle node.

Next, we define our two dimensional interpolation polynomials as follows:

$$R_1(u, v) = L_1(u)L_1(v) \tag{7.4}$$

$$R_2(u, v) = L_2(u)L_1(v) \tag{7.5}$$

$$R_3(u, v) = L_3(u)L_1(v) \tag{7.6}$$

$$R_4(u,v) = L_1(u)L_2(v) \tag{7.7}$$

$$R_5(u,v) = L_2(u)L_2(v) \tag{7.8}$$

$$R_6(u,v) = L_3(u)L_2(v) \tag{7.9}$$

$$R_7(u,v) = L_1(u)L_3(v) \tag{7.10}$$

$$R_8(u,v) = L_2(u)L_3(v) \tag{7.11}$$

$$R_9(u,v) = L_3(u)L_3(v) \tag{7.12}$$

This development allows us to use the same half-Gauss-Lobatto grid scheme developed for the constant and bilinear panels. Initially, this didn't work properly. The biquadratic interpolation calculated a significantly higher lift for a given deflection, leading to a significantly lower required trim angle of attack, roughly half of what was predicted by the other methods.

Some graphical visualization revealed the problem. The pressure field calculated by FAST is shown in figure 33. The field is heavily dominated by a huge spike along the leading edge. The constant and bilinear fits were able to deal with what is effectively an impulse in the field. The biquadratic representation could not. As it tried to fit a curve through the zero pressure on the leading edge, through the huge value at the next node, and back to a fraction of that value on the third node, it encountered numerical difficulties.

The solution to the problem was to reduce the gradient of the pressure field at the leading edge. For this purpose, the edge values were set equal to the values at the nearest internal node. Thus, the edge pressure gradient was set to zero. The biquadratic interpolation then worked correctly.

To understand the magnitude of the net change in the pressure field, the bilinear and constant convergence tests were rerun. The converged value of trim angle of attack

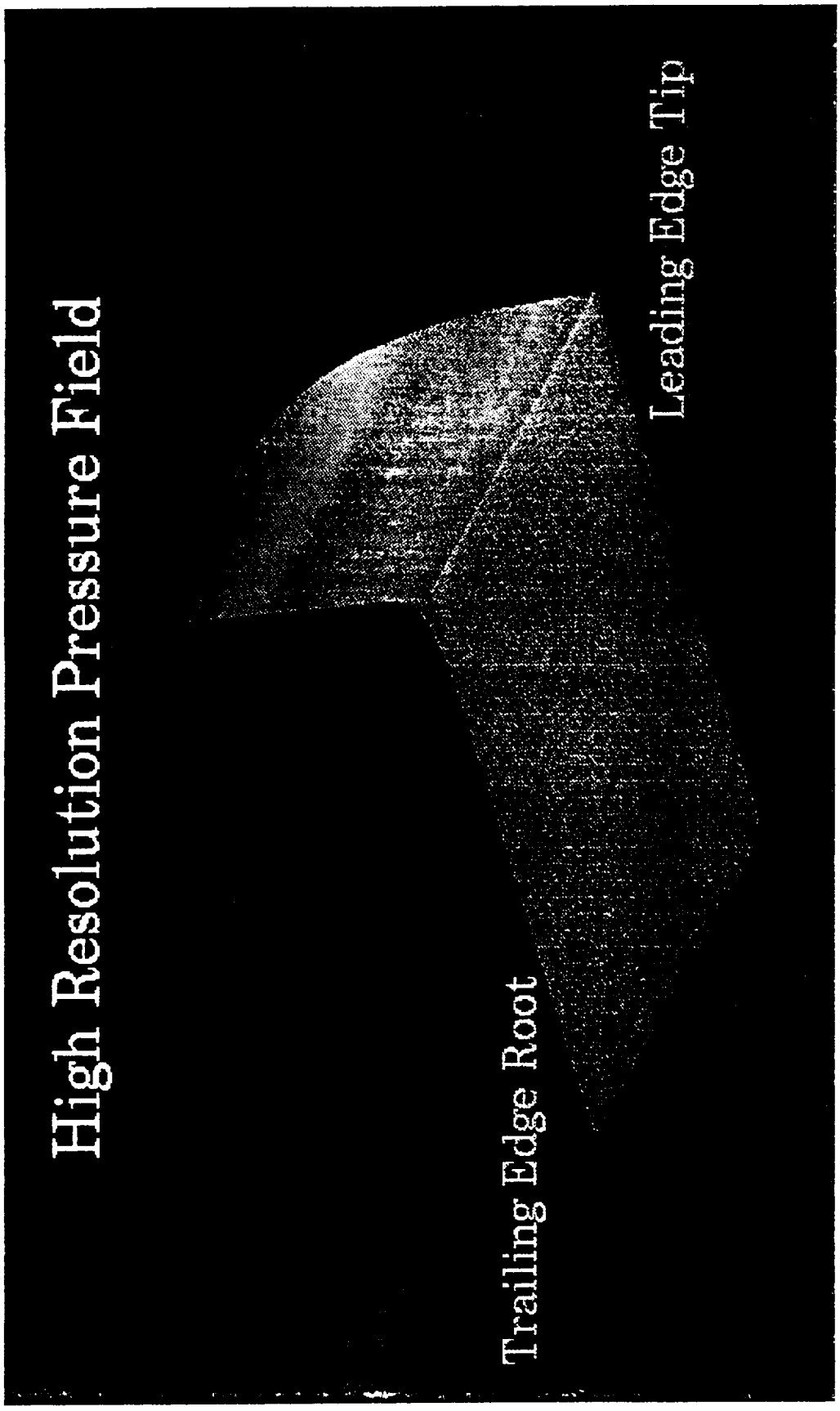

Figure 43. Wing Pressure Field

was reduced by about 2%. The change is small because the area of the panels effected is extremely tiny.

7.1 Biquadratic Results

Figures 44-47 show the biquadratic pressure representation results for trim angle of attack and the sensitivity derivatives. Figures 48 - 51 show the tip deflection values and their sensitivity derivatives. These plots are nearly identical to those produced by the other pressure schemes.

Chapter 8 discusses the relative performance of the schemes in detail.

Equation 3.4 was also used to try to represent the global sensitivities of the point pressures to the shape parameters. It was anticipated that as with deflection coefficients it would be difficult to model the individual sensitivities of the 1600 coefficients. As with the Chebyshev version of da/dr_ℓ, the results were mixed. Figures 52-59 are representative of the large number of point pressures examined.

Figures 52-53 show da/dS at two points along the leading edge. Figures 54-55 show da/dAR's mediocre performance. As with the chebyshev approach, $da/d\Lambda$ and $da/d\lambda$ perform much better. Representative plots are shown in figures 56-57 and 58-59 respectively.

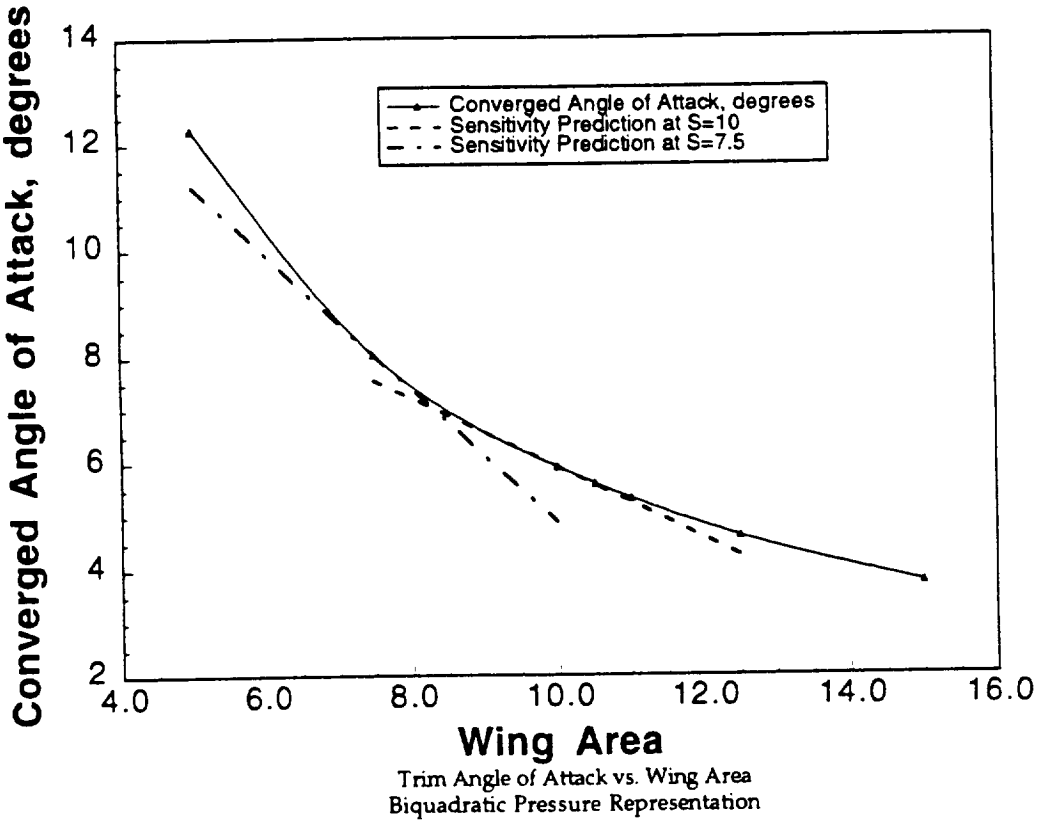

Figure 44. Trim Angle of Attack vs. Wing Area, Biquadratic Pressure Representation

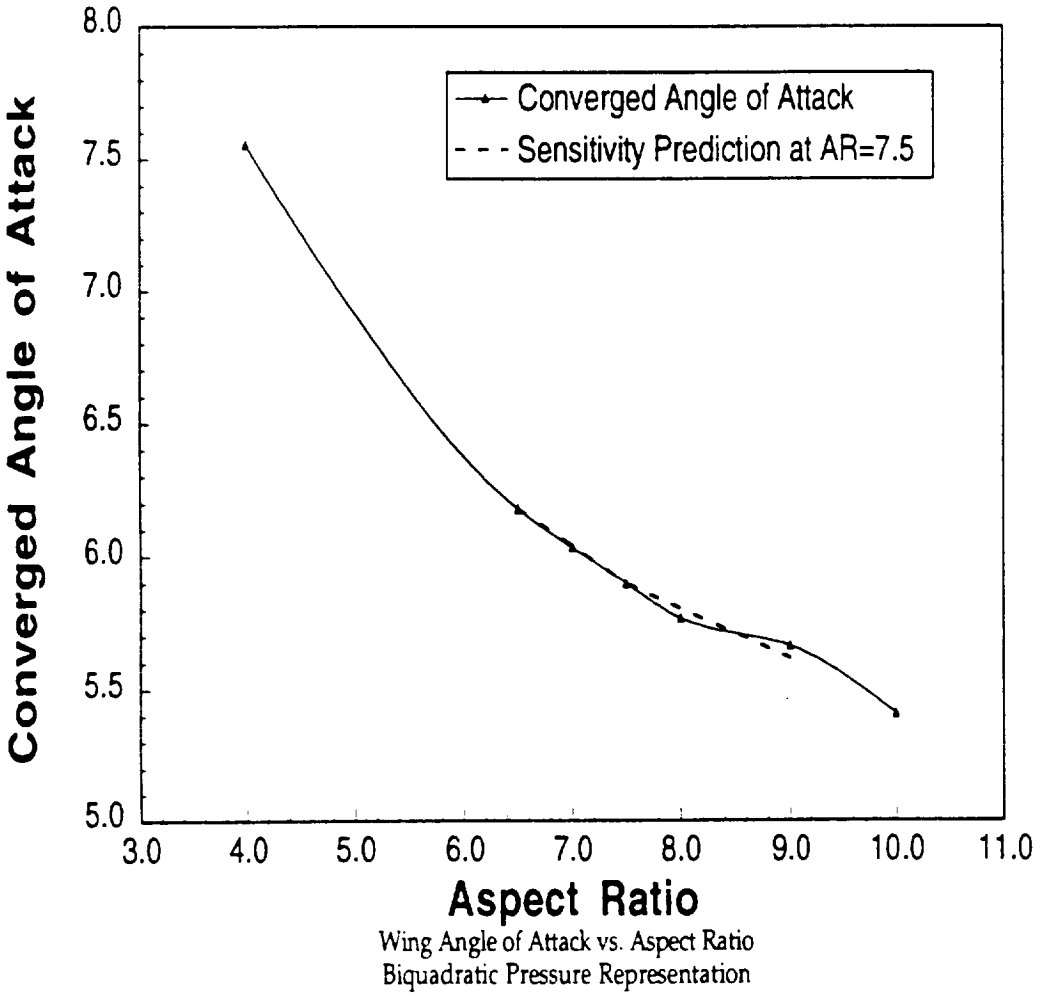

Figure 45. Trim Angle of Attack vs. Wing Aspect Ratio, Biquadratic Pressure Representation

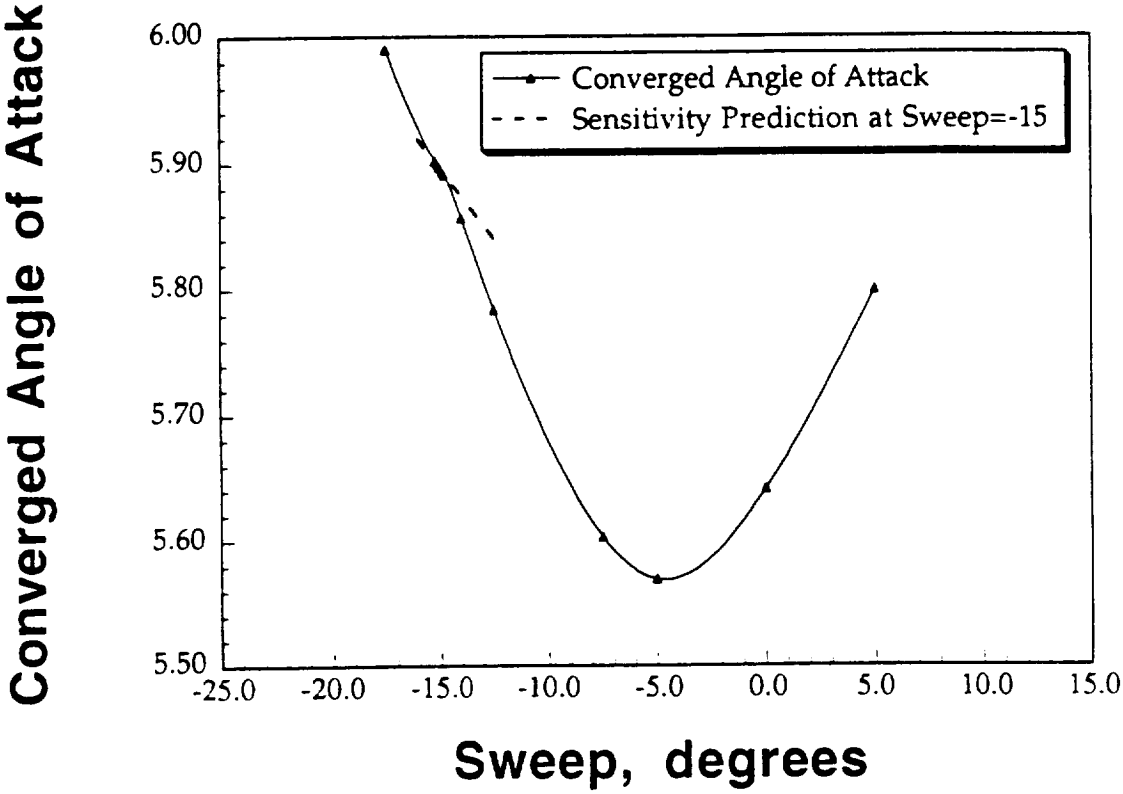

Figure 46. Trim Angle of Attack vs. Wing Sweep, Biquadratic Pressure Representation

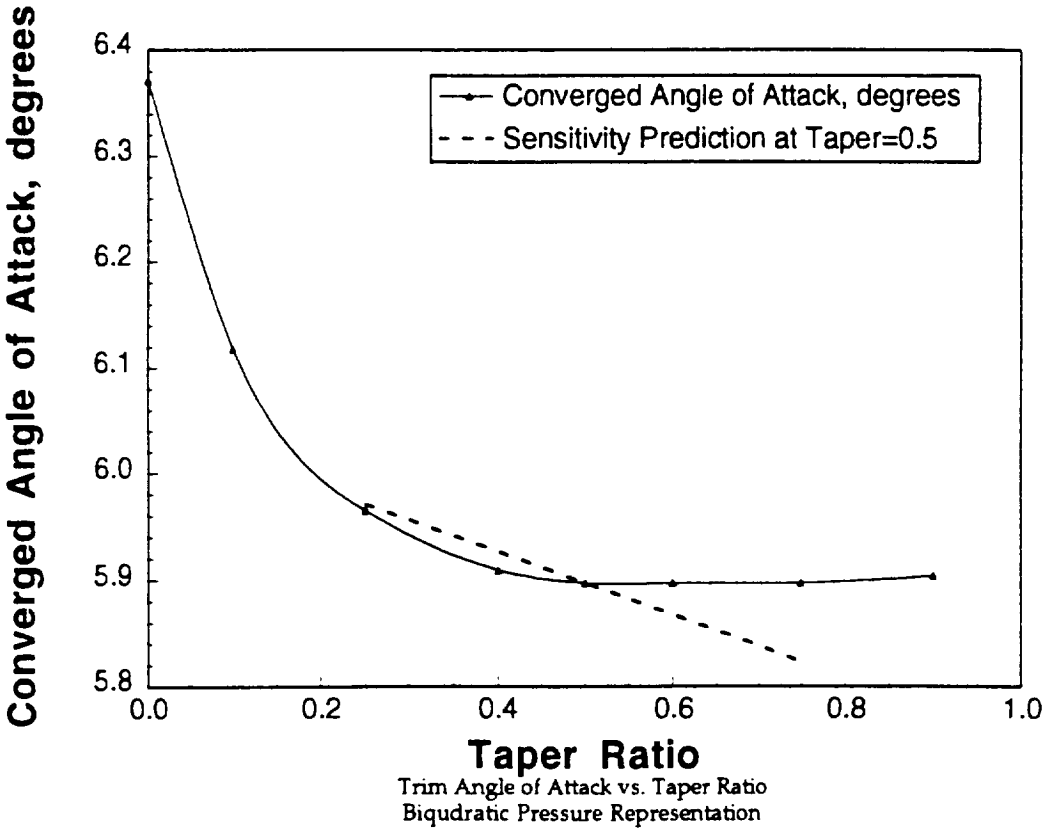

Figure 47. Trim Angle of Attack vs. Wing Taper Ratio, Biquadratic Pressure Representation

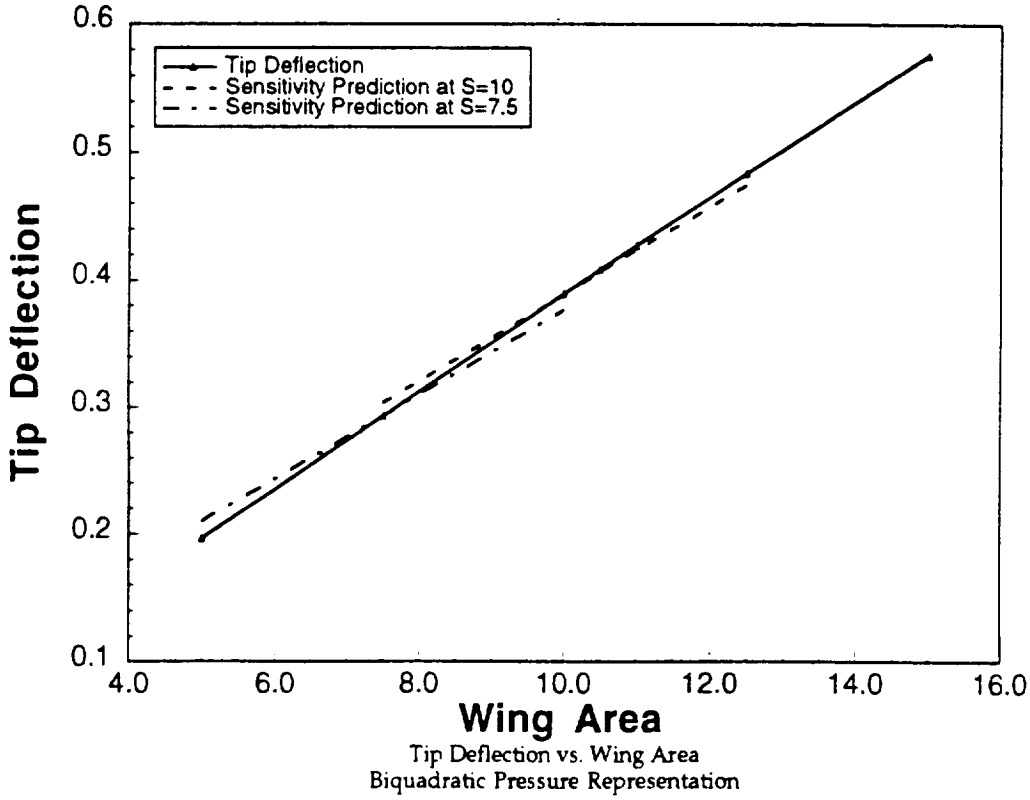

Figure 48. Tip Deflection vs. Wing Area, Biquadratic Pressure Representation

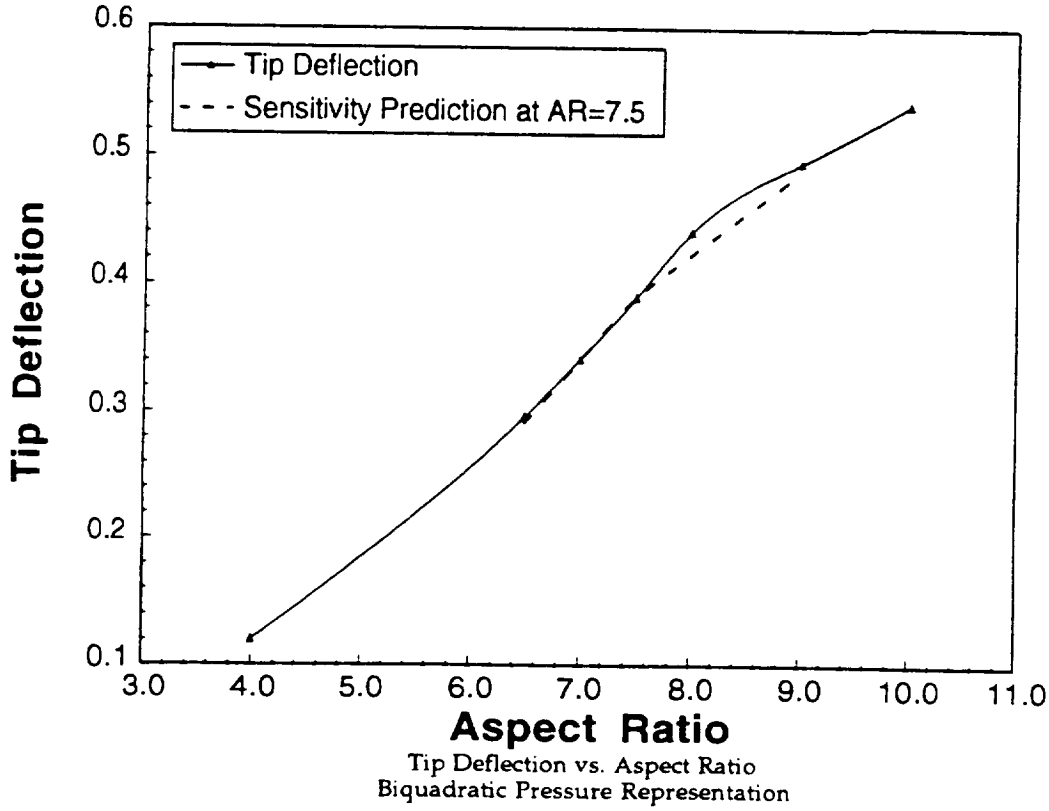

Figure 49. Tip Deflection vs. Wing Aspect Ratio, Biquadratic Pressure Representation

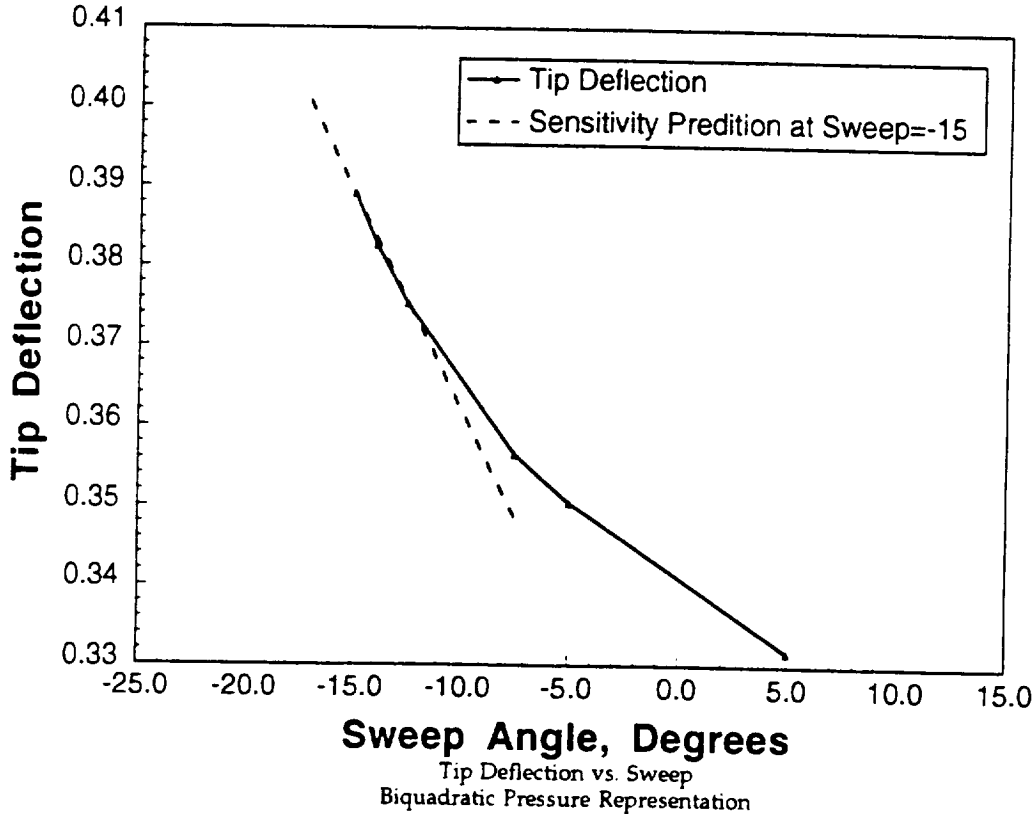

Figure 50. Tip Deflection vs. Wing Sweep, Biquadratic Pressure Representation

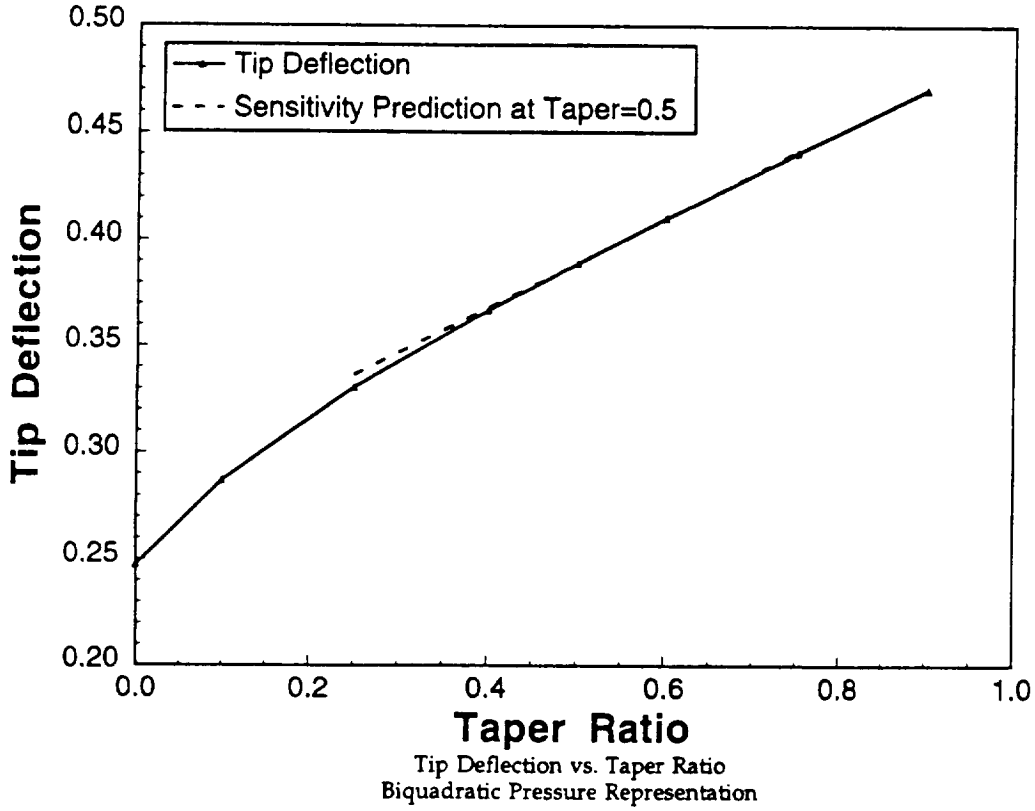

Figure 51. Tip Deflection vs. Wing Taper Ratio, Biquadratic Pressure Representation

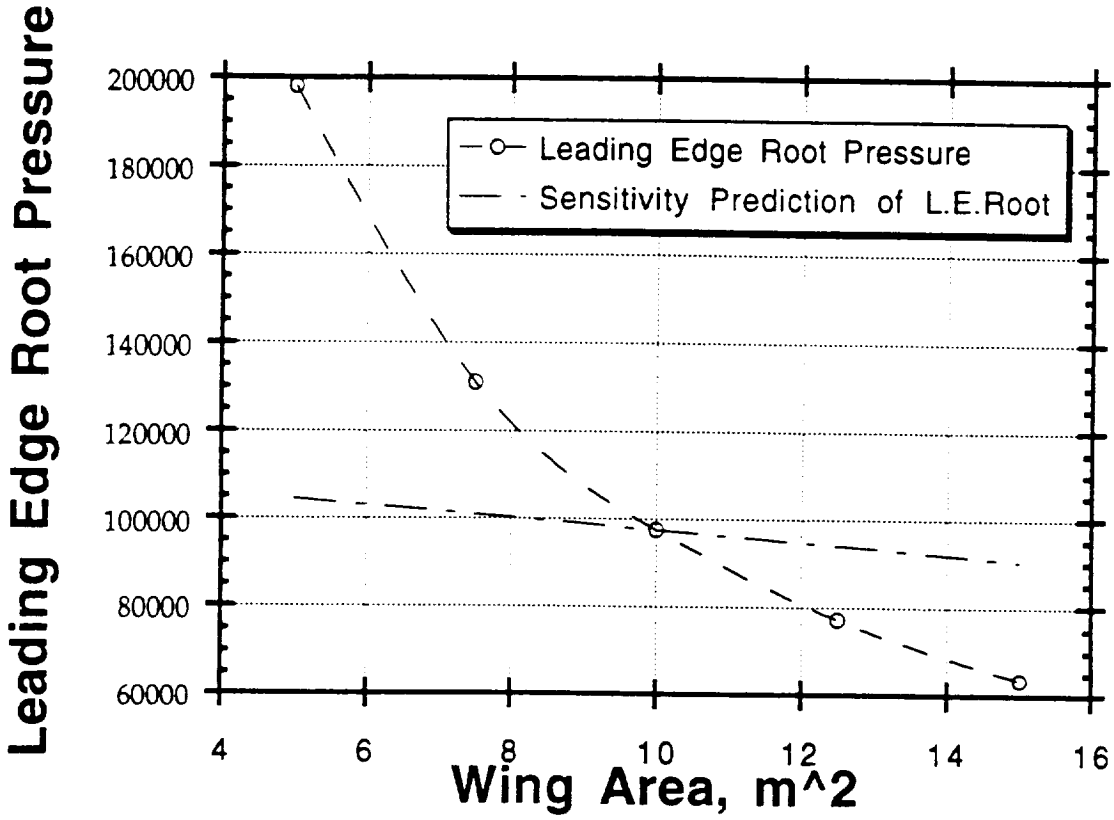

Figure 52. L.E. Root Pressure vs. Area, Biquadratic Pressure Representation

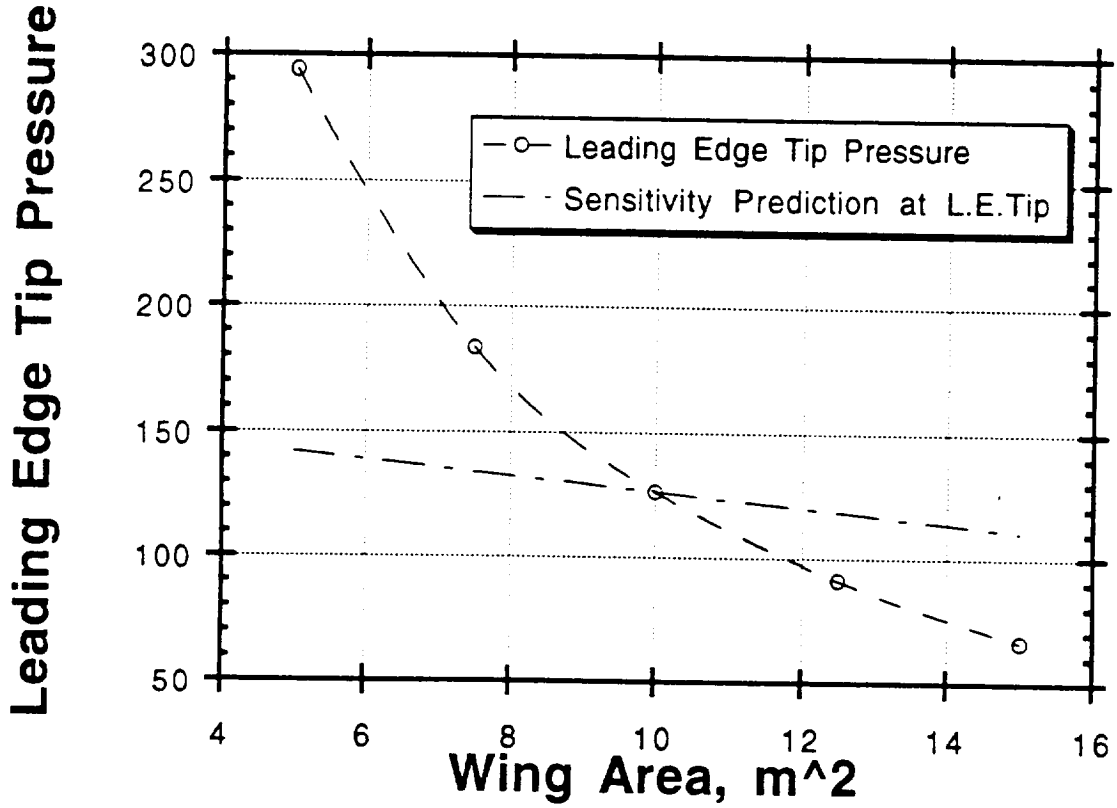

Figure 53. L.E. Tip Pressure vs. Area, Biquadratic Pressure Representation

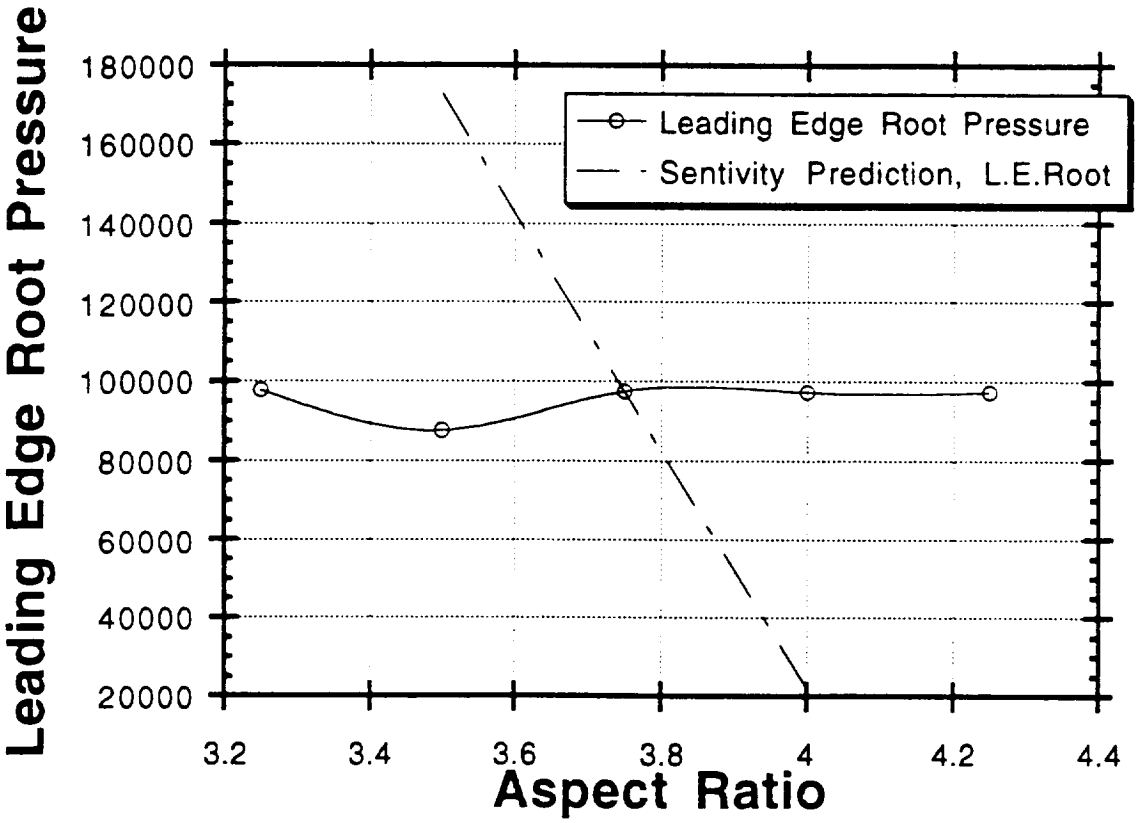

Figure 54. L.E. Root Pressure vs. Aspect Ratio, Biquadratic Pressure Representation

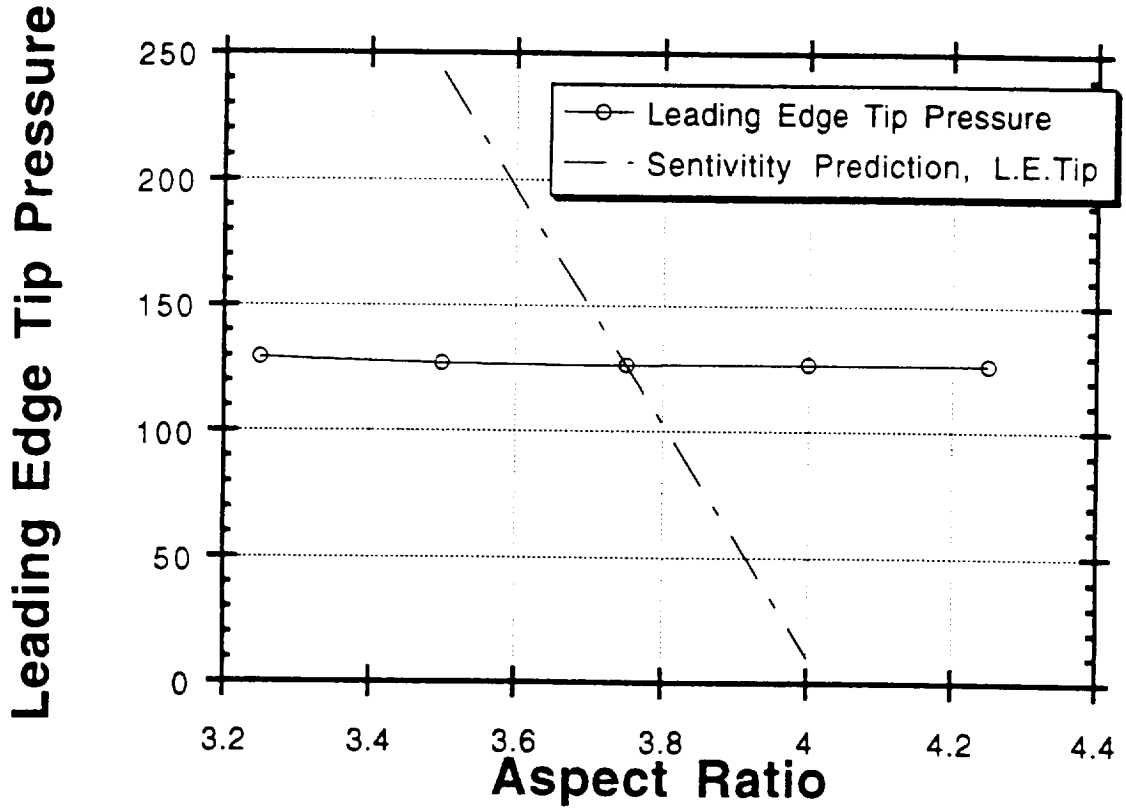

Figure 55. L.E. Tip Pressure vs. Aspect Ratio, Biquadratic Pressure Representation

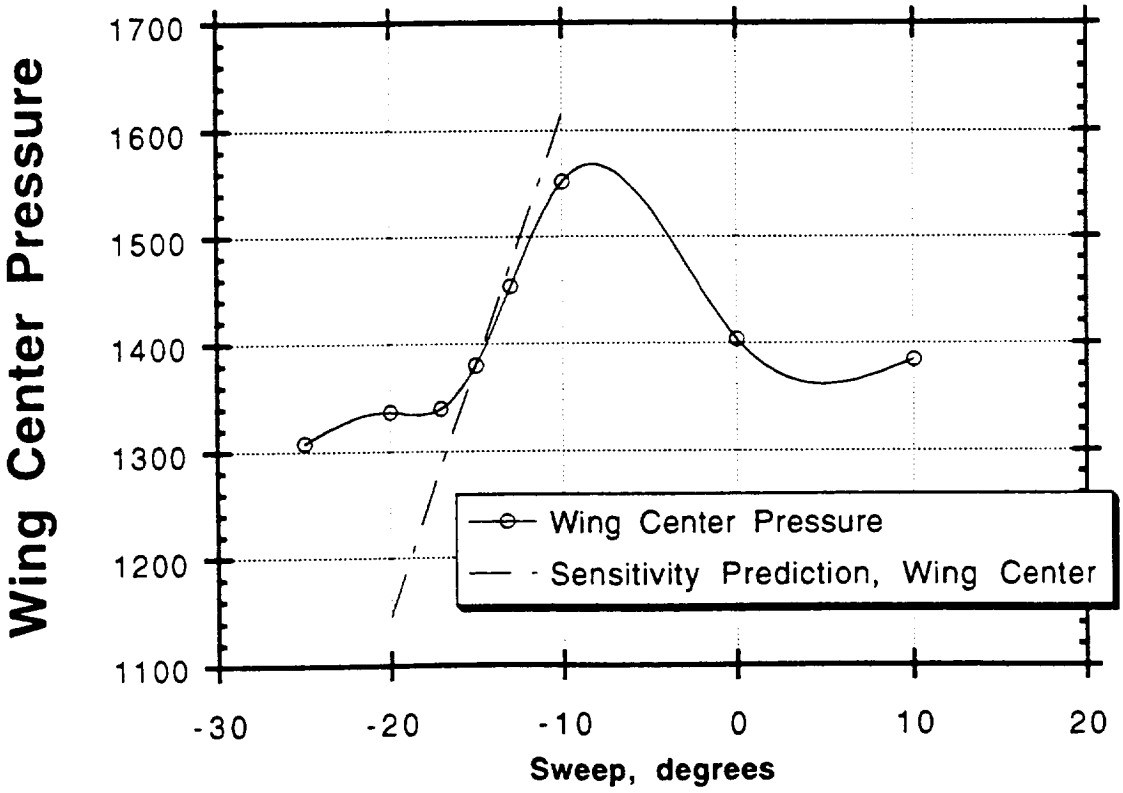

Figure 56. Wing Center Pressure vs. Sweep, Biquadratic Pressure Representation

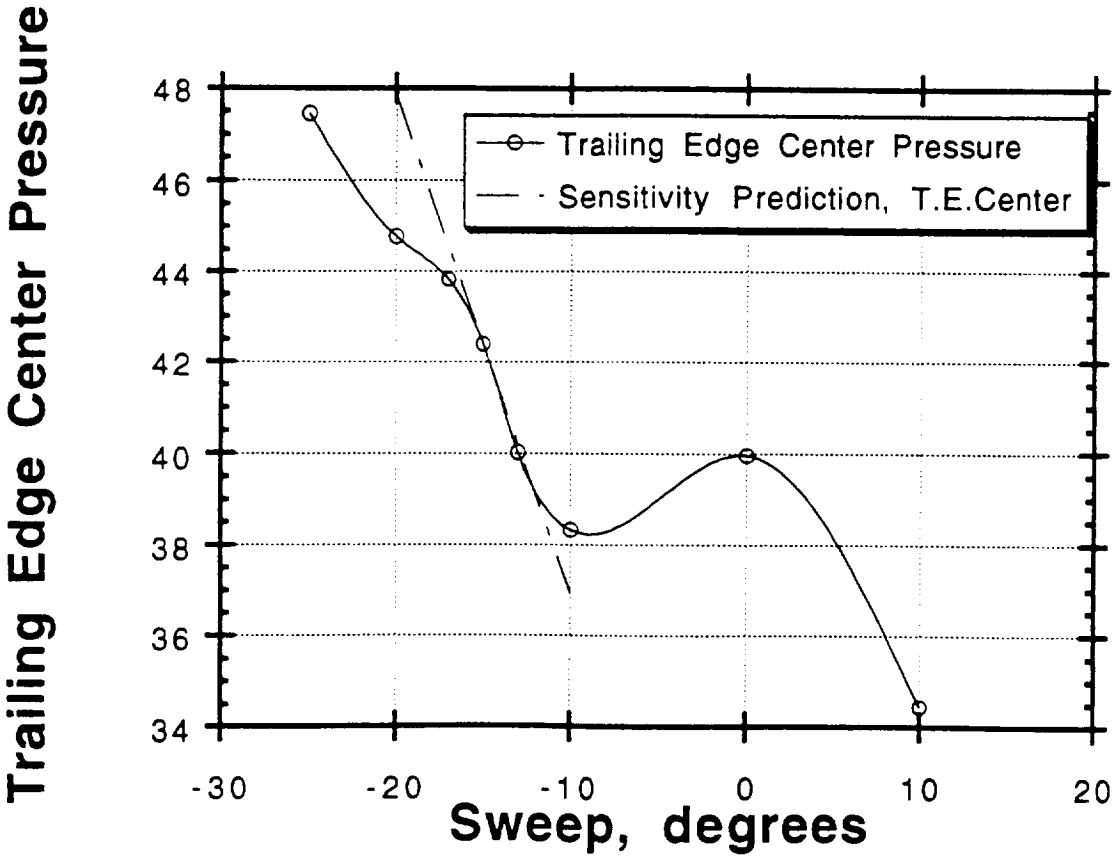

Figure 57. T.E. Center Pressure vs. Sweep, Biquadratic Pressure Representation

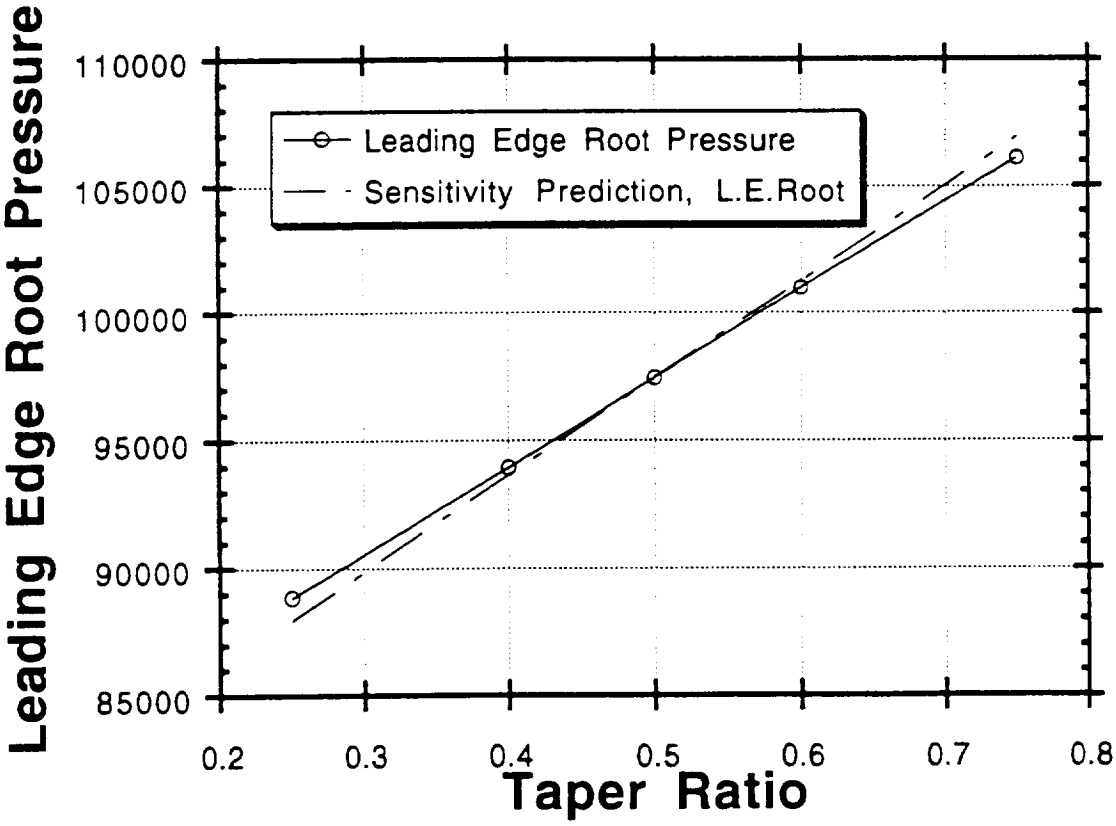

Figure 58. L.E. Root Pressure vs Taper Ratio, Biquadratic Pressure Representation

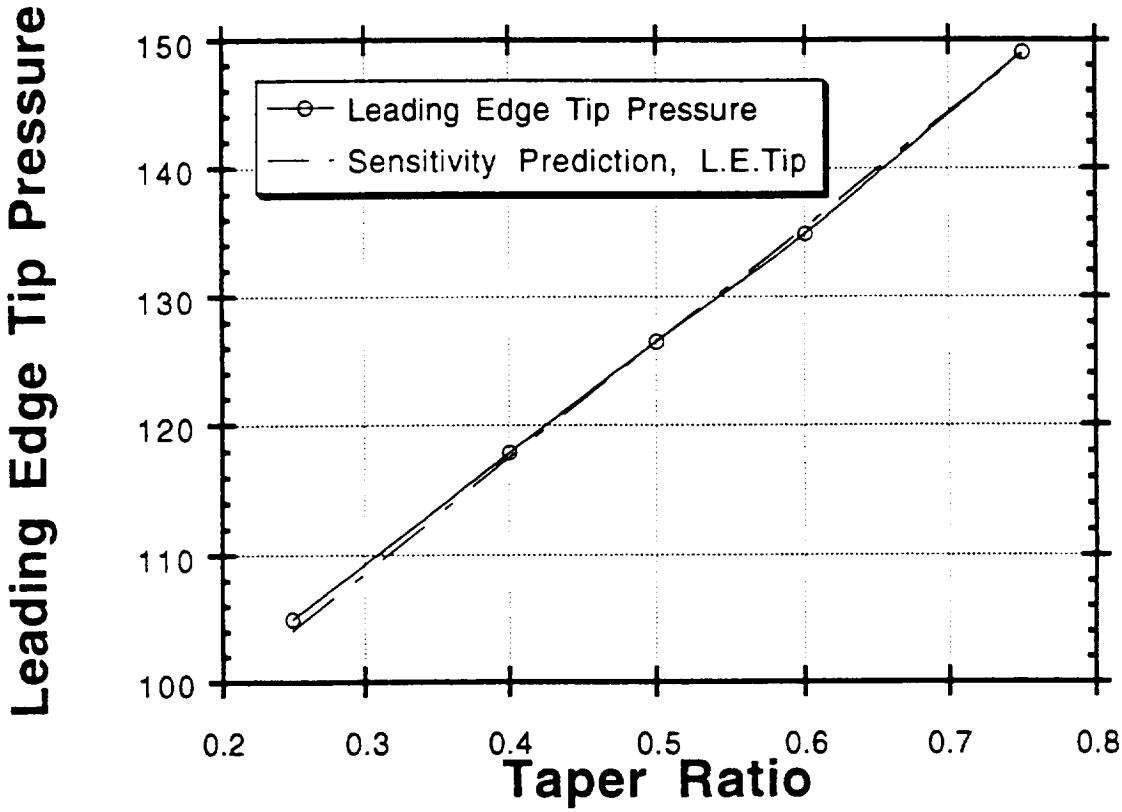

Figure 59. L.E. Tip Pressure vs. Taper Ratio, Biquadratic Pressure Representation

8.0 Method Comparison

In this research, a variation of Sobieski's Global Sensitivity Equations is implemented to obtain the global sensitivity of the static aeroelastic responses. The scheme is independent of the analysis code used to obtain aerodynamic data.

8.1 CPU Time Comparison

Each method produced very similar final results. The remaining question is how well they performed costwise. The following chart shows a comparison of CPU times on the VAX mainframe for a complete analysis run. Here, Nx is the number of pressure nodes in the x, or chord-wise, direction. Ny is the number of pressure nodes in the y, or span-wise, direction.

Table 3: CPU Times

Case		**CPUTime**
		HR : MIN : SEC
Chebyshev		1 : 31 : 55.31
Constant	Nx=Ny=15	1 : 11 : 42.02
Constant	Nx=Ny=39	1 : 24 : 41.62
Bilinear	Nx=Ny=15	1 : 20 : 52.99
Bilinear	Nx=Ny=39	1 : 23 : 00.35
Biquadratic	Nx=Ny=15	1 : 14 : 17.58
Biquadratic	Nx=Ny=39	1 : 24 : 41.40

Thus, the differences in CPU run times for the various schemes and resolutions vary by less than 20%.

8.2 Performance Comparison

The next issue for the local schemes is just how much resolution is necessary. This is not a simple issue.

Tables 4-33 show the various converged results for all three local pressure schemes. A wide range of resolutions is investigated. The tables also list each value's percentage difference from the highest resolution grid's value. These percentage differences give an indication of how well a particular grid has done at producing a converged result. The senstivity derivative charts also give the logarithmic derivative of the highest resolution grid's value. This value gives some indication of how accurately it is possible to model the derivative.

Some grid conclusions are valid across all of the cases. It is obvious that N_x has a much more significant effect on the solution than N_y. This is because the main variation in the pressure field is in the x, or chordwise, direction. A certain minimum resolution in the y, or spanwise, direction seems necessary, perhaps $N_y = 15$. After that, increasing spanwise resolution accomplishes little compared to a similar increase in chordwise resolution.

Since the difference in CPU times between high and low resolution cases is not very large, in most cases running the program at the highest resolution available makes sense. If however, one wishes to minimize the CPU time used, then some choices must be made. One has to decide how close to a converged value one is willing to be. The convergence tables give some qualitative feel for what grid spacings are necessary to be as close as you desire to convergence for a particular technique.

For instance, assume a 10 % difference from the highest resolution value is permissable

for a certain application. A look through the Biquadratic results shows that a 15x15 grid will provide this accuracy. The bilinear approach requires a 15x5 grid to get this result. The constant pressure panel approach requires a 15x15 grid.

The choice of which scheme to use remains. All four schemes work well. Of the three local schemes, the higher order schemes converge faster than the lower schemes, but the difference isn't overwhelming. Since the CPU times for the three schemes are comparable, the biquadratic scheme produces the best results for similar computational effort. However, the polynomial overshoot problems encountered in this approach could be problematical for other cases. The bilinear approach is more robust and only slightly slower to converge.

Table 4. Trim Angle of Attack, Local Constant Pressure Representation

Trim Angle of Attack, Degrees

Local Constant Pressure Representation with Zero Gradient Edges
(percentage difference from 39x39 value)

	$N_y = 5$	N_y=15	N_y=25	N_y=35	Ny=39
N_x=5	5.63679 (4.49%)	5.59279 (5.23%)	5.58864 (5.30%)	5.58747 (5.32%)	5.58724 (5.33%)
N_x=15	5.85874 (0.727%)	5.81303 (1.50%)	5.80872 (1.57%)	5.80747 (1.60%)	5.80720 (1.60%)
N_x=25	5.91893 (0.290%)	5.87255 (0.493%)	5.86821 (0.567%)	5.86694 (0.588%)	5.86670 (0.592%)
N_x=35	5.94700 (0.769%)	5.90062 (0.017%)	5.89623 (0.092%)	5.89498 (0.113%)	5.89472 (0.117%)
N_x=39	5.95400 (0.887%)	5.90755 (0.100%)	5.90317 (0.026%)	5.90193 (0.005%)	5.90164 (0.0%)

Leading Edge Tip Deflection

Local Constant Pressure Representation with Zero Gradient Edges
(percentage difference from 39x39 value)

	$N_y = 5$	N_y=15	N_y=25	N_y=35	Ny=39
N_x=5	0.38294 (1.53%)	0.38684 (0.525%)	0.38731 (0.405%)	0.38745 (0.370%)	0.38748 (0.362%)
N_x=15	0.38443 (1.15%)	0.38834 (0.141%)	0.38881 (0.020%)	0.38895 (0.016%)	0.38897 (0.023%)
N_x=25	0.38440 (1.15%)	0.38831 (0.147%)	0.38878 (0.027%)	0.38892 (0.009%)	0.38895 (0.016%)
N_x=35	0.38435 (1.16%)	0.38826 (0.160%)	0.38873 (0.039%)	0.38887 (0.004%)	0.38890 (0.004%)
N_x=39	0.38434 (1.17%)	0.38825 (0.163%)	0.38872 (0.043%)	0.38885 (0.008%)	0.38888 (0.0%)

Table 5. Leading Edge Tip Deflection, Local Constant Pressure Representation

$d\alpha/dS$

Local Constant Pressure Representation with Zero Gradient Edges
(percentage difference from 39x39 value)

	$N_y = 5$	N_y=15	N_y=25	N_y=35	Ny=39
N_x=5	-0.63289 (4.52%)	-0.63033 (4.90%)	-0.62984 (4.98%)	-0.62994 (4.96%)	-0.62985 (4.98%)
N_x=15	-0.65666 (0.933%)	-0.65366 (1.39%)	-0.65320 (1.46%)	-0.65347 (1.41%)	-0.65323 (1.45%)
N_x=25	-0.66269 (0.024%)	-0.65999 (0.430%)	-0.65939 (0.522%)	-0.65954 (0.499%)	-0.65925 (0.542%)
N_x=35	-0.66565 (0.423%)	-0.66304 (0.029%)	-0.66245 (0.060%)	-0.66254 (0.046%)	-0.66222 (0.095%)
N_x=39	-0.66649 (0.549%)	-0.66332 (0.072%)	-0.66300 (0.023%)	-0.66327 (0.063%)	-0.66285 (0.0%)

Logarithmic Derivative: -1.12315

Table 6. $d\alpha/dS$, Local Constant Pressure Representation

Table 7. dTipDeflection / dS, Local Constant Pressure Representation

dTipDeflection/dS
Local Constant Pressure Representation with Zero Gradient Edges
(percentage difference from 39x39 value)

	$N_y = 5$	N_y=15	N_y=25	N_y=35	Ny=39
N_x=5	3.370×10^{-2} (1.32%)	3.400×10^{-2} (0.437%)	3.402×10^{-2} (0.401%)	3.404×10^{-2} (0.333%)	3.403×10^{-2} (0.350%)
N_x=15	3.383×10^{-2} (0.948%)	3.411×10^{-2} (0.124%)	3.414×10^{-2} (0.020%)	3.417×10^{-2} (0.043%)	3.417×10^{-2} (0.042%)
N_x=25	3.382×10^{-2} (0.962%)	3.411×10^{-2} (0.112%)	3.414×10^{-2} (0.037%)	3.416×10^{-2} (0.020%)	3.416×10^{-2} (0.025%)
N_x=35	3.382×10^{-2} (0.982%)	3.410×10^{-2} (0.144%)	3.414×10^{-2} (0.026%)	3.416×10^{-2} (0.034%)	3.415×10^{-2} (0.005%)
N_x=39	3.382×10^{-2} (0.968%)	3.411×10^{-2} (0.121%)	3.414×10^{-2} (0.034%)	3.415×10^{-2} (0.013%)	3.415×10^{-2} (0.0%)

Logarithmic Derivative: 0.87825

$d\alpha/dAR$

Local Constant Pressure Representation with Zero Gradient Edges
(percentage difference from 39x39 value)

	$N_y = 5$	N_y=15	N_y=25	N_y=35	Ny=39
N_x=5	-0.51897 (12.6%)	-0.53669 (9.66%)	-0.52121 (12.3%)	-0.63050 (6.14%)	-0.53589 (9.79%)
N_x=15	-0.58179 (2.06%)	-0.58693 (1.20%)	-0.55031 (7.36%)	-0.55992 (5.75%)	-0.55041 (7.35%)
N_x=25	-0.59863 (0.771%)	-0.52004 (12.5%)	-0.59675 (0.455%)	-0.56276 (5.27%)	-0.53861 (9.33%)
N_x=35	-0.60087 (1.15%)	-0.59868 (0.780%)	-0.55204 (7.07%)	-0.57248 (3.63%)	-0.53695 (9.61%)
N_x=39	-0.57091 (3.90%)	-0.57658 (2.94%)	-0.54057 (9.00%)	-0.63523 (6.93%)	-0.59405 (0.0%)

Logarithmic Derivative: -0.37747

Table 8. $d\alpha/dAR$, Local Constant Pressure Representation

Table 9. dTipDeflection / dAR, Local Constant Pressure Representation

dTipDeflection/dAR

Local Constant Pressure Representation with Zero Gradient Edges
(percentage difference from 39x39 value)

	$N_y = 5$	N_y=15	N_y=25	N_y=35	Ny=39
N_x=5	0.19335 (1.09%)	0.19524 (0.125%)	0.19699 (0.775%)	0.19714 (0.848%)	0.19799 (1.28%)
N_x=15	0.19461 (0.443%)	0.19627 (0.407%)	0.19542 (0.029%)	0.19450 (0.501%)	0.19542 (0.032%)
N_x=25	0.19397 (0.774%)	0.19501 (0.242%)	0.19702 (0.786%)	0.19501 (0.240%)	0.19625 (0.395%)
N_x=35	0.19464 (0.431%)	0.19577 (0.147%)	0.19442 (0.544%)	0.19555 (0.038%)	0.19621 (0.373%)
N_x=39	0.19299 (1.27%)	0.19561 (0.067%)	0.19476 (0.367%)	0.19701 (0.783%)	0.19548 (0.0%)

Logarithmic Derivative: 1.88501

$d\alpha/d\Lambda$

Local Constant Pressure Representation with Zero Gradient Edges
(percentage difference from 39x39 value)

	$N_y = 5$	N_y=15	N_y=25	N_y=35	Ny=39
N_x=5	3.474×10^{-2} (53.5%)	2.886×10^{-2} (27.5%)	2.915×10^{-2} (28.8%)	2.928×10^{-2} (29.4%)	2.930×10^{-2} (29.5%)
N_x=15	2.924×10^{-2} (29.2%)	2.363×10^{-2} (4.44%)	2.391×10^{-2} (5.65%)	2.403×10^{-2} (6.20%)	2.406×10^{-2} (6.30%)
N_x=25	2.822×10^{-2} (24.7%)	2.267×10^{-2} (0.202%)	2.295×10^{-2} (1.43%)	2.308×10^{-2} (1.98%)	2.310×10^{-2} (2.09%)
N_x=35	2.782×10^{-2} (22.9%)	2.230×10^{-2} (1.46%)	2.256×10^{-2} (0.288%)	2.268×10^{-2} (0.243%)	2.272×10^{-2} (0.380%)
N_x=39	2.772×10^{-2} (22.5%)	2.219×10^{-2} (1.92%)	2.248×10^{-2} (0.662%)	2.260×10^{-2} (0.127%)	2.263×10^{-2} (0.0%)

Logarithmic Derivative: -5.75×10^{-2}

Table 10. $d\alpha/d\Lambda$, Local Constant Pressure Representation

Table 11. dTip Deflection/d Λ, Local Constant Pressure Representation

dTipDeflection/dΛ
Local Constant Pressure Representation with Zero Gradient Edges
(percentage difference from 39x39 value)

	$N_y = 5$	N_y=15	N_y=25	N_y=35	Ny=39
N_x=5	-5.427×10^{-3} (0.784%)	-5.262×10^{-3} (2.29%)	-5.249×10^{-3} (2.53%)	-5.245×10^{-3} (2.59%)	-5.245×10^{-3} (2.60%)
N_x=15	-5.547×10^{-3} (3.01%)	-5.384×10^{-3} (0.008%)	-5.372×10^{-3} (0.242%)	-5.369×10^{-3} (0.303%)	-5.368×10^{-3} (0.311%)
N_x=25	-5.558×10^{-3} (3.21%)	-5.396×10^{-3} (0.202%)	-5.384×10^{-3} (0.017%)	-5.381×10^{-3} (0.074%)	-5.380×10^{-3} (0.086%)
N_x=35	-5.561×10^{-3} (3.27%)	-5.400×10^{-3} (0.286%)	-5.388×10^{-3} (0.054%)	-5.384×10^{-3} (0.009%)	-5.383×10^{-3} (0.033%)
N_x=39	-5.562×10^{-3} (3.29%)	-5.401×10^{-3} (0.296%)	-5.388×10^{-3} (0.060%)	-5.385×10^{-3} (0.004%)	-5.385×10^{-3} (0.0%)

Logarithmic Derivative: 0.20771

$d\alpha/d\lambda$

Local Constant Pressure Representation with Zero Gradient Edges
(percentage difference from 39x39 value)

	$N_y = 5$	N_y=15	N_y=25	N_y=35	Ny=39
N_x=5	-0.18999 (35.3%)	-0.27932 (4.87%)	-0.29077 (2.17%)	-0.28959 (1.37%)	-0.29028 (1.13%)
N_x=15	-0.18872 (35.7%)	-0.28202 (3.95%)	-0.29077 (0.965%)	-0.29274 (0.295%)	-0.29274 (0.297%)
N_x=25	-0.18787 (36.0%)	-0.28206 (3.93%)	-0.28963 (1.35%)	-0.29250 (0.376%)	-0.29336 (0.083%)
N_x=35	-0.18725 (36.2%)	-0.28206 (4.07%)	-0.28980 (1.30%)	-0.29283 (0.264%)	-0.29329 (0.109%)
N_x=39	-0.18756 (36.1%)	-0.28224 (3.87%)	-0.29018 (1.17%)	-0.29255 (0.361%)	-0.29361 (0.0%)

Logarithmic Derivative: -2.49×10^{-2}

Table 12. $d\alpha/d\lambda$, Local Constant Pressure Representation

dTipDeflection/dλ
Local Constant Pressure Representation with Zero Gradient Edges
(percentage difference from 39x39 value)

	$N_y = 5$	N_y=15	N_y=25	N_y=35	Ny=39
N_x=5	0.22339 (5.76%)	0.21184 (0.296%)	0.21082 (0.186%)	0.21061 (0.286%)	0.21054 (0.320%)
N_x=15	0.22420 (6.15%)	0.21249 (0.602%)	0.21154 (0.151%)	0.21130 (0.042%)	0.21124 (0.011%)
N_x=25	0.22420 (6.15%)	0.21250 (0.608%)	0.21155 (0.159%)	0.21129 (0.034%)	0.21123 (0.008%)
N_x=35	0.22420 (6.15%)	0.21247 (0.594%)	0.21151 (0.137%)	0.21127 (0.025%)	0.21120 (0.006%)
N_x=39	0.22415 (6.12%)	0.21245 (0.586%)	0.21152 (0.145%)	0.21127 (0.024%)	0.21122 (0.0%)

Logarithmic Derivative: 0.27157

Table 13. dTip Deflection/d λ, Local Constant Pressure Representation

Table 14. Trim Angle of Attack, Local Bilinear Pressure Representation

Trim Angle of Attack, Degrees

Local Bilinear Pressure Representation with Zero Gradient Edges
(percentage difference from 39x39 value)

	$N_y = 5$	N_y=15	N_y=25	N_y=35	Ny=39
N_x=5	5.62957 (4.61%)	5.58954 (5.29%)	5.58563 (5.35%)	5.58449 (5.37%)	5.58429 (5.38%)
N_x=15	5.85385 (0.808%)	5.81228 (1.51%)	5.80819 (1.58%)	5.80703 (1.60%)	5.80677 (1.61%)
N_x=25	5.91405 (0.212%)	5.87204 (0.500%)	5.86794 (0.570%)	5.86673 (0.590%)	5.86649 (0.594%)
N_x=35	5.94236 (0.691%)	5.90017 (0.024%)	5.89605 (0.093%)	5.89481 (0.114%)	5.89459 (0.118%)
N_x=39	5.94936 (0.810%)	5.90715 (0.095%)	5.90298 (0.024%)	5.90178 (0.004%)	5.90156 (0.0%)

Leading Edge Tip Deflection
Local Bilinear Pressure Representation with Zero Gradient Edges
(percentage difference from 39x39 value)

	$N_y = 5$	N_y=15	N_y=25	N_y=35	Ny=39
N_x=5	0.38185 (1.81%)	0.38740 (0.378%)	0.38798 (0.229%)	0.38815 (0.185%)	0.38819 (0.176%)
N_x=15	0.38269 (1.59%)	0.38826 (0.158%)	0.38884 (0.008%)	0.38901 (0.036%)	0.38905 (0.045%)
N_x=25	0.38260 (1.61%)	0.38817 (0.180%)	0.38875 (0.031%)	0.38892 (0.013%)	0.38896 (0.022%)
N_x=35	0.38254 (1.63%)	0.38810 (0.197%)	0.38869 (0.048%)	0.38886 (0.004%)	0.38889 (0.005%)
N_x=39	0.38252 (1.63%)	0.38809 (0.202%)	0.38867 (0.052%)	0.38884 (0.008%)	0.38887 (0.0%)

Table 15. Leading Edge Tip Deflection, Local Bilinear Pressure Representation

$d\alpha/dS$

Local Bilinear Pressure Representation with Zero Gradient Edges
(percentage difference from 39x39 value)

	$N_y = 5$	N_y=15	N_y=25	N_y=35	Ny=39
N_x=5	-0.63269 (4.54%)	-0.63036 (4.89%)	-0.63012 (4.93%)	-0.62981 (4.98%)	-0.62986 (4.97%)
N_x=15	-0.65592 (1.04%)	-0.65354 (1.40%)	-0.65324 (1.44%)	-0.65326 (1.44%)	-0.65308 (1.47%)
N_x=25	-0.66228 (0.078%)	-0.65974 (0.461%)	-0.65942 (0.510%)	-0.65977 (0.457%)	-0.65934 (0.521%)
N_x=35	-0.66545 (0.401%)	-0.66273 (0.010%)	-0.66254 (0.038%)	-0.66227 (0.080%)	-0.66244 (0.054%)
N_x=39	-0.66587 (0.464%)	-0.66353 (0.111%)	-0.66302 (0.033%)	-0.66326 (0.069%)	-0.66280 (0.0%)

Logarithmic Derivative: -1.12328

Table 16. *dα/dS*, Local Bilinear Pressure Representation

dTipDeflection/dS
Local Bilinear Pressure Representation with Zero Gradient Edges
(percentage difference from 39x39 value)

	$N_y = 5$	$N_y=15$	$N_y=25$	$N_y=35$	Ny=39
$N_x=5$	3.356×10^{-2} (1.73%)	3.402×10^{-2} (0.369%)	3.408×10^{-2} (0.208%)	3.409×10^{-2} (0.170%)	3.409×10^{-2} (0.166%)
$N_x=15$	3.365×10^{-2} (1.47%)	3.410×10^{-2} (0.140%)	3.414×10^{-2} (0.021%)	3.416×10^{-2} (0.039%)	3.416×10^{-2} (0.044%)
$N_x=25$	3.364×10^{-2} (1.50%)	3.409×10^{-2} (0.172%)	3.415×10^{-2} (0.003%)	3.416×10^{-2} (0.032%)	3.416×10^{-2} (0.017%)
$N_x=35$	3.362×10^{-2} (1.54%)	3.409×10^{-2} (0.161%)	3.415×10^{-2} (0.013%)	3.415×10^{-2} (0.009%)	3.415×10^{-2} (0.013%)
$N_x=39$	3.364×10^{-2} (1.50%)	3.409×10^{-2} (0.181%)	3.414×10^{-2} (0.028%)	3.415×10^{-2} (0.007%)	3.415×10^{-2} (0.0%)

Logarithmic Derivative: 0.87827

Table 17. dTipDeflection / dS, Local Bilinear Pressure Representation

$d\alpha/dAR$

Local Bilinear Pressure Representation with Zero Gradient Edges
(percentage difference from 39x39 value)

	$N_y = 5$	N_y=15	N_y=25	N_y=35	Ny=39
N_x=5	-0.55212 (9.82%)	-0.53544 (6.50%)	-0.53018 (5.45%)	-0.56241 (11.9%)	-0.55457 (10.3%)
N_x=15	-0.58632 (16.6%)	-0.57447 (14.3%)	-0.50664 (0.770%)	-0.54610 (8.62%)	-0.58610 (16.6%)
N_x=25	-0.59189 (17.7%)	-0.53844 (7.09%)	-0.57613 (14.6%)	-0.56644 (12.7%)	-0.58734 (16.8%)
N_x=35	-0.58232 (15.8%)	-0.56233 (11.8%)	-0.60060 (19.5%)	-0.55088 (9.57%)	-0.60950 (21.2%)
N_x=39	-0.57146 (13.7%)	-0.50848 (5.45%)	-0.54456 (8.31%)	-0.57537 (14.4%)	-0.50277 (0.0%)

Logarithmic Derivative: -0.56865

Table 18. *dα/dAR*, Local Bilinear Pressure Representation

Table 19. dTipDeflection / dAR, Local Bilinear Pressure Representation

dTipDeflection/dAR
Local Bilinear Pressure Representation with Zero Gradient Edges
(percentage difference from 39x39 value)

	$N_y = 5$	N_y=15	N_y=25	N_y=35	Ny=39
N_x=5	0.19442 (0.429%)	0.19838 (1.60%)	0.19560 (0.172%)	0.19636 (0.564%)	0.19504 (0.114%)
N_x=15	0.19159 (1.88%)	0.19536 (0.050%)	0.19741 (1.10%)	0.19663 (0.700%)	0.19673 (0.754%)
N_x=25	0.19177 (1.79%)	0.19604 (0.399%)	0.19716 (1.01%)	0.19517 (0.044%)	0.19657 (0.670%)
N_x=35	0.19522 (0.020%)	0.19700 (0.891%)	0.19583 (0.290%)	0.19802 (1.41%)	0.19541 (0.074%)
N_x=39	0.19097 (2.20%)	0.19508 (0.095%)	0.19585 (0.302%)	0.19572 (0.238%)	0.19526 (0.0%)

Logarithmic Derivative: 1.87290

$d\alpha/d\Lambda$

Local Bilinear Pressure Representation with Zero Gradient Edges
(percentage difference from 39x39 value)

	$N_y = 5$	N_y=15	N_y=25	N_y=35	Ny=39
N_x=5	2.185×10^{-2} (2.48%)	2.641×10^{-2} (17.9%)	2.759×10^{-2} (23.1%)	2.798×10^{-2} (24.9%)	2.806×10^{-2} (25.2%)
N_x=15	1.790×10^{-2} (20.1%)	2.214×10^{-2} (1.17%)	2.328×10^{-2} (3.876%)	2.364×10^{-2} (5.52%)	2.372×10^{-2} (5.86%)
N_x=25	1.703×10^{-2} (24.0%)	2.128×10^{-2} (5.03%)	2.241×10^{-2} (0.034%)	2.277×10^{-2} (1.60%)	2.284×10^{-2} (1.93%)
N_x=35	1.669×10^{-2} (25.5%)	2.092×10^{-2} (6.64%)	2.205×10^{-2} (1.586%)	2.241×10^{-2} (0.032%)	2.249×10^{-2} (0.349%)
N_x=39	1.661×10^{-2} (25.9%)	2.084×10^{-2} (7.00%)	2.197×10^{-2} (1.97%)	2.233×10^{-2} (0.364%)	2.241×10^{-2} (0.0%)

Logarithmic Derivative: -5.70×10^{-2}

Table 20. $d\alpha/d\Lambda$, Local Bilinear Pressure Representation

Table 21. dTip Deflection/d Λ, Local Bilinear Pressure Representation

dTipDeflection/dΛ
Local Bilinear Pressure Representation with Zero Gradient Edges
(percentage difference from 39x39 value)

	$N_y = 5$	N_y=15	N_y=25	N_y=35	Ny=39
N_x=5	-5.341×10^{-3} (0.779%)	-5.285×10^{-3} (1.82%)	-5.281×10^{-3} (1.89%)	-5.280×10^{-3} (1.91%)	-5.280×10^{-3} (1.92%)
N_x=15	-5.429×10^{-3} (0.847%)	-5.374×10^{-3} (0.171%)	-5.371×10^{-3} (0.225%)	-5.371×10^{-3} (0.227%)	-5.370×10^{-3} (0.239%)
N_x=25	-5.437×10^{-3} (0.998%)	-5.383×10^{-3} (0.003%)	-5.380×10^{-3} (0.059%)	-5.379×10^{-3} (0.070%)	-5.379×10^{-3} (0.072%)
N_x=35	-5.440×10^{-3} (1.05%)	-5.386×10^{-3} (0.051%)	-5.383×10^{-3} (0.001%)	-5.383×10^{-3} (0.011%)	-5.382×10^{-3} (0.013%)
N_x=39	-5.440×10^{-3} (1.06%)	-5.387×10^{-3} (0.070%)	-5.384×10^{-3} (0.009%)	-5.383×10^{-3} (0.006%)	-5.383×10^{-3} (0.0%)

Logarithmic Derivative: 0.20764

$d\alpha/d\lambda$

Local Bilinear Pressure Representation with Zero Gradient Edges
(percentage difference from 39x39 value)

	$N_y = 5$	N_y=15	N_y=25	N_y=35	Ny=39
N_x=5	-0.18013 (38.5%)	-0.27965 (4.58%)	-0.28801 (1.72%)	-0.29100 (0.701%)	-0.29095 (0.720%)
N_x=15	-0.17859 (39.1%)	-0.28131 (4.01%)	-0.29008 (1.02%)	-0.29219 (0.294%)	-0.29275 (0.104%)
N_x=25	-0.17771 (39.4%)	-0.28142 (3.97%)	-0.29006 (1.02%)	-0.29246 (0.204%)	-0.29330 (0.082%)
N_x=35	-0.17702 (39.6%)	-0.28121 (4.04%)	-0.29003 (1.03%)	-0.29291 (0.051%)	-0.29298 (0.027%)
N_x=39	-0.17680 (39.7%)	-0.28107 (4.09%)	-0.29068 (0.812%)	-0.29262 (0.149%)	-0.29306 (0.0%)

Logarithmic Derivative: -2.49×10^{-2}

Table 22. $d\alpha/d\lambda$, Local Bilinear Pressure Representation

Table 23. dTip Deflection/d λ, Local Bilinear Pressure Representation

dTipDeflection/dλ
Local Bilinear Pressure Representation with Zero Gradient Edges
(percentage difference from 39x39 value)

	$N_y = 5$	N_y=15	N_y=25	N_y=35	Ny=39
N_x=5	0.21531 (1.80%)	0.21118 (0.150%)	0.21091 (0.280%)	0.21083 (0.319%)	0.21081 (0.326%)
N_x=15	0.21569 (1.98%)	0.21149 (0.003%)	0.21122 (0.133%)	0.21116 (0.164%)	0.21115 (0.166%)
N_x=25	0.21565 (1.96%)	0.21145 (0.024%)	0.21173 (0.107%)	0.21113 (0.174%)	0.21111 (0.186%)
N_x=35	0.21563 (1.95%)	0.21145 (0.026%)	0.21118 (0.154%)	0.21109 (0.197%)	0.21107 (0.203%)
N_x=39	0.21562 (1.95%)	0.21144 (0.030%)	0.21112 (0.180%)	0.21108 (0.200%)	0.21150 (0.0%)

Logarithmic Derivative: 0.27136

Table 24. Trim Angle of Attack, Local Biquadratic Pressure Representation

Trim Angle of Attack, Degrees
Local Biquadratic Pressure Representation
(percentage difference from 39x39 value)

	$N_y = 5$	N_y=15	N_y=25	N_y=35	Ny=39
N_x=5	5.48210 (7.04%)	5.43253 (7.88%)	5.43140 (7.90%)	5.43120 (7.90%)	5.43119 (7.90%)
N_x=15	5.84153 (0.943%)	5.78820 (1.85%)	5.78704 (1.87%)	5.78684 (1.87%)	5.78682 (1.87%)
N_x=25	5.91327 (0.273%)	5.85923 (0.643%)	5.85805 (0.663%)	5.85786 (0.666%)	5.85782 (0.667%)
N_x=35	5.94483 (0.809%)	5.89055 (0.112%)	5.88936 (0.132%)	5.88914 (0.136%)	5.88913 (0.136%)
N_x=39	5.95289 (0.945%)	5.89855 (0.024%)	5.89737 (0.004%)	5.98719 (0.0006%)	5.89715 (0.0%)

Table 25. Leading Edge Tip Deflection, Local Biquadratic Pressure Representation

Leading Edge Tip Deflection
Local Biquadratic Pressure Representation
(percentage difference from 39x39 value)

	$N_y = 5$	N_y=15	N_y=25	N_y=35	Ny=39
N_x=5	0.38146 (1.95%)	0.39013 (0.279%)	0.39039 (0.346%)	0.39044 (0.358%)	0.39044 (0.359%)
N_x=15	0.38051 (2.19%)	0.38915 (0.027%)	0.38941 (0.093%)	0.38945 (0.104%)	0.38946 (0.106%)
N_x=25	0.38024 (2.26%)	0.38888 (0.042%)	0.38914 (0.024%)	0.38918 (0.035%)	0.38919 (0.037%)
N_x=35	0.38013 (2.29%)	0.38877 (0.071%)	0.38903 (0.005%)	0.38907 (0.006%)	0.38907 (0.007%)
N_x=39	0.38010 (2.30%)	0.38874 (0.078%)	0.38900 (0.012%)	0.38904 (0.001%)	0.38904 (0.0%)

Table 26. $d\alpha/dS$, Local Biquadratic Pressure Representation

$d\alpha/dS$
Local Biquadratic Pressure Representation
(percentage difference from 39x39 value)

	$N_y = 5$	N_y=15	N_y=25	N_y=35	Ny=39
N_x=5	-0.61947 (6.54%)	-0.61419 (7.34%)	-0.61431 (7.32%)	-0.61409 (7.35%)	-0.61421 (7.33%)
N_x=15	-0.65702 (0.874%)	-0.65128 (1.74%)	-0.65129 (1.74%)	-0.65116 (1.76%)	-0.65121 (1.75%)
N_x=25	-0.66440 (0.240%)	-0.65839 (0.667%)	-0.65848 (0.653%)	-0.65836 (0.671%)	-0.65883 (0.601%)
N_x=35	-0.66786 (0.761%)	-0.66146 (0.204%)	-0.66167 (0.173%)	-0.66161 (0.182%)	-0.66162 (0.181%)
N_x=39	-0.66876 (0.897%)	-0.66247 (0.052%)	-0.66243 (0.058%)	-0.66263 (0.028%)	-0.66281 (0.0%)

Logarithmic Derivative: -1.12396

Table 27. dTipDeflection / dS, Local Biquadratic Pressure Representation

dTipDeflection/dS
Local Biquadratic Pressure Representation
(percentage difference from 39x39 value)

	$N_y = 5$	$N_y=15$	$N_y=25$	$N_y=35$	Ny=39
$N_x=5$	0.38146 (1016%)	3.425×10^{-2} (0.239%)	3.427×10^{-2} (0.269%)	3.429×10^{-2} (0.331%)	3.428×10^{-2} (0.298%)
$N_x=15$	3.346×10^{-2} (2.08%)	3.417×10^{-2} (0.028%)	3.419×10^{-2} (0.054%)	3.419×10^{-2} (0.053%)	3.420×10^{-2} (0.086%)
$N_x=25$	3.344×10^{-2} (2.15%)	3.416×10^{-2} (0.047%)	3.417×10^{-2} (0.004%)	3.418×10^{-2} (0.010%)	3.417×10^{-2} (0.008%)
$N_x=35$	3.342×10^{-2} (2.20%)	3.414×10^{-2} (0.091%)	3.416×10^{-2} (0.037%)	3.417×10^{-2} (0.004%)	3.416×10^{-2} (0.037%)
$N_x=39$	3.343×10^{-2} (2.18%)	3.414×10^{-2} (0.111%)	3.417×10^{-2} (0.021%)	3.417×10^{-2} (0.027%)	3.418×10^{-2} (0.0%)

Logarithmic Derivative: 0.80755

Table 28. *dα/dAR*, Local Biquadratic Pressure Representation

$d\alpha/dAR$
Local Biquadratic Pressure Representation
(percentage difference from 39x39 value)

	$N_y = 5$	$N_y=15$	$N_y=25$	$N_y=35$	Ny=39
$N_x=5$	-0.56738 (1.21%)	-0.54087 (3.52%)	-0.49941 (10.9%)	-0.58304 (4.00%)	-0.53266 (4.99%)
$N_x=15$	-0.56117 (0.100%)	-0.54882 (2.10%)	-0.62450 (11.4%)	-0.51247 (8.59%)	-0.59946 (6.93%)
$N_x=25$	-0.58890 (5.05%)	-0.55829 (0.414%)	-0.58667 (4.65%)	-0.49677 (11.4%)	-0.56710 (1.16%)
$N_x=35$	-0.57685 (2.90%)	-0.51383 (8.35%)	-0.60211 (7.40%)	-0.59464 (6.07%)	-0.58032 (3.52%)
$N_x=39$	-0.56466 (0.722%	-0.54942 (2.00%)	-0.61138 (9.06%)	-0.63159 (12.7%)	-0.56061 (0.0%)

Logarithmic Derivative: -0.35649

Table 29. dTipDeflection / dAR, Local Biquadratic Pressure Representation

dTipDeflection/dAR
Local Biquadratic Pressure Representation
(percentage difference from 39x39 value)

	$N_y = 5$	N_y=15	N_y=25	N_y=35	Ny=39
N_x=5	0.19069 (3.18%)	0.19637 (0.299%)	0.19567 (0.652%)	0.19550 (0.740%)	0.19384 (1.58%)
N_x=15	0.19246 (2.28%)	0.19589 (0.541%)	0.19788 (0.468%)	0.19770 (0.379%)	0.19551 (0.966%)
N_x=25	0.19050 (3.28%)	0.19753 (0.290%)	0.19647 (0.245%)	0.19673 (0.115%)	0.19647 (0.244%)
N_x=35	0.19169 (2.67%)	0.19591 (0.532%)	0.19551 (0.733%)	0.19533 (0.823%)	0.19623 (0.368%)
N_x=39	0.19105 (3.00%)	0.19626 (0.352%)	0.19779 (0.424%)	0.19667 (0.145%)	0.19695 (0.0%)

Logarithmic Derivative: 1.89844

Table 30. $d\alpha/d\Lambda$, Local Biquadratic Pressure Representation

$d\alpha/d\Lambda$
Local Biquadratic Pressure Representation
(percentage difference from 39x39 value)

	$N_y = 5$	$N_y=15$	$N_y=25$	$N_y=35$	Ny=39
$N_x=5$	-2.110×10^{-3} (109%)	2.582×10^{-2} (14.4%)	2.730×10^{-2} (20.9%)	2.757×10^{-2} (22.1%)	2.762×10^{-2} (22.3%)
$N_x=15$	-5.690×10^{-3} (125%)	2.208×10^{-2} (2.20%)	2.352×10^{-2} (4.17%)	2.378×10^{-2} (5.34%)	2.383×10^{-2} (5.54%)
$N_x=25$	-6.384×10^{-3} (128%)	2.126×10^{-2} (5.81%)	2.269×10^{-2} (0.492%)	2.294×10^{-2} (1.62%)	2.298×10^{-2} (1.80%)
$N_x=35$	-6.651×10^{-3} (129%)	2.094×10^{-2} (7.25%)	2.237×10^{-2} (0.926%)	2.261×10^{-2} (0.158%)	2.266×10^{-2} (0.366%)
$N_x=39$	-6.714×10^{-3} (130%)	2.086×10^{-2} (7.58%)	2.230×10^{-2} (1.24%)	2.253×10^{-2} (0.192%)	2.258×10^{-2} (0.0%)

Logarithmic Derivative: -5.74×10^{-2}

Table 31. dTip Deflection/d Λ, Local Biquadratic Pressure Representation

dTipDeflection/dΛ
Local Biquadratic Pressure Representation
(percentage difference from 39x39 value)

	$N_y = 5$	N_y=15	N_y=25	N_y=35	Ny=39
N_x=5	-5.192×10^{-3} (3.57%)	-5.354×10^{-3} (0.566%)	-5.357×10^{-3} (0.496%)	-5.358×10^{-3} (0.476%)	-5.359×10^{-3} (0.471%)
N_x=15	-5.243×10^{-3} (2.61%)	-5.377×10^{-3} (0.125%)	-5.380×10^{-3} (0.077%)	-5.381×10^{-3} (0.062%)	-5.380×10^{-3} (0.068%)
N_x=25	-5.244×10^{-3} (2.59%)	-5.379×10^{-3} (0.091%)	-5.383×10^{-3} (0.027%)	-5.383×10^{-3} (0.026%)	-5.382×10^{-3} (0.035%)
N_x=35	-5.246×10^{-3} (2.57%)	-5.380×10^{-3} (0.065%)	-5.383×10^{-3} (0.010%)	-5.384×10^{-3} (0.0002%)	-5.384×10^{-3} (0.001%)
N_x=39	-5.247×10^{-3} (2.55%)	-5.380×10^{-3} (0.068%)	-5.384×10^{-3} (0.008%)	-5.384×10^{-3} (0.005%)	-5.384×10^{-3} (0.0%)

Logarithmic Derivative: 0.20758

Table 32. $d\alpha/d\lambda$, Local Biquadratic Pressure Representation

$d\alpha/d\lambda$
Local Biquadratic Pressure Representation
(percentage difference from 39x39 value)

	$N_y = 5$	N_y=15	N_y=25	N_y=35	Ny=39
N_x=5	-0.26751 (9.35%)	-0.28939 (1.94%)	-0.29215 (1.00%)	-0.29228 (0.959%)	-0.29195 (1.07%)
N_x=15	-0.26875 (8.93%)	-0.29155 (1.20%)	-0.29388 (0.417%)	-0.29533 (0.075%)	-0.29481 (0.102%)
N_x=25	-0.26779 (9.26%)	-0.29155 (1.21%)	-0.29457 (0.182%)	-0.29540 (0.100%)	-0.29493 (0.061%)
N_x=35	-0.26774 (9.28%)	-0.29168 (1.16%)	-0.29513 (0.007%)	-0.29490 (0.072%)	-0.29577 (0.224%)
N_x=39	-0.26793 (9.21%)	-0.29180 (1.12%)	-0.29454 (0.193%)	-0.29510 (0.004%)	-0.29511 (0.0%)

Logarithmic Derivative: -2.50×10^{-2}

Table 33. dTip Deflection/d λ, Local Biquadratic Pressure Representation

dTipDeflection/dλ
Local Biquadratic Pressure Representation
(percentage difference from 39x39 value)

	$N_y = 5$	N_y=15	N_y=25	N_y=35	Ny=39
N_x=5	0.21073 (0.135%)	0.21117 (0.074%)	0.21123 (0.103%)	0.21123 (0.100%)	0.21125 (0.110%)
N_x=15	0.21066 (0.166%)	0.21110 (0.039%)	0.21117 (0.073%)	0.21119 (0.081%)	0.21120 (0.087%)
N_x=25	0.21054 (0.225%)	0.21101 (0.003%)	0.21107 (0.029%)	0.21109 (0.036%)	0.21108 (0.030%)
N_x=35	0.21046 (0.261%)	0.21094 (0.033%)	0.21101 (0.036%)	0.21105 (0.015%)	0.21102 (0.047%)
N_x=39	0.21045 (0.268%)	0.21093 (0.040%)	0.21103 (0.008%)	0.21104 (0.010%)	0.21101 (0.0%)

Logarithmic Derivative: 0.27119

9.0 Conclusions

The results show good accuracy for integrated quantities such as tip displacements but less accuracy for individual displacement coefficients or trim angle of attack. In general, the accuracy decreases noticably when the size of the logarithmic derivative decreases.

The global sensitivity approach does an excellent job of predicting global sensitivities with the input of just local sensitivities. It does this without the expense of multiple runs of an entire aeroelastic system.

A few of the capabilities of the current system have never been explored, and could expand the utility of the system. The aerodynamic-code input filter code supports cambered and twisted wings, for instance. The system also allows easy replacement of the various modules with higher performance models. A non-linear aerodynamic code or a fancier structural module could be easily integrated into the system.

The code implemented for this research can be of significant utility in the early configuration determining stage of a design project. Coupled with an appropriate optimizer, the code could produce a reasonable baseline design for a minimum effort.

References

1. Adelman, H.M., and Haftka, R. T., *Sensitivity Analysis in Engineering* NASA, CP-2457, 1987.

2. Adelman, H.M. and Haftka, R. T., "Sensitivity Analysis of Discrete Structural Systems," *AIAA Journal*, Vol. 24, No. 5, May 1986, pp. 823-832.

3. Hawk, J.D., and Bristow, D. R., "Development of MCAERO Wing Design Panel Method with Interactive Graphics Module," NASA CR- 3775.

4. Yates, E.C., Jr., "Aerodynamic Sensitivities From Subsonic, Sonic, and Supersonic Unsteady, Nonplanar Lifting Surface Theory," NASA TM-100502, 1987.

5. Haftka, R.T., and Yates, E.C., "Repetitive Flutter Calculations in Structural Design," *Journal of Aircraft*, Vol.13, No. 7, July 1976, pp. 456-461.

6. Haftka R.T., Grossman, B., Eppard, W. M., and Kao, P.J., "Efficient Optimization of Integrated Aerodynamic-Structural Design," Paper presented at International Conference on Inverse Design Concepts and Optimization in Engineering Sciences - II, ICIDES-II, Pennsylvania State University, University Park, Pennsylvania, Oct., 1987.

7. Barthelemy, J.-F., and Bergen F. D., "Shape Sensitivity Analysis of Wing Static Aeroelastic Characteristics," NASA Technical Paper 2808, May 1988. See also *Journal of Aircraft*, Vol 26, No. 8, Aug 1989, pp. 712-717.

8. Rudisill, C. S., and Bhatia, K. G., "Optimization of Complex Structures to Satisfy Flutter Requirements," *AIAA Journal*, Vol. 9, No. 8, Aug. 1971, pp. 1486-1491.

9. Pedersen, P., and Seyranian, A. P., "Sensitivity Analysis for Problems of Dynamic Stability," *International Journal of Solids and Structures*, Vol. 19, No. 4, 1983, pp. 315-335.

10. Kapania, R. K., Bergen F. D., and Barthelemy J.-F.M., "Shape Sensitivity Analysis of Flutter Response of a Laminated Wing," Presented at the AIAA / ASME / ASCE

/ AHS / ASC 30th Structures, Structural Dynamics & Materials Conference, Apr., 1989, Mobile. *AIAA Journal*, Vol 29, No. 4, 1991, pp. 611-612.

11. Giles, G. L., "Equivalent Plate Analysis of Aircraft Wing Box Structures with General Planform Geometry," *Journal of Aircraft*, Vol. 23, No. 11, Nov. 1986, pp. 859-864.

12. Giles, G. L., "Further Generalization of an Equivalent Plate Representation for Aircraft Structural Analysis," *Journal of Aircraft*, Vol. 26, No. 1, Jan 1989, pp. 67-74.

13. Yates, E. C., "Calculation of Flutter Characteristics for Finite-Span Swept or Unswept Wings at Subsonic and Supersonic Speeds by a Modified Strip Analysis," NASA RM L57110, March 1958, (Declassified Feb. 6, 1962)

14. Landsberger, B. J., and Dugundji, J., "Experimental Aeroelastic Behavior of Unswept and Forward-Swept Cantilever Graphite/Epoxy Wings," *Journal of Aircraft*, Vol. 22, No. 8, August 1985.

15. Spielberg, I.N., "The Two Dimensional Incompressible Aerodynamic Coefficients for Oscillatory Changes in Airfoil Camber," *Journal of the Aeronautical Sciences*, Vol. 20, June 1953, pp. 389-396.

16. Unger, E.R., Hutchison, M.G., Rais-Rohani, M., Haftka, R.T., Grossman, B., "Variable-Complexity Multidisciplinary Design of a Transport Wing," *International Journal of Systems Automation: Research and Applications (SARA)*, Vol 2, 1992, pp. 87-113.

17. Borland, C., "A Multidisciplinary Approach to Aeroelastic Analysis," *Computing Systems in Engineering*, Vol 1, Nos 2-4, 1990, pp. 197-209.

18. Kapania, R.K., Eldred, L.B., and Barthelemy, J-F.,M. "Shape Sensitivity Analysis of a Wing Aeroelastic Response," Paper presented at 32nd AIAA / ASCE / ASME / AMS / ASC Structures, Stuctural Dynamics and Materials Conference, Baltimore, MD., April 1991. Updated version to appear in *Journal of Aircraft*, Vol 30, No. 2, March-April, 1993.

19. Sobieszczanski-Sobieski, J., "Sensitivity of Complex, Internally Coupled Systems," *AIAA Journal*, Vol. 28, No. 1, Jan 1990, pp. 153-160.

20. Desmarais, R. N., and Bennet, R. M., "User's Guide for a Modular Flutter

Analysis Software System", NASA TM 78720, May,1978.

21. Burden, R. L., and Faires, J. D., *Numerical Analysis*, Fourth Ed., PWS-KENT Publishing Company, Boston, 1989, pp. 85- 144, 425-482.

22. de Boor, C., *A Practical Guide to Splines*, Springer- Verlag, New York, 1978.

23. Haftka, R. T. and Gürdal, Z., *Elements of Structural Optimization*, 3rd Ed., Kluwer Publications, 1992.

Vita

The author was born on [redacted] in [redacted]. He received his B.S. degree in Aerospace and Ocean Engineering from Virginia Polytechnic Institute and State University in June, 1986, and his M.S. in Aerospace Engineering from VPI&SU in December, 1989. Upon completion of his Ph.D. he hopes to find interesting and rewarding work out in the real world.